공학석사 학위논문

A Study of Reinforced Concrete Flat Plate-Column Interior Connections with Shearbands

전단밴드로 보강된 철근콘크리트 플랫 플레이트 내부 접합부의 실험적 연구

2015년 8 월

서울대학교 대학원

건축학과

이 주 동

공학석사 학위논문

A Study of Reinforced Concrete Flat Plate-Column Interior Connections with Shearbands

전단밴드로 보강된 철근콘크리트 플랫 플레이트 내부 접합부의 실험적 연구

2015년 8 월

서울대학교 대학원

건축학과

이 주 동

A Study of Reinforced Concrete Flat Plate-Column Interior Connections with Shearbands

지도 교수 강 현 구

이 논문을 공학석사 학위논문으로 제출함
2015 년 4 월

서울대학교 대학원
건축학과
이 주 동

이주동의 공학석사 학위논문을 인준함
2015 년 7 월

위 원 장 **홍 성 걸** (인)

부위원장 **강 현 구** (인)

위 원 **이 철 호** (인)

Abstract

A Study of Reinforced Concrete Flat Plate-Column Interior Connections with Shearbands

Lee, Ju Dong
Department of Architecture and Architectural Engineering
College of Engineering
Seoul National University

Because a flat plate system is a system whose columns support slab without beams, it allows for relatively small floor height and simple formwork; however, this system is vulnerable to seismic actions, as punching failure of flat plate-column connection may occur. To ensure its structural safety during earthquakes, an important design consideration is to obtain seismic ductility at the connection between column and slab. In this study, a shear band reinforcement is suggested as a method to improve overall performance of slab-column connections. The shearbands have many advantages over conventional shear reinforcement in terms of convenient installation and overall cost.

An experimental study was conducted to estimate the seismic and punching shear performance of the shear reinforcement for flat plate slab-column connections. A total of six specimens were constructed on one-half scale slab-

column connections and included slab-column connections without shear reinforcement and with stirrups / shearbands. Three specimens were tested under reversed cyclic lateral loading subjected to a constant gravity shear ratio of about one-third of the nominal concrete shear strength, and the remaining specimens were tested under only gravity load. The test results indicate that both shear reinforcements used in this study substantially increased the punching shear strength, the ductility of the slab-column connections, and the dissipation energy capacity. Although the connections strengthened with shear band were not as effective as connections strengthened with stirrup, they showed sufficient capacity for use in nonparticipating and lateral-force resisting systems. Most of all, the feasibility of the shearbands in the figure is promising because its installation process is quite simple.

Keywords : flat plate system, shear reinforcement, punching shear, unbalanced moment, shearbands
Student Number : 2013-20569

Contents

List of Tables

List of Figures

List of Equations

Chapter 1. Introduction

1.1 Introduction

A flat plate system is a system whereby the columns support the slab without beams (**Figure 1-1**). Since the system has no beams and girders, it is possible to have a relatively smaller floor to floor height. Additionally, it can reduce construction time, while improving constructability due to its relatively simple form work. Finally, the use of flat plate systems allows a flexible floor plan for building users and fewer restrictions for the building's remodeling in the future in comparison to beam-column frame or bearing wall systems (Choi and Song, 2007).

Figure 1-1 Flat plate construction

However, the punching failure of the slab can become brittle, resulting in an unstable and drastic fracture mechanism. Therefore shear failure of the slab may lead to severe damage to the entire building, and eventually cause serious accidents resulting in irreparable harm to victims (Ahn and Park, 2005). For example, 502 people were killed and 937 thousand were injured in a Sampoong department store collapse on June 29, 1995 in Seoul, Korea. Other accidents due to the collapse of structures utilizing the flat plate system have been reported as shown in **Figure 1-2**.

Figure 1-2 Failure of flat plate system

Another concern with the design of a flat plate system is that it can be vulnerable to seismic actions if it is not carefully detailed. Stress concentration often develops at the RC slab-column(s) under combined large gravity and moderate lateral loads; unexpected story deformation is thus not negligible. Reinforcement details and thickness of slab need to be considered (Choi et al., 2007).

Despite these disadvantages, the use of a flat plate system has increased because of the demand for flexible floor plans and the increase in high-rise building construction. Accordingly, many studies have been conducted to prove the effective performance of the flat plate system through experiments and simulation models.

To secure its structural safety, the most important factor is obtaining ductility and integrity for the column-slab connection; several common approaches can be taken to improve the connection integrity (Ahn and Park, 2005): 1) Material approach: use of high performance concrete; 2) Design approach: increase the size of the column section and slab thickness, or use a shear capital; and 3) Reinforcement approach: arrange shear reinforcement. Among these approaches, the reinforcement approach is considered to be the most efficient and economical solution (Pilakoutas and Li, 1995).

The need for more convenient shear reinforcement has been reported, and many types of methods such as stud type and lattice type have been developed

to overcome the above-mentioned drawbacks. The band type shear reinforcement is suggested in this study. In this shear reinforcement, the rebar is replaced with a manufactured steel band. The band type shear reinforcement has many advantages over conventional shear reinforcement. For example, the installation is extremely simple and increased slab thickness is not required. Additionally, since the steel bands are manufactured in advance in a factory, the quality is uniform and any time delay required to bend the rebar on the construction site is avoided.

1.2 Objectives

A major objective of this study is to validate the structural performance of an isolated slab-column connection specimen with band type shear reinforcement. To estimate its performance, a specimen without shear reinforcement and a specimen with stirrup shear reinforcement were tested. To compare several aspects, analyses of drift ratio, ductility capacity, moment and shear strength, and dissipation energy were conducted using obtained experiment data. If a specimen using band type shear reinforcement shows corresponding performance with a specimen using stirrup shear reinforcement, it could replace the stirrup shear reinforcement, given the many advantages mentioned in the introduction.

Additionally, although all specimens are designed to satisfy ACI 318-11 (“Building”, 2011), analysis of specimens’ strength using the latest versions of two other design codes, Eurocode 2 (“Design”, 2004) and KCI 2012 (“Korean”, 2012) was also carried out. Design fundamentals and processes are briefly introduced, and similarities and differences are examined in **Chapter 3**. By comparing experiment results with the design strengths obtained using the codes, it is possible to observe whether a code is conservative or pragmatic in terms of safety.

Another objective of this study is to determine the transfer width assumed by ACI code for delivering unbalanced moment. For many decades, ACI 318-11 has considered c_2+3h as the transfer width, while KCI 2012 (which previously followed the same concept), has not considered transfer width since their latest code version in 2012. Even in the U.S., this matter is still controversial, although the ACI code recommends the use of c_2+3h as an effective transfer depth. For example, some codes insist c_2+5h is more reasonable and some claim that the column strip is more appropriate (Hawkins et al., 1989; Hwang, 1989; "Prestandard", 2000). This is because too many variables need to be considered when determining the transfer width. In this study, strain gauges are installed within the column area, at transfer widths of c_2+3h and c_2+5h and at the column strip to determine the effects of external load on reinforcement arranged at these locations. The obtained data after tests are analyzed and discussion is given regarding the reasons why KCI 2012 and Eurocode 2 no longer consider the concept of transfer width.

1.3 Organization

This thesis is organized into eight main chapters. The introduction (**Chapter 1**) is followed by a discussion on the previous research carried out in this area (**Chapter 2**). **Chapter 3** includes details of the six test specimens, the construction process, the test setup, the loading plan, and gauge work plan. The properties of used material in the entire experiment are also presented in **Chapter 3**. Design philosophies and processes suggested by ACI 318-11 ("Building", 2011), KCI 2012 ("Korean", 2012) and Eurocode 2 ("Design", 2004) are considered in **Chapter 3**. Experimental results are included in **Chapter 5**. Result analyses and considerations are described in **Chapter 6**. Finally, conclusions are given in **Chapter 7**.

Chapter 2. Previous Studies

An option for the use of shearbands as punching shear reinforcement is available in the Joint ACI-ASCE Committee 352 report (ACI 352.1R-11), Guide for Design of Slab-Column Connections in Monolithic Concrete Structures. However, the database for slab-column connections with shearbands is still quite limited. To the best of the author's knowledge, only three studies on shearbands have been conducted since shearbands were first suggested by Pilakoutas and Li (1994). In three previous experimental programs, specimens were tested under two different loading conditions: 1) monotonic gravity loading and 2) combined constant gravity and reversed cyclic lateral loading. The former was applied to assess the direct punching shear strength, while the latter was applied to assess the unbalanced moment capacity. This chapter introduces the different types of shearbands used in three experimental programs, and summarizes the test results.

2.1 Monotonic gravity load test

Pilakoutas and Li (2003) introduced a new concept for shear reinforcement, called the 'shearbands' system for flat slabs. They conducted an experimental study at the University of Sheffield, the details of which were published in "Alternative Shear Reinforcement for Reinforced Concrete Flat Slabs (2003)". A total of four specimens were tested under four types of load phases (**Table 2-1**).

Table 2-1 Four types of load phases in Pilakoutas and Li's study

Phase	Load
A	Two cycles up to service load (150 kN)
B	Two cycles up to the design capacity (250 kN)
C	One cycle up to 450 kN
D	The slab was loaded to failure

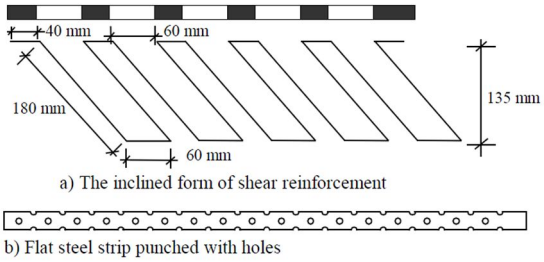

(a) The schematic way of representing shearbands

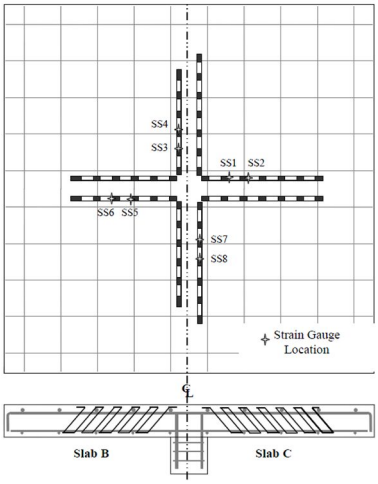

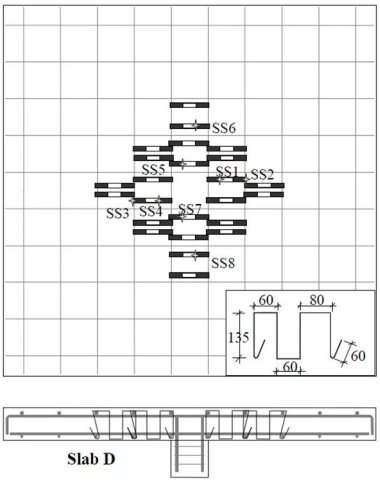

(b) PSS-B and PSS-C (c) PSS-D

Figure 2-1 Layout of shearbands (Pilakoutas and Li, 2003)

The slabs were named PSS (punching shear slab) A to D. The PSS-A was a control specimen without shear reinforcement, and slabs PSS-B, PSS-C, and PSS-D were reinforced with different forms of shearbands. For PSS-B, the

strip with 8 mm diameter circular holes was bent in an inclined form to be placed perpendicular to the shear crack, of which the angle is assumed to be 45 degrees at the bottom of the slab-column connection. The hole in the strip was thought to improve the anchorage capacity between the concrete and shear reinforcement. To examine the performance of the shearbands without holes, PSS-C was shear-reinforced with the shearbands having no holes. Shearbands were placed in the two principal directions instead of being arranged evenly over the critical section as specified in ACI 318-02 ("Building", 2002). All conditions were similar for PSS-B and PSS-C, but two additional legs were extended for PSS-C. Vertical steel strip with holes were used for Specimen PSS-D as shear reinforcement. The shearbands were made of a high strength, high ductility flat steel strip of 25.4 mm width and 0.8 mm thickness, and its details are diagrammatically described in **Figure 2-1**.

Unlike traditional punching shear tests (where the concentrated load is applied to the bottom of the column using one hydraulic jack and specimens are supported through tie rods on their various corners), eight hydraulic jacks of 100 kN capacity were used to apply the load symmetrically at eight points of contraflexure on a circle of 1.7 m diameter (**Figure 2-2**), according to the research carried out by Pilakoutas and Li (2003).

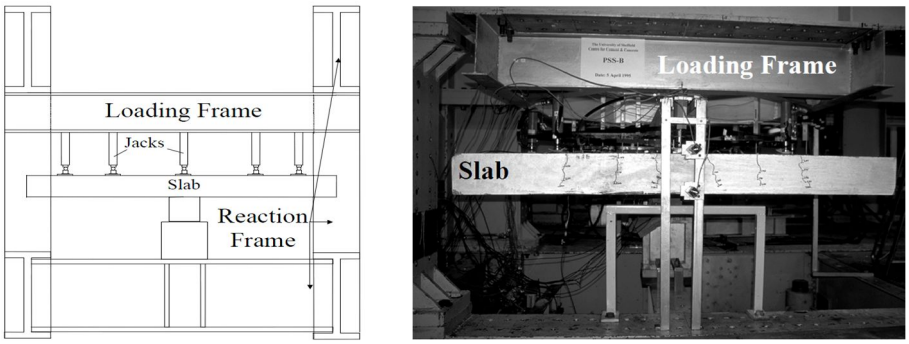

(a) Test elevation (b) Test setting

Figure 2-2 Gravity load test setting (Pilakoutas and Li, 2003)

The test result (**Figure 2-3**) revealed that the shear strengths of PSS-B, PSS-C, and PSS-D improved 1.23 times, and the deformation capacity of these improved 2.23, 2.11 and 1.88 times, respectively, compared to the specimen without shear reinforcement (PSS-A). The test result and a comparison of results are summarized in **Table 2-2**.

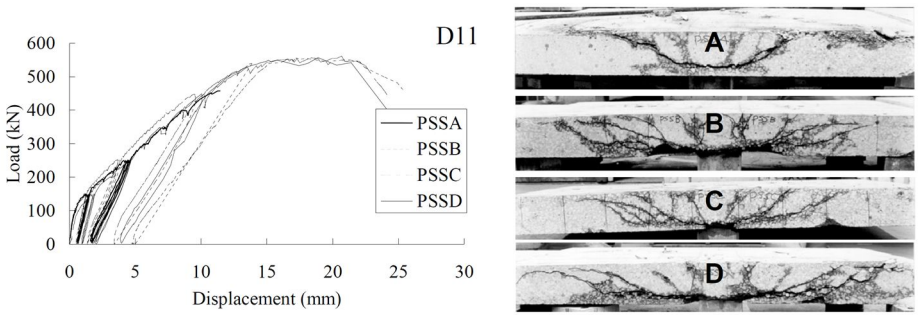

(a) Load-displacement curve (b) Section at failure

Figure 2-3 Load-displacement and section through the slab (Pilakoutas and Li, 2003)

Table 2-2 Test result (Pilakoutas and Li, 2003)

ID	Test results		Comparison of results	
	Strength	Deformability	Strength ratio(1)	Deformability ratio(2)
PSS-A	454 kN	11.4 mm	–	–
PSS-B	560 kN	25.4 mm	1.23	2.23
PSS-C	560 kN	24.1 mm	1.23	2.11
PSS-D	560 kN	21.4 mm	1.23	1.88

Note: (1), (2) The ratio were calculated by dividing the values of shear-reinforced specimens by those of unreinforced specimens

Pilakoutas and Li (2003) proved the effectiveness of the shearbands and this led to several subsequent studies.

2.2 Seismic load test

Another experimental study of flat plate using shearbands was carried out by Kang and Wallace (2008). In their study, a total of four specimens were tested under combined constant gravity and reversed cyclic lateral loading. Except for the type of shear reinforcement, all parameters were the same for the four specimens, including top and bottom reinforcement, loading conditions, slab thickness, and span length. Specimen C0 was a control specimen and had no shear steel reinforcement while PS2.5 and PS3.5 were reinforced with thin-plate stirrups and HS2.5 was strengthened with headed studs. The same type of shearbands with holes at 30 mm spacing was installed for specimens PS2.5 and PS3.5, although further shearbands were distributed in a wider area near the connection for Specimen PS2.5. Details of each specimen are referred from the special publication about shearbands by Kang and Park (2012), and suggested in **Figure 2-4**.

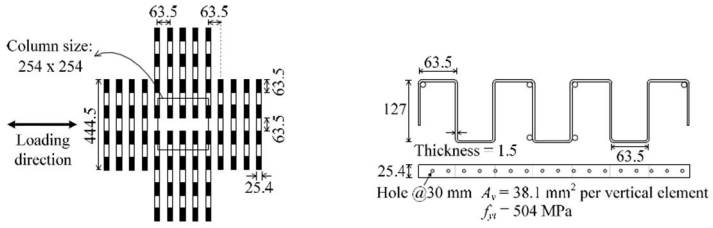

(a) PS2.5

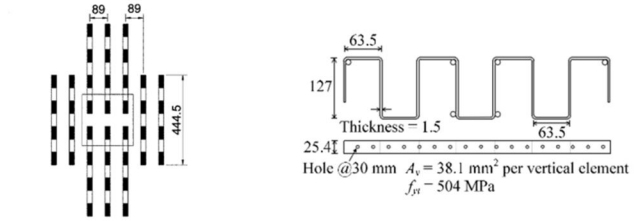

(b) PS3.5

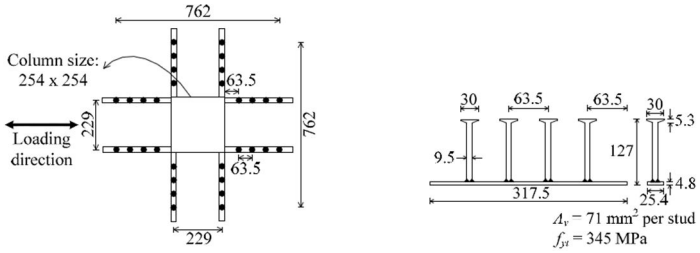

(c) HS2.5

Figure 2-4 Layout of shearbands (Kang and Wallace, 2012)

All specimens were designed to undergo punching failure after flexural yielding of the slab reinforcement because the reinforcing ratio was moderate. The test result (**Figure 2-5**) also revealed that the failure modes of all specimens were drift-induced failures prior to shear failures.

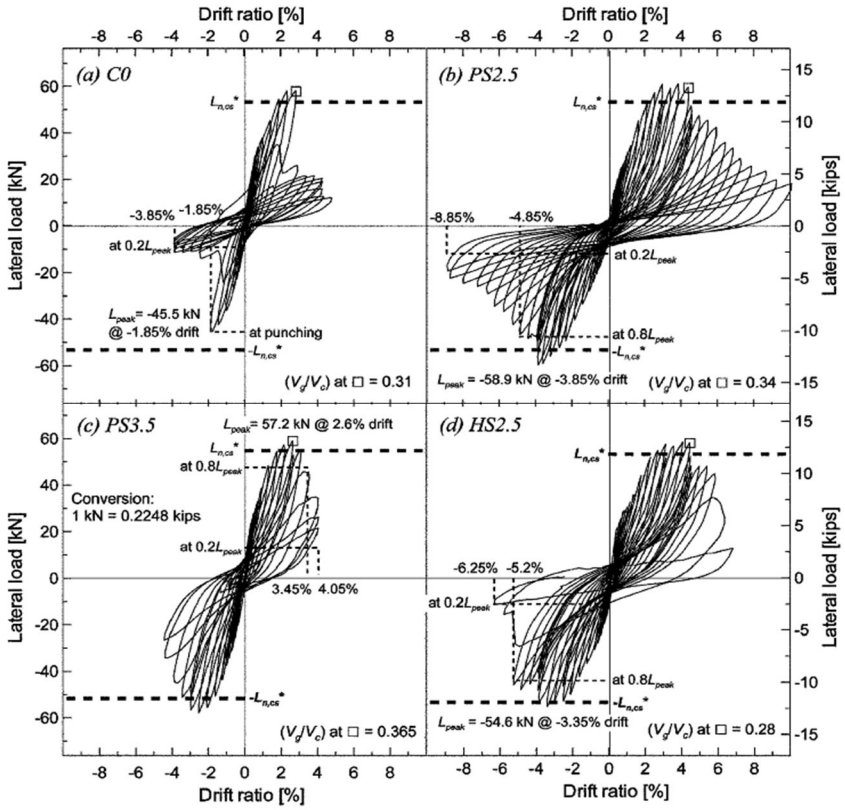

Figure 2-5 Test results (Kang and Wallace, 2008)

Although all specimens exhibited similar lateral load carrying capacities because drift induced failure occurred, remarkable differences were observed for the deformation capacity depending on the presence of shear reinforcement. Kang and Wallace (2008) defined the drift ratio at 80% of peak moment as a drift inducing punching failure. Experimental results from their study are summarized in **Table 2-3**. As shown in the table, specimens PS2.5 and PS3.5 exhibited 2.23 times and 2.11 times deformability, respectively, than specimen C0 (without shear reinforcement). The shearbands showed better performance than the headed studs, where specimen PS2.5 exhibited the ideal behavior, maintaining ductility at the end of the test.

Table 2-3 Test result (Kang and Wallace, 2008)

ID	V_g/V_c	Test result		Comparison of results	
		Strength [kN-m]	Deformability [%]	Strength ratio(1)	Deformability ratio(2)
C0	0.33	83.2	1.85	1.00	1.00
PS2.5	0.33	107.7	4.85	1.29	2.62
PS3.5	0.33	104.6	3.45	1.26	1.86
HS2.5	0.33	99.9	5.20	1.20	2.81

Note: (1), (2) The ratio was calculated by dividing the values of shear-reinforced specimens by those of unreinforced specimens. V_g is the gravity force to be transferred from the slab to the column; V_c is the nominal concrete shear strength calculated by **Eq. (3-3)**

Kang and Wallace (2008) tested slab-column connections where top and bottom reinforcement was not engaged by the shearband and revealed that those connections showed remarkable improvement regarding both strength and ductility. Therefore, this result is meaningful because it can reduce construction time and make placement of shearbands more convenient although it was not consistent with ACI 318-11 (“Building”, 2011) recommendations.

An experimental program to validate the effectiveness of lattice shear

reinforcement was conducted by Park et al. (2012). Four types of shear reinforcement (lattice, stud rails, shearbands and stirrups) were tested and compared. Among them, only experiments of control specimens and specimens with stud rails/shearbands were discussed in this paper, and more information about other shear reinforcement can be found in the paper by Park et al. (2012). The specimens were divided into two groups and the only difference between two groups was the concrete strength. The 22.5 MPa concrete was used for Group A, and the 38.7 MPa concrete was used for Group B. The layout of each shear reinforcements installed at the slab-column connections is given in **Figure 2-6**. Three strips of the shearbands were placed per column face perpendicular to each column side to have similar nominal shear strength provided by shear reinforcement (V_s).

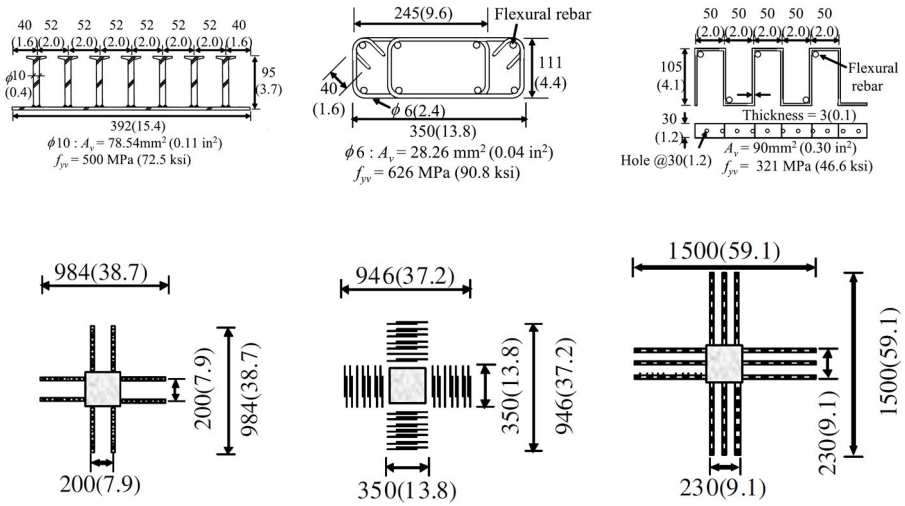

(a) SR-A and SR-B (b) ST-A and ST-B (c) SB-A and SB-B

Figure 2-6 Layout of shearbands (Park et al., 2012)

The relationships of unbalanced moment versus drift ratio for each group are drawn in **Figures 2-7** and **2-8**, respectively. From the figure, it is known that the seismic performance of both shear-reinforced specimens remarkably

improved. In contrast to RC-A and RC-B (no shear reinforcement), which exhibited brittle punching shear, SB-A and SB-B (with shearbands), ST-A and ST-B (with stirrup) and SR-A and SR-B (with stud rails) showed ductile behaviors while improving unbalanced moment carrying capacity.

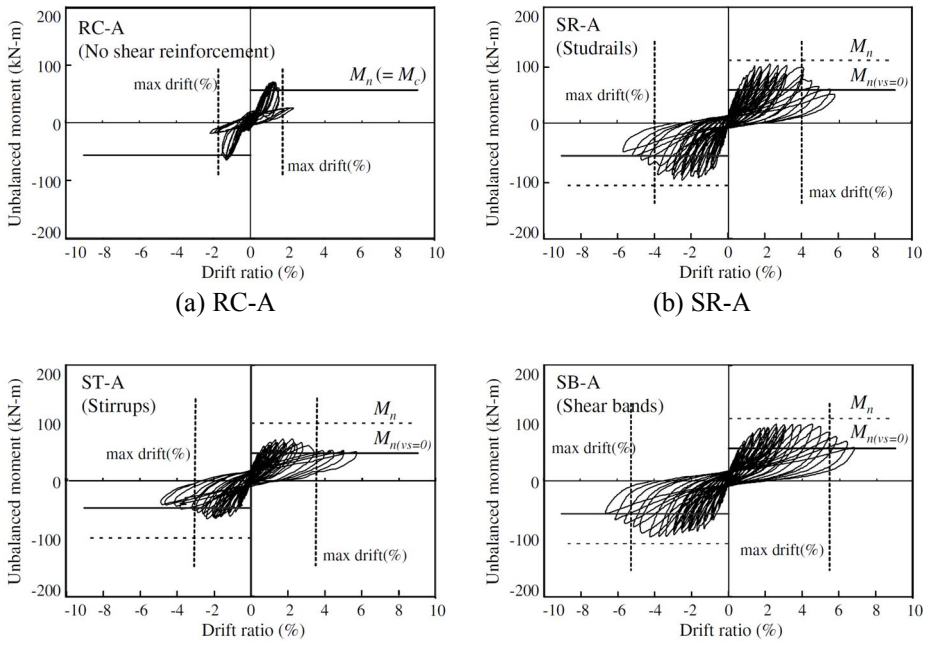

(a) RC-A (b) SR-A

(c) ST-A (d) SB-A

Figure 2-7 Unbalanced moment vs. drift of specimens in Group A (Park et al., 2012)

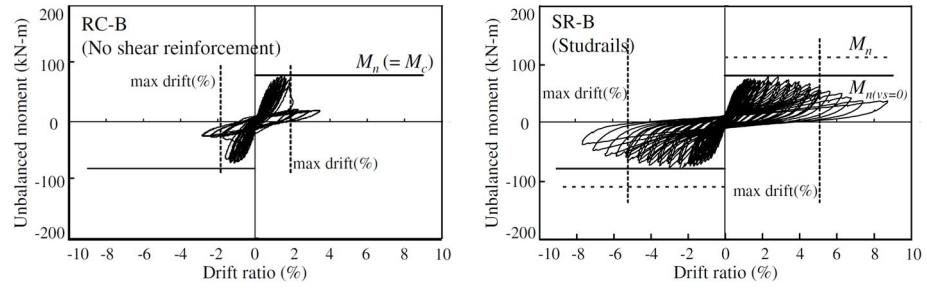

(a) RC-B (b) SR- B

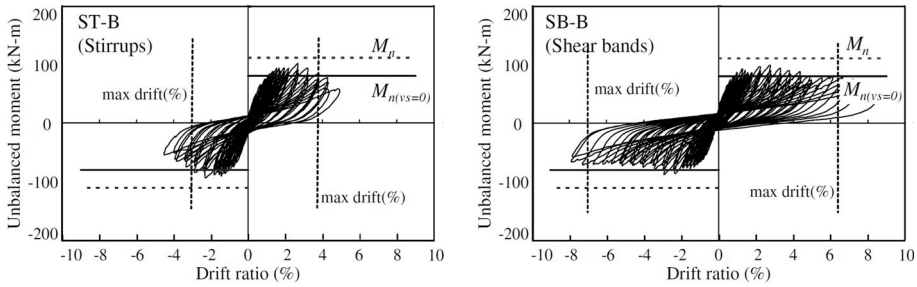

(c) ST- B (d) SB- B

Figure 2-8 Unbalanced moment vs. drift of specimens in Group B (Park et al., 2012)

As suggested in **Table 2-4**, drift capacities at punching shear (drift at 80% of peak load) of the connections with shearbands were 5.1% and 6.5% for SB-A and SB-B, respectively, whereas those with stud rails or stirrups were 4.0% and 5.1% for SR-A and SR-B or 3.0% and 3.2% for ST-A and ST-B, respectively.

Table 2-4 Test result (Park et al., 2012)

ID	Shear reinforcement	V_g/V_c	Test result		Comparison	
			M_{peak}[(1)] [kN-m]	δ_{exp}[(2)]	M_{exp}/M_{exp} (control)[(3)]	$\delta_{exp}/\delta_{exp}$ (control)[(4)]
RC-A	None	0.45	64.5	1.5	–	–
SR-A	Stud rails	0.45	98.9	4.0	1.53	2.67
ST-A	Stirrup	0.54	66.1	3.0	1.02	2.00
SB-A	Shearbands	0.45	96.7	5.1	1.49	3.10
RC-B	None	0.41	70.5	1.6	–	–
SR-B	Stud rails	0.41	77.1	5.1	1.09	3.19
ST-B	Stirrup	0.41	93.8	3.2	1.33	2.00
SB-B	Shearbands	0.41	86.8	6.5	1.23	4.06

Note: V_g is the gravity force to be transferred from the slab to the column; V_c is the nominal concrete shear strength calculated by **Eq. (3-3)**; M_{peak} is the maximum measured unbalanced moment during the test; [(1)] Maximum value of the unbalanced moment; [(2)] Maximum drift ratio at $0.8M_{peak}$; [(3)] Ratio of strength of shear-reinforced specimen to that of control specimen; [(4)] Ratio of maximum drift ratio of shear-reinforced specimen to that of control specimen;

According to Park et al. (2012), test results of all specimens with stud rails/ stirrup/shearbands did not reach to the design moment strength (M_n) predicted by ACI 318-08 ("Building", 2008). This observation throws a doubt on flat plate design in accordance with ACI 318 -11 (ACI 318-08 and ACI 318-11 have the same design method for two way slab subjected to unbalanced moment).

Chapter 3. Design Code

3.1 ACI 318-11

3.1.1 Punching shear design

The punching shear design specified in the ACI 318-11 code is generally based on the same principle as that of KCI 2012 ("Korean", 2012), whereby the factored shear force should not be greater than the nominal shear strength ($V_u \leq V_n$). However, the method of calculating each concrete shear strength (V_c) and nominal shear strength provided by shear reinforcement (V_s) differ between the two codes.

The major difference is that ACI 318-11 ("Building", 2011) suggests different equations to obtain the nominal concrete shear strength (V_c) according to the existence of shear reinforcement, where V_c is the smallest value among the following three equations when there is no shear reinforcement.

$$V_c = 0.17(1+2/\beta)\lambda\sqrt{f'_c}b_o d \tag{3-1}$$

$$V_c = 0.083(\alpha_s d/b_o + 2)\lambda\sqrt{f'_c}b_o d \tag{3-2}$$

$$V_c = 0.33\lambda\sqrt{f'_c}b_o d \tag{3-3}$$

Where,

V_c : nominal shear strength provided by concrete, N
β : ratio of long side to short side of the column, concentrated load or reaction area

λ : modification factor reflecting the reduced mechanical properties of lightweight concrete

f'_c : specified compressive strength of concrete, MPa

b_o : perimeter of critical section for shear in slabs, mm

d : distance from extreme compression fiber to centroid of longitudinal tension reinforcement, mm

α_s : 40 for interior columns, 30 for edge column, 20 for corner columns.

If shear reinforcement is arranged, two critical sections need to be considered: a section through the slab shear reinforcement and a section through an area outside the shear reinforcement, as described in **Figure 3-1**.

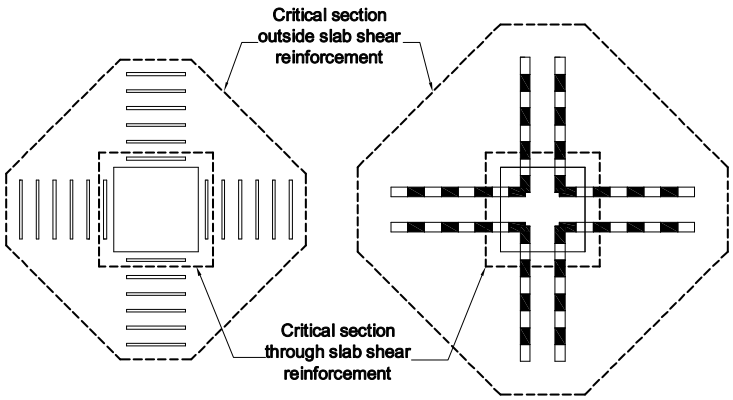

Figure 3-1 Critical section in shear reinforced concrete

The strength of the two critical sections shall be computed and compared to determine which critical section governs failure. The shear strength of the critical section through the slab shear reinforcement is determined using **Eqs. (3-4)** ~ **(3-6)**, but V_n shall not be greater than $0.5\sqrt{f'_c}b_o d$. The shear strength of the critical section outside the shear reinforcement is determined from **Eqs. (3-1)** ~ **(3-3)**.

$$V_c + V_s = V_n \leq 0.5\sqrt{f'_c}b_o d \tag{3-4}$$

$$V_c \le 0.17\lambda\sqrt{f'_c}\,b_o d \tag{3-5}$$

$$V_s = \frac{A_v f_{yt} d}{s} \tag{3-6}$$

Where,

V_c	:	nominal shear strength provided by concrete, N
V_s	:	nominal shear strength provided by shear reinforcement, N
V_s	:	nominal shear strength, N
f'_c	:	specified compressive strength of concrete, MPa
b_o	:	perimeter of critical section for shear in slabs, mm
d	:	distance from extreme compression fiber to centroid of longitudinal tension reinforcement, mm
λ	:	modification factor reflecting the reduced mechanical properties of lightweight concrete
A_v	:	area of shear reinforcement within spacing s, mm^2
f_{yt}	:	specified yield strength f_y of transverse reinforcement, MPa
s	:	center-to-center spacing of reinforcement, mm

3.1.2 Unbalanced moment design

In Chapter 11.11.7 of ACI 318-11 ("Building", 2011), the design of the transfer of moment in slab-column connections is specified. Members without shear reinforcement and with shear reinforcement are considered separately.

When there is no shear reinforcement, the area $d/2$ distant from the column surface is considered as b_0 (critical section), as shown in **Figure 3-2**, and the shear stress is calculated from the following equations.

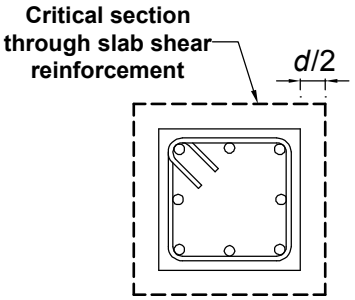

Figure 3-2 Critical section of non-shear-reinforced concrete (from ACI 318-11)

$$\phi v_n = \phi V_c / (b_o d) \tag{3-7}$$

It is noted that 0.75 is recommended as the strength reduction factor ϕ in ACI 318-11, but reduction factor was not considered in this study.

The assumed distribution of shear stress is drawn in **Figure 3-3**, and the maximum factored shear stress can be calculated from **Eq. (3-8)**.

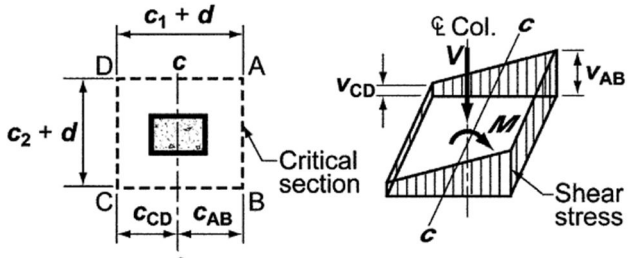

Figure 3-3 Assumed distribution of shear stress (from ACI 318-11)

$$v_u = \frac{V_u}{A_c} \pm \frac{\gamma_v M_{u,unb} c}{J_c} \le v_n = v_c + v_s \tag{3-8}$$

Where,

v_u : maximum factored shear stress, MPa
v_u : nominal stress capacity provided by the concrete, MPa

v_u : nominal stress capacity provided by shear reinforcement, MPa
V_u : factored direct force to be transferred from the slab to the column, N
A_c : area of concrete of assumed critical section, mm^2
γ_v : factor used to determine the unbalanced moment transferred by eccentricity of shear at slab-column connections
$M_{u,unb}$: unbalanced moment, N-mm
c : distance from the centroid of the critical section to the perimeter of the critical section, mm
J_c : property of assumed critical section analogous to polar moment of inertia, mm^4

When failure occurs due to shear failure, factored shear stress v_u is equal to the nominal shear stress v_n, and the maximum unbalanced can be obtained from this relationship.

In the case of no shear reinforcement, shear failure occurs when v_u reaches v_n (= v_c, since only concrete resists shear force) and the unbalanced moment is derived from **Eq. (3-9)** at the moment of shear failure.

$$\frac{V_u}{A_c} \pm \frac{\gamma_v M_{u,unb} c}{J_c} = v_c \tag{3-9}$$

For members with shear reinforcement, v_u corresponding to $v_n = (v_c + v_s)$ causes shear failure, and the unbalanced moment is obtained from **Eqs. (3-10)** and **(3-11)**.

$$\phi v_n = \phi(V_c + V_s)/(b_o d) \tag{3-10}$$

$$\frac{V_u}{A_c} \pm \frac{\gamma_v M_{u,unb} c}{J_c} = v_c + v_s \tag{3-11}$$

Two critical sections should be computed and compared to determine the more severe critical section in the same manner as that for punching shear design in **Chapter 3.1.1**. Along with column critical section $d/2$ from the

column faces, the ends and connection lines of the octagon section (which is $d/2$ distant from shear reinforcement) are also considered as critical sections (**Figure 3-4**).

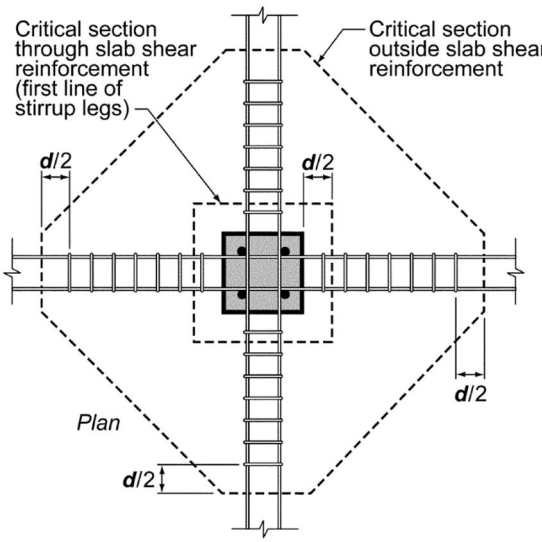

Figure 3-4 Two critical sections

A connection subjected to large unbalanced moment can have two different failure modes: punching shear failure by concrete fracture and flexural failure by flexural reinforcement failure. The failure mode of each connection depends on its flexural strength (M_{slab}) and the maximum unbalanced moment (M_{unb}). The flexural strength (M_{slab}) varies depending on the transfer widths considered. Although ACI 318-11 suggests taking c_2+3h to be a moment transfer width, determination of the transfer width is still a controversial issue (e.g., FEMA 356 (2000) allows the use of c_2+5h). Therefore, c_2+3h is validated as the transfer width by comparing it with c_2+5h and column strip. Flexural strength (M_{slab}) within considered transfer width is calculated using **Eqs. (3-12)** and **(3-13)**.

$$\sum M_{n\_*} = M^{+}{}_{n\_*} + M^{-}{}_{n\_*} \tag{3-12}$$

$$M_{Slab\_*} = \frac{\sum M_{n\_*}}{\gamma_f} \tag{3-13}$$

Where, $*$ varies depending on what transfer is considered (c_2+3h, c_2+5h and column strip);

$M^{+}_{n\_*}$	:	positive nominal flexural strength within the considered section, N-mm
$M^{-}_{n\_*}$	:	negative nominal flexural strength within the considered section, N-mm
ΣM_{n_*}	:	sum of positive and negative nominal moment strength of the slab over the considered section, N-mm
M_{Slab_*}	:	flexural moment capacity within the considered section, N-mm
γ_f	:	factor used to determine the unbalanced moment transferred by flexure at slab-column connections (a representative value equal to 0.6 is used)

3.2 KCI 2012

3.2.1 Punching shear design

KCI 2012 (“Korean”, 2012) demands design shear strength (ϕV_n) of a section where shear force is applied to be greater than the factored shear force (V_u).

$$V_u \le \phi V_n \tag{3-14}$$

$$V_n = V_c + V_s \tag{3-15}$$

The design of the nominal shear strength (V_c) of structures having two-way behavior such as a two way slab or footing is particularly stated in KCI 2012 (“Korean”, 2012) Section 7.12.2 by considering various factors. Choi et al. (2014) suggested detail information about following procedure.

$$V_c = v_c b_o d \tag{3-16}$$

$$v_c = \lambda k_s k_{bo} f_{te} \cot\psi (c_u / d) \tag{3-17}$$

$$k_s = (300/d)^{0.25} \le 1.0 \tag{3-18}$$

$$k_{bo} = 4/\sqrt{\alpha_s (b_0/d)} \le 1.25 \tag{3-19}$$

$$f_{te} = 0.21\sqrt{f_{ck}} \tag{3-20}$$

$$\cot\psi = \sqrt{f_{te}(f_{te} + f_{cc})} / f_{te} \tag{3-21}$$

$$c_u = c\,[25\sqrt{\rho / f_{ck}} - 300(\rho / f_{ck})] \tag{3-22}$$

$$f_{cc} = (2/3) f_{ck} \tag{3-23}$$

Note that ratio of reinforcement ρ is used when $\rho \le 0.03$, however when ρ is smaller than 0.005, then use 0.005.

Where,

λ	:	modification factor reflecting the reduced mechanical properties of lightweight concrete
v_c	:	nominal shear stress, MPa
b_0	:	perimeter of critical section, mm
k_s	:	size effect factor
k_{bo}	:	aspect ratio factor
f_{te}	:	effective tensile strength reduced by the transverse compressive stress, , MPa
ψ	:	crack angle of slab in flexure zone
c_u	:	depth of compression zone, neglecting compressive reinforcement
f_{cc}	:	mean value of compressive stress applying to compression zone at critical section, MPa
α_s	:	coefficient factor when deciding V_c in two way slab or footing slab; take 1.0 for interior column, 1.33 for exterior column (except corner column), 2.0 for corner column

When shear reinforcement is installed additional shear strength by shear reinforcement is added, and nominal shear strength provided by shear reinforcement (V_s) is determined from **Eq. (3-24)**.

$$V_s = \frac{0.5 A_v f_{yt} d}{s} \tag{3-24}$$

Where,

A_v : area of shear reinforcement within spacing s, mm^2
s : center-to-center spacing of transverse reinforcement, mm
f_{yt} : specified yield strength of transverse reinforcement, MPa
(**f_{yt}** shall not exceed 400 MPa)

3.2.2 Unbalanced moment design

In Chapter 7.12 of the KCI 2012 code, the eccentric shear design used to transfer unbalanced moment is specified.

$$M_u \le \phi M_n \tag{3-25}$$

The code suggests different procedures depending on whether connection is exterior or interior. In case of interior connection, design unbalanced moment strength is suggested as the sum of three moments (front moment, rear moment and side moment) as shown in **Figure 3-5** and **Eq. (3-26)**.

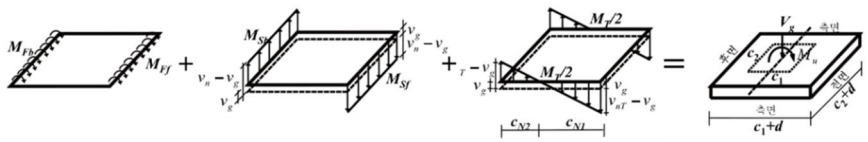

Figure 3-5 Model of unbalanced moment and eccentric shear stress's neutral axis in slab-column connection given in KCI 2012

$$\phi M_n = \phi_f M_F + \phi_v M_S + \phi_v M_T \tag{3-26}$$

Where,

M_{Ff} : flexural strength of top main reinforcement within critical section, N-mm

M_{Fb} : flexural strength of bottom main reinforcement within critical section, N-mm

M_F : sum of moment strengths of front and rear slab, N-mm

M_S : flexural strength by eccentric shear in front and rear slab, N-mm

M_T : torsion strength by eccentric shear in sides, N-mm

ϕ_f : strength reduction factor (= 0.85)

ϕ_v : strength reduction factor (= 0.75)

The design procedure of the interior connections is suggested specifically in KCI 2012, Section 7.12.7, and some of them are excerpted as shown in following figures and equations.

Firstly, to obtain the moment strength by main slab reinforcement (**Figure 3-6**), the flexural strengths of the top and bottom main reinforcements are calculated using **Eqs. (3-27)** ~ **(3.29)**. It is noted that main reinforcement only within c_2+d is considered.

Figure 3-6 Moment strength of front and rear slab (KCI 2012)

$$M_F = M_{Ff} + M_{Fb} \tag{3-27}$$

$$M_{Ff} = A_{Sf} f_y jd \tag{3-28}$$

$$M_{Fb} = A_{Sb} f_y jd \tag{3-29}$$

Where,

A_{Sf} : area of the tensile reinforcement at the front of the critical section, mm^2

A_{Sb} : area of the tensile reinforcement at the back of the critical section, mm^2

jd : distance from the resultant tensile force to the resultant compressive force in the cross section, mm

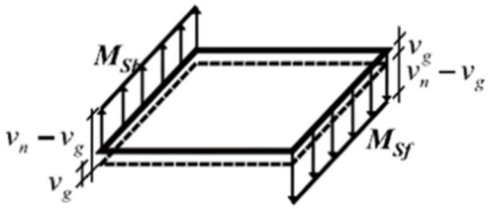

Figure 3-7 Unbalanced moment from rear and front slab

As shown in **Figure 3-7**, the rear and front eccentric shear stresses that occur in interior connections generate unbalanced moment M_s. Allowable shear stress due to the unbalanced moment is limited to (v_n−v_g) due to the direct shearing stress v_g (= V_g/b_0d) applied to the compression zone at the front side. Direct shear stress does not induce unbalanced moment and the front and rear unbalanced moment M_s is calculated from **Eq. (3-29)**, considering the contribution of eccentric shear.

$$M_S = [(v_n - v_g)(c_2 + d)d](c_1 + d) \geq 0 \tag{3-30}$$

$$v_n = v_c + v_p + 0.4v_s \leq 0.34 f_{ck} c_u / d \tag{3-31}$$

$$v_g = V_G / (b_0 d) \tag{3-32}$$

Where,

v_n : eccentric stress strength, MPa

v_g : direct shearing stress applied to critical section (= V_g/b_0d), MPa

v_p : stress by prestressing at the critical section, MPa

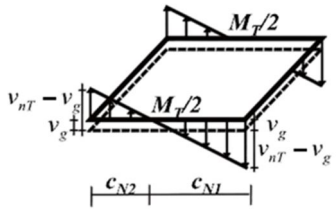

Figure 3-8 Moment by side eccentric shear

Flexural moment M_T due to side eccentric shear is calculated by using effective shear stress strength ($v_{nT} - v_g$) at the sides.

$$M_T = \frac{4}{3}(v_{nT} - v_g)\left(\frac{c_1 + d}{2}\right)^2 d \geq 0 \tag{3-33}$$

$$v_{nT} = 0.63\lambda + v_p + v_s \leq 0.34 f_{ck} c_u / d \tag{3-34}$$

Where,

v_{nT} : maximum shear stress at the sides at the intersections, MPa

3.3 Eurocode 2

In Sections 6.4.4 and 6.4.5, Eurocode 2 (“Design”, 2004) gives detail design procedures for punching shear resistance of slabs and column bases with/without shear reinforcement. Depending on the existence of shear reinforcement, two critical sections including the adjacent to the column (column periphery) and the control perimeter within 2d from the periphery of the column or three critical sections including previous two critical sections and outer perimeter shall be considered (Gardner, 2011; Ferreira et al, 2014).

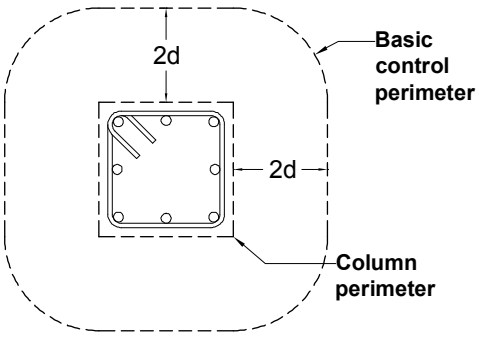

Figure 3-9 Basic control section and control perimeter (Eurocode 2)

3.3.1 Punching shear capacity in slabs

Chapter 6.4.4 in Eurocode 2 ("Design", 2004) deals with the punching shear resistance of slabs and column bases without shear reinforcement. According to 6.4.4(1), the punching shear resistance of a slab at the basic control perimeter should be assessed for the basic control section (**Figure 3-9**) using **Eq. (3-35)**.

$$v_{Rd,c} = C_{Rd,c} k (100 \rho_1 f_{ck})^{1/3} + k_1 \sigma_{cp} \geq (v_{\min} + k_1 \sigma_{cp}) \tag{3-35}$$

$$k = 1 + \sqrt{\frac{200}{d}} \leq 2d \tag{3-36}$$

$$\rho_l = \sqrt{\rho_{ly} \rho_{lz}} \leq 0.02 \tag{3-37}$$

It is noted that the values ρ_{ly} and ρ_{lz} should be calculated as mean values taking into account a slab width equal to the column width plus 3d each side.

$$\sigma_{cp} = (\sigma_{cy} + \sigma_{cz})/2 \tag{3-38}$$

Where,

$v_{Rd,c}$: design shear resistance of concrete without shear reinforcement

expressed as a stress, MPa

$C_{Rd,c}$: recommended value is $0.18/\gamma_c$

γ_c : partial factor for concrete

k : coefficient or factor

ρ_l : reinforcement ratio for longitudinal reinforcement

v_{min} : $0.035k^{3/2}f_{ck}^{1/2}$, MPa

ρ_{ly} : relate to bounded tension steel in z-direction

ρ_{lz} : relate to bounded tension steel in z-direction

Along with the basic control perimeter, punching shear calculation at the column perimeter should be carried out using **Eq. (3-39)**, and the obtained value shall not be greater than the capacity of the concrete struts $v_{Rd,max}$ (The recommended value of $v_{Rd,max}$ is $0.5vf_{cd}$).

$$v_{Ed} = \frac{\beta V_{Ed}}{u_o d} \le v_{Rd,\max} \tag{3-39}$$

Where,

u_0 : length of column periphery, mm

β : factor dealing with eccentricity (punching shear)

$v_{Rd,max}$: capacity of concrete struts expressed as a stress, MPa

$$v = 0.6\left(1 - \frac{f_{ck}}{250}\right) \tag{3-40}$$

$$f_{cd} = \alpha_{cc}\eta f_{ck} / \gamma_c \tag{3-41}$$

Where,

v : strength reduction factor for concrete cracked in shear, MPa

f_{cd} : design value of the concrete compression force in the direction of the longitudinal member axis, N

α_{cc} : coefficient taking into account long term effects of compressive (tensile) load and the way load is applied

η : factor defining effective strength (=1 for ≤ C50/60)

The calculation of the punching shear resistance of slabs and column bases having shear reinforcement is specified in Section 6.4.5 of Eurocode 2. Calculation should be carried out for three sections: 1) at the adjacent to the column; 2) at control perimeters within 2*d* from the periphery of the column; and 3) outermost perimeter of shear reinforcement. The sections at 1) and 2) are shown in **Figure 3-9**, and the section at 3) is suggested in **Figure 3-10**.

First, at section 1) at the adjacent to the column, the punching shear stress (v_{Ed}) is calculated from **Eq. (3-39)** as the same as without shear reinforcement. Similarly, the obtained value shall not be greater than the capacity of the concrete struts $v_{Rd,max}$ (The recommended value of $v_{Rd,max}$ is $0.5vf_{cd}$).

Secondly, at basic control perimeters within 2*d* from the periphery of the column (which is an area strengthened by shear reinforcement), **Eq. (3-42)** is used to determine the design punching shear stress capacity $v_{Rd,cs}$

$$v_{Rd,cs}=0.75v_{Rd,c}+1.5(d/s_r)A_{sw}f_{ywd,ef}(1/(u_1 d))\sin\alpha \qquad (3\text{-}42)$$

Where,

$v_{Rd,cs}$: design punching shear resistance of concrete with shear reinforcement expressed as a stress (punching shear), MPa
A_{sw} : area of one perimeter of shear reinforcement around the column, mm^2
s_r : radial spacing of perimeters of shear reinforcement, mm
$f_{ywd,ef}$: effective design strength of punching shear reinforcement ($f_{ywd,ef} = 250 + 0.25d \le f_{ywd}$), N
f_{ywd} : design yield strength of shear reinforcement, MPa
d : mean of the effective depths in the orthogonal directions, mm
α : angle between the shear reinforcement and the plane of the slab
u_1 : basic control perimeter (at 2*d* from face of load), mm

Lastly, punching shear resistance at u_{out} (outermost perimeter of shear

reinforcement shown in **Figure 3-10**), for which shear reinforcement is not required, should be checked using **Eq. (3-43)**.

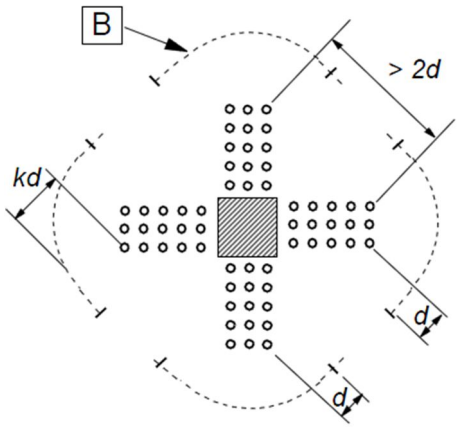

Figure 3-10 Outer perimeter of shear reinforcement (Eurocode 2)

$$u_{out,ef}=\beta V_{Ed}/(v_{Rd,c}d) \tag{3-43}$$

Where,

u_{out} : perimeter at which shear reinforcement is no longer required, mm

In this study, the outermost perimeter is already determined, and **Eq. (3-43)** is modified to **Eq. (3-44)** in order to obtain V_{Ed}.

$$V_{Ed} = u_{out,ef} v_{Rd,c} d / \beta \tag{3-44}$$

3.3.2 Unbalanced moment design

In Section 6.4.3(3) of Eurocode 2 (“Design”, 2004), the design of a section is designated where the support reaction is eccentric with regard to the control perimeter. The maximum shear stress is calculated according to **Eq. (3-45)**

when unbalanced moment occurs.

$$v_{Ed} = \beta \frac{V_{Ed}}{u_i d} \tag{3-45}$$

$$\beta = 1 + k \frac{M_{Ed}}{V_{Ed}} \frac{u_1}{W_1} \tag{3-46}$$

Where,

V_{Ed} : applied shear force, N
u_i : length of control perimeter being considered, mm
β : given by **Eq. (3-46)**
d : mean of effective depths in orthogonal directions, mm
α : angle between shear reinforcement and plane of the slab
u_1 : length of basic control perimeter, mm
k : coefficient dependent on ratio between the column dimensions

c_1/c_2	0.5	1.0	2.0	3.0
k	0.45	0.6	0.7	0.8

W_1 : function of basic control perimeter u_1 and corresponds to distribution of shear as illustrated in following figure

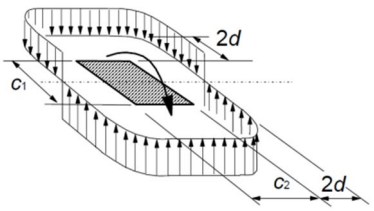

Note: for rectangular columns: W_1 is obtained by the equation below.

$$W_1 = \frac{c_1^2}{2} + c_1 c_2 + 4 c_2 d + 16 d^2 + 2\pi d c_1$$

where c_1 and c_2 are the column dimensions parallel or perpendicular to the eccentricity of the load, respectively.

The design value of the applied internal bending moment (M_{Ed}) is obtained by rearranging **Eqs. (3-45)** and **(3-46)**, and the transformed equation is suggested

in **Eq. (3-47)**.

$$M_{Ed} = \left(v_{Ed} \frac{u_i d}{V_{Ed}} - 1 \right) \frac{V_{Ed} W_1}{k u_1} \tag{3-47}$$

The unbalanced moment capacity at critical sections mentioned in **Chapter 3.3.1** are calculated and compared. The smallest value is considered as the design strength and critical section with the smallest value is regarded as the governing section.

Chapter 4. Specimen Design and Construction

In this study, an experimental program was planned. A total of six specimens of interior slab-column connections were constructed at the plant of Total PC Industrial Co. Ltd. The specimens used in the current study were designed to compare punching and seismic performance of a reinforced concrete (RC) flat plate system with/without shear reinforcement and a reinforced concrete flat plate system strengthened with band type shear reinforcement. Three of the specimens were used for an unbalanced moment experiment and the remaining specimens were used for a punching shear experiment. Each of the specimens is described in detail in the following subsection. The first letter of the specimen name indicates a type of experiment (**P**: Punching shear experiment and **U**: Unbalanced moment experiment), and the second letter implies the type of shear reinforcement used (**N**: No shear reinforcement, **S**: Stirrup reinforcement, and **B**: Band type reinforcement). While fabricating specimens, details (bar arrangement, bar spacing, covering depth) were directly measured. The construction error is ±5 mm compared with the notated details on the floor plan. The process of construction for both the unbalanced moment test and the punching shear test are shown in **Figure 4-1** and **4-2**.

(a) Bar arrangement

(b) Specimen construction

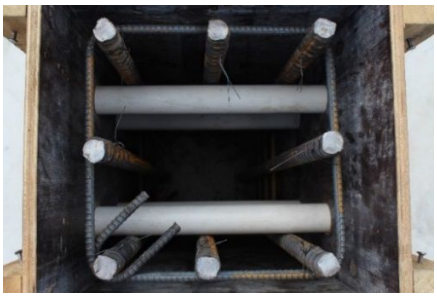

(c) Column detail

(d) Constructed specimen

Figure 4-1 Construction of unbalanced moment specimen

(a) Bar arrangement

(b) Specimen construction

(c) Concrete placement

(d) Concrete curing

Figure 4-2 Construction of punching shear specimen

The specimens were tested in a structural laboratory at Kongju National University. Two different types of experiments are planned: an unbalanced moment experiment and a punching shear experiment. In order to simulate similar moments generated in the interior connections of flat plate buildings

having large gravity and moderate lateral loads, three unbalanced moment specimens were tested under reversed cyclic and gravity loads, and controlled by displacement. The concept is shown in **Figure 4-3**.

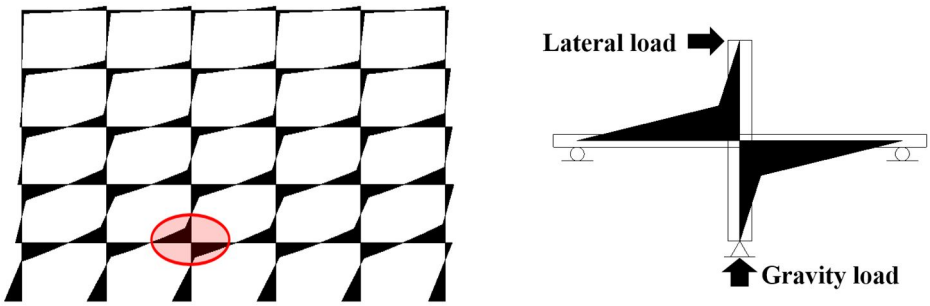

Figure 4-3 Moment diagram in unbalanced moment specimen

The other three specimens for punching shear were tested under only gravity load, and also managed by displacement. The moment diagram developed from the punching shear experiment is shown in **Figure 4-4**.

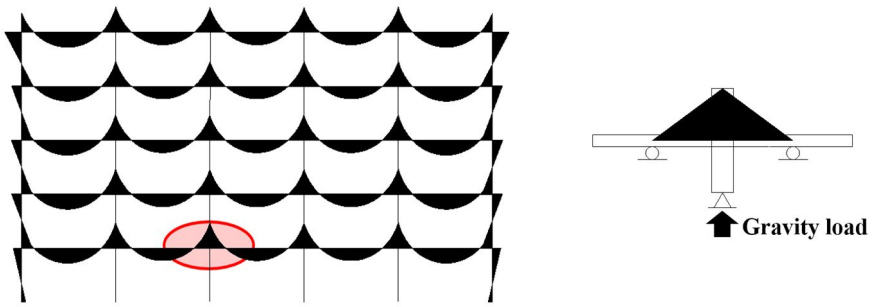

Figure 4-4 Moment diagram in punching specimen

4.1 Specimen Modeling

The prototype of this experiment is an interior flat plate floor system having a 5 m span. Due to limitations of the laboratory size and actuator's capacity, a scale factor of one-half was used for the specimens as shown in **Figure 4-5**.

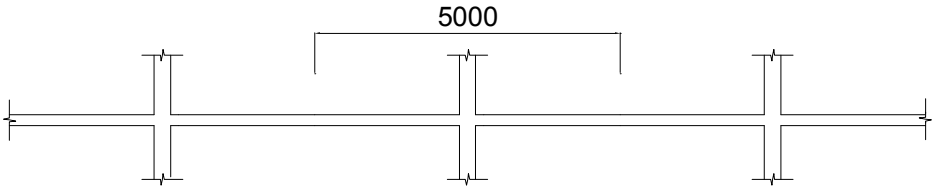

Figure 4-5 Proto type of the study

The major difference between the unbalanced moment and punching shear experiment is the location at which the inflection point occurs. **Figure 4-6** shows that an inflection point is located near the middle of the span when a large lateral load is applied with a gravity load.

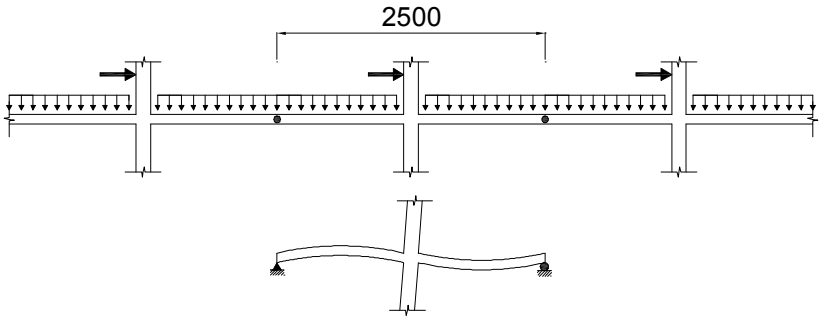

Figure 4-6 Specimen modeling for unbalanced moment

On the other hand, an inflection point is generated at 1/4 of the span when only gravity load is applied. The specimen was designed considering the inflection difference for each experiment as shown in **Figure 4-7**.

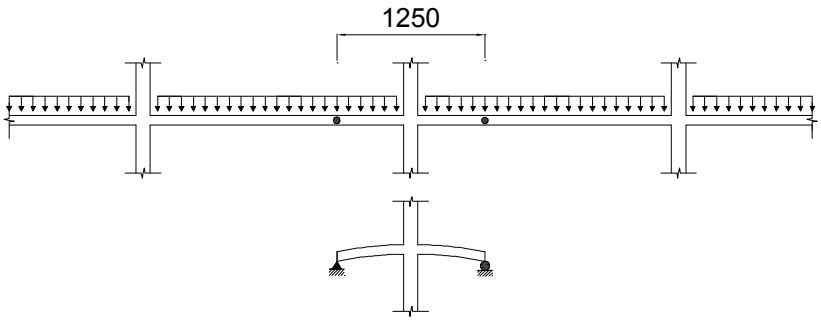

Figure 4-7 Specimen modeling for punching shear

4.2 Detailed description of specimens

4.2.1 Details of shear reinforcement

The band type shear reinforcement used in this experiment is shown in **Figure 4-8**. Since it was manufactured in a factory in advance and designed to be easily assembled, any additional work such as welding or bending of the rebar at the construction site was not required. The band type shear reinforcement had a folded shape and each band was connected to another band. To ensure convenient and simple assembly, the reinforcement is designed to be connected using pins through two holes at both ends of the plate.

A band consisted of five vertical plates and four plates in the horizontal direction: the total section size is 300 mm x 110 mm. Each vertical plate connected to the top and bottom horizontal plates had a length of 110 mm and it plays the role of improving the punching shear resistance. The horizontal plates held the vertical plates and controlled the spacing between the vertical plates. Since the spacing between shear reinforcement was designed to be 60 mm in this experiment, the length of each horizontal plate was 60 mm. The section size of the bands was 35 mm × 3 mm. To assist understanding, illustrations of a band, the assembled bands, and the method of connecting the bands using pins are presented in **Figure 4-8**.

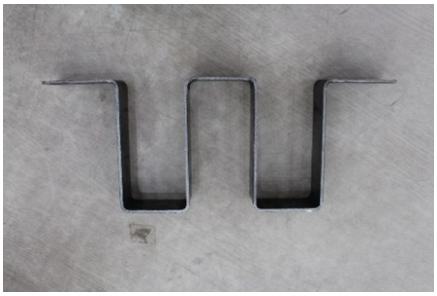

(a) Shearbands

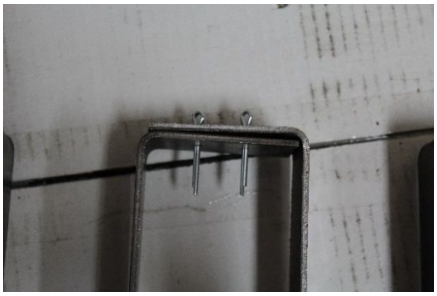

(b) Shearbands connection

(c) Connected shearbands

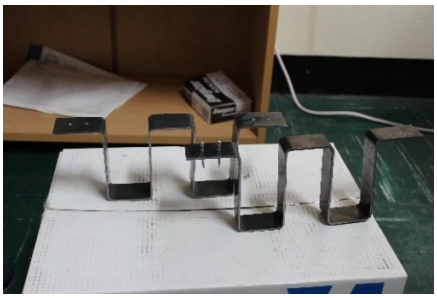

(d) Connected shearbands

Figure 4-8 Details of band type shear reinforcement.

The shear reinforcement arrangements in the two experiments were the same. From a point 30 mm from the side of the column, a 330 mm length of shear reinforcements was arranged in four directions. Six stirrups made of D10 rebar, with a size of 210 mm × 135 mm, were set up at 60 mm intervals, which is approximately the half of the effective depth, in the conventional stirrup type shear reinforcement.

In the band type shear reinforcement, two bands were connected to reach 540 mm, and two of the assembled bands were installed in one direction. The band started from a point 90 mm inside the column, and ended at a point 390 mm from the side of the column. A total of eight bands were used for the four directions and the effective length of shear reinforcement was 390 mm (60 mm of plate at the end was not counted as part of the shear reinforcement length, since it was not confined by a vertical plate). Specific details and construction processes are shown in **Figures 4-9** and **4-10**.

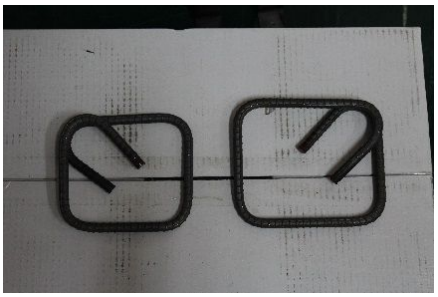

(a) Stirrups

(b) Shearbands

(c) Stirrups installation

(d) Shearbands installation

Figure 4-9 Manufactured product and installation of shear reinforcement

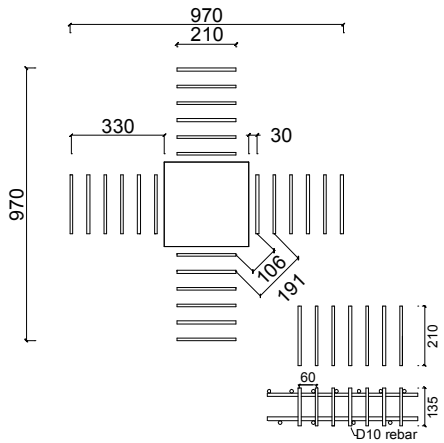

(a) Stirrups

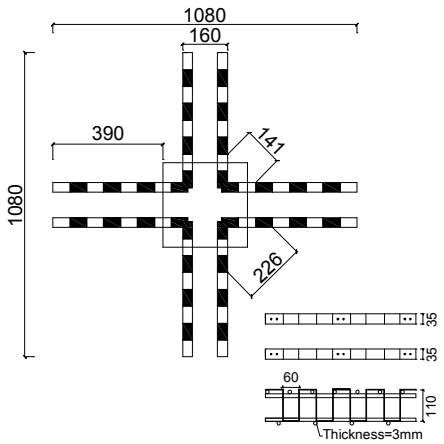

(b) Shearbands

Figure 4-10 Floor plan and elevation of stirrups and shearbands reinforcement (Units: mm)

While shear reinforcement for both punching shear and unbalanced moment experiments was planned to be the same, the size of slabs, column length, and rebar arrangement differ. Each main slab bar arrangement and sizes of specimens are described in the following subsection.

4.2.2 Unbalanced moment specimens

A slab, having 150 mm thickness and 2,800 mm for the entire span, was simply supported at points 150 mm from the ends of the slab. The cross section of the column was 300 mm × 300 mm, and the total height of each specimen was 1,900 mm. Since the specimens were part of a lateral-force resisting system, the slab reinforcement was designed to satisfy the requirements for intermediate moment frames (ACI 318-11, Section 21.3.6), whereby the reinforcement placed within the effective width shall be proportioned to resist $\gamma_f M_{slab}$, and not less than one-half of the reinforcement in the column strip shall be placed within the effective slab width. All top and bottom bars were continuous throughout the span in accordance with ACI 318-11, Section 13.3.8 and Section 21.3.6.

Table 4-1 Reinforcing bar ratios

Unbalanced moment test			
Current test program			
ρ^-_{c+3h} 0.0147	ρ^+_{c+3h} 0.0088	$\rho^-_{c.s}$ 0.0141	$\rho^+_{c.s}$ 0.0088
Kang and Wallace (2008)			
ρ^-_{c+3h} 0.0052	ρ^+_{c+3h} 0.0022	$\rho^-_{c.s}$ 0.0052	$\rho^+_{c.s}$ 0.0021
Park et al. (2010)			
ρ^-_{c+3h} 0.0095	ρ^+_{c+3h} 0.0054	$\rho^-_{c.s}$ 0.0096	$\rho^+_{c.s}$ 0.0064

Note: ρ is the ratio of A_s to bd ($=A_s/bd$); A_s is the cross-sectional area of slab reinforcement within b; b is the considered width; d is the effective depth (top layer); ρ_{c+3h} is the reinforcing ratio for the width of c_2+3h; c_2 is the column width; h is the slab thickness; $\rho_{c.s}$ is the reinforcing ratio for the column strip; – means top bars for negative bending; + means bottom bars for positive bending

A considerable amount of reinforcement was arranged in specimens for the unbalanced moment experiment, compared with previous studies, in order to generate stress-induced punching failure (**Table 4-1**).

Compared to flexural yielding followed by punching failure, stress-induced punching failure is more brittle and critical, and this experiment was designed to observe and compare the effect of shear reinforcement when a failure occurs in an extreme situation. Specific details for each specimen are summarized in **Table 4-2**.

Table 4-2 Dimensions and properties of unbalanced moment specimens

ID	L [mm]	f'_c [MPa]	Col. [mm]	d [mm]	ρ_{c+3h}		$\rho_{c.s}$	
					Top	Bottom	Top	Bottom
UN	2,500	24.1	300	105	0.0145	0.0106	0.0145	0.0113
US	2,500	24.1	300	105	0.0145	0.0106	0.0145	0.0113
UB	2,500	24.1	300	105	0.0145	0.0106	0.0145	0.0113

Note: L is the length of specimen's span; f'_c is the specified compressive strength of concrete; Col. is the size of column, d is the effective depth; ρ_{c+3h} is the reinforcing ratio for the width of c_2+3h; $\rho_{c.s}$ is the reinforcing ratio for the width of column strip

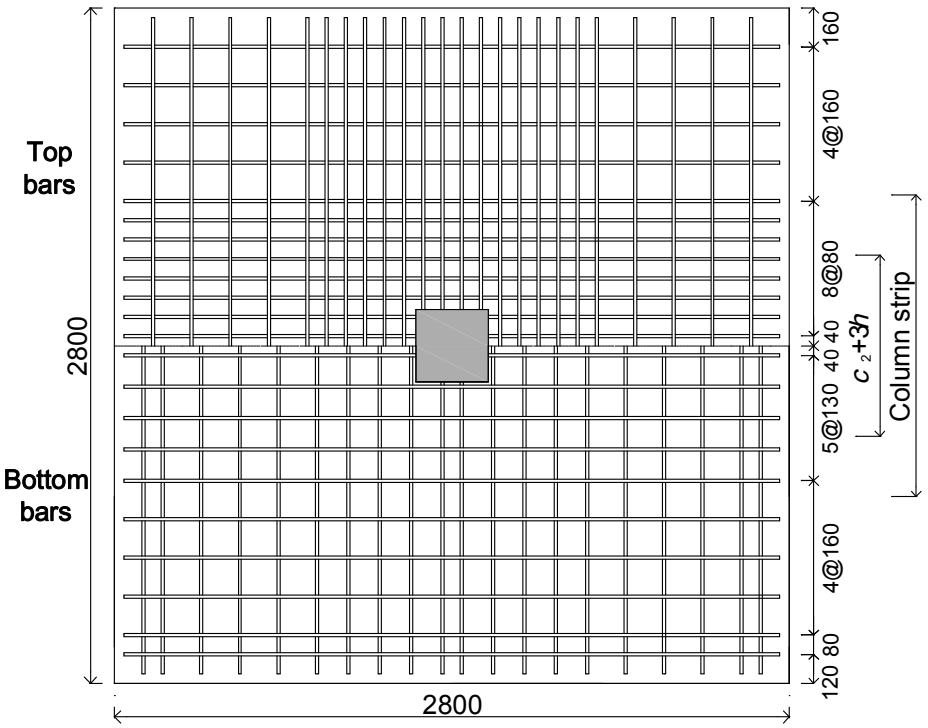

Figure 4-11 Top and bottom slab bar arrangement (Unbalanced moment test)
(Units: mm)

The D13 reinforcing bars were used for all slab main bars and the arrangement of rebars varied depending on the column strip and middle strip. For the top bar of the slab, a total of 24 D13s were installed for each transverse and longitudinal direction. Among these 24 rebars, 16 rebars were carefully placed within 1,250 mm of the column strip at intervals of 80 mm, and 8 rebars were placed at intervals of 160 mm within the middle strip. In the bottom of slab, a total of 20 rebars were distributed for each direction similar to the placement in the top of the slab. Ten reinforcing bars were installed within the column strip at intervals of 160 mm and the remaining rebars were placed at 160 mm spacing within the middle strip. Transverse and longitudinal directions had the same rebar distribution for all spans. Plans of the rebar arrangement for the top and bottom of the slab are shown in **Figure 4-11**

The aim of this study was to determine the failure of slab rather than the failure of the column, so the columns needed to remain undamaged for the entire experiment procedure. To prevent column failure occurring before slab failure, 8 D22s were used as the main reinforcement and 19 D10s were placed to tie the main reinforcement at intervals of 100 mm in the column. The elevation and details of the column are drawn in **Figure 4-12**.

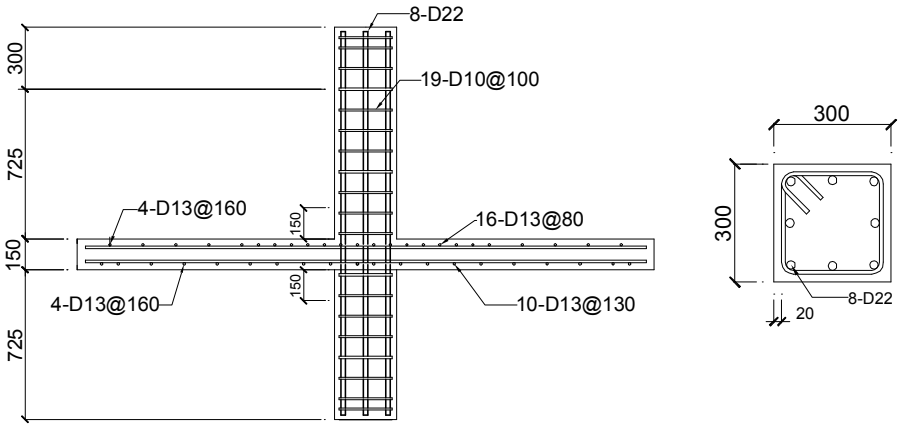

Figure 4-12 Elevation of unbalanced moment specimen and details of column (Units: mm)

4.2.3 Punching shear specimens

In the research performed by Pilakoutas and Li (2003), all specimens exhibited flexural failure mode except the unreinforced specimen, which showed brittle punching failure; this result rendered it difficult to make a performance comparison between the different types of shearbands. Thus, to avoid all shear reinforced specimens having the same strength, significantly more top and bottom reinforcing bars were arranged in this current study than in Pilakoutas and Li's study.

The flexural capacity of the slab is calculated as Broms (1990) suggested in his paper "Shear Reinforcement for Deflection Ductility of Flat Plates", but the procedure iss a bit simplified. Determining the moment transfer width in

two-way slab is a controversial matter, and four supports in longitudinal direction were assumed to generate moment in this study. Calculated flexural capacity of the slab was 573 kN, and the following presents used equations to obtain the flexural capacity of the slab.

$$V_{f\_f} = \left(4 \cdot M_{f\_f}\right) / l_0 \tag{4-1}$$

$$M^{-}_{n\_c.s} = M_{f\_f} = \left(V_{f\_f} \cdot l_0\right) / 4 \tag{4-2}$$

$$M^{-}_{n\_c.s} = n_{c.s} f_y A_s \left(d - \frac{a}{2}\right) \tag{4-3}$$

$$a = \frac{n_{c.s} A_s f_y}{0.85 f'_c b} \tag{4-4}$$

Where,

$P_{f.f}$	:	load inducing flexural failure and obtained when $M_{f.f}$ equals $M^{-}_{n\_c.s}$
$M_{f.f}$	:	moment caused by $P_{f.f}$
l_0	:	distance between column face line and support line
$M^{-}_{n\_c.s}$	:	negative moment capacity within column strip
$n_{c.s}$	:	number of top bars within column strip
f_y	:	specified yield strength of reinforcement (= 530 MPa)
A_s	:	section area of top bar (= 126.7 mm^2)
d	:	effective depth
a	:	depth of equivalent rectangular stress block
f'_c	:	specified compressive strength of concrete
$b_{c.s}$	:	width of column strip

As shown in **Table 4-3**, flexural capacity of all slabs is greater than design shear strength calculated by ACI 318-11; thus, all specimens were expected to exhibit the brittle punching shear failure by concrete fracture before yielding of slab flexural reinforcement like the seismic test.

Table 4-3 Summarized calculation of flexural capacity of slabs

	$n_{c.s}$ [EA]	a [mm]	$b_{c.s}$ [mm]	l_0 [mm]	$M_{c.s}$ (= $M_{f.f}$) [kN-m]	$V_{f.f}$ [kN]	V_{n_ACI} [kN]
PN	15	39.3	1,250	600	85.9	573	276
PS	15	39.3	1,250	600	85.9	573	418
PB	15	39.3	1,250	600	85.9	573	418

Note: V_{n_ACI} is the design shear strength calculated by ACI 318-11

As the same as the unbalanced moment experiment, D13 rebars were used as main slab reinforcement. Total of 26 rebars were arranged for each transverse and longitudinal directions for top slab reinforcement. The top slab reinforcement was evenly distributed at 86.7 mm spacing through the entire slab. Likewise, 23 rebars were installed in the bottom part of slab at intervals of 106.5 mm for each direction. Both top and bottom slab reinforcement arrangement is drawn in **Figure 4-13**.

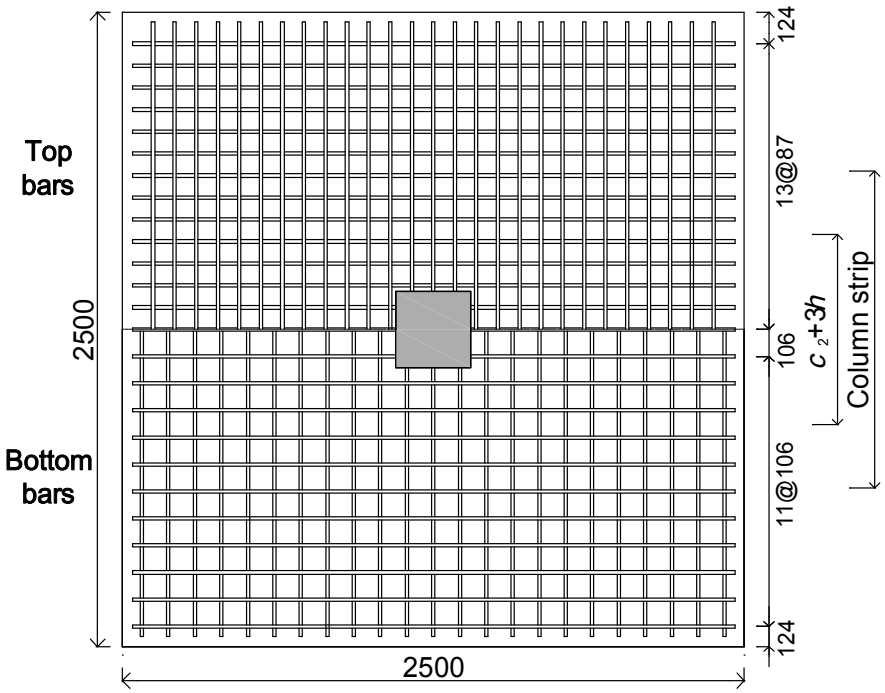

Figure 4-13 Top and bottom slab bar arrangement (Punching shear test) (Units: mm)

Similar to the preceding unbalanced moment experiment, failure at the slab would occur without column failure. The same column with an unbalanced moment experiment was constructed, except with a shorter column height (750 mm). An elevation and details of the column are shown in **Figure 4-14**

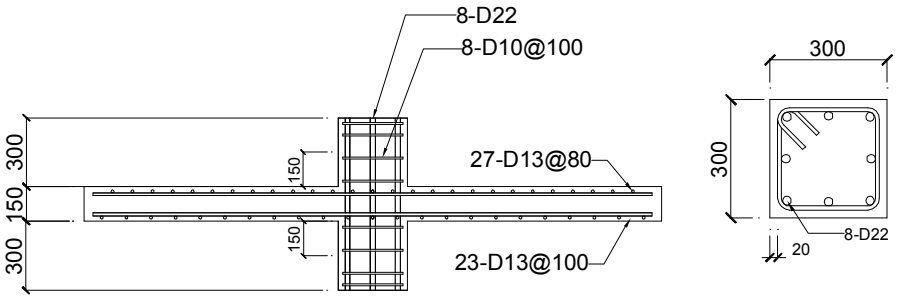

Figure 4-14 Elevation of punching shear specimen (Units: mm)

4.3 Specimen Setting

4.3.1 Unbalanced moment test

To avoid generating moment at both ends, hinge supports were set up at both ends and fixed with H-steel in a longitudinal direction. Gravity load, generated by an actuator (300 kN capacity) under the column, was applied by pushing up the column through a 25 mm steel plate. Cyclic lateral load was added on the top of the column using a 1,000 kN capacity actuator. Four shores were installed at each corner to prevent deviation of the specimen. Detail information is shown in **Figure 4-15**.

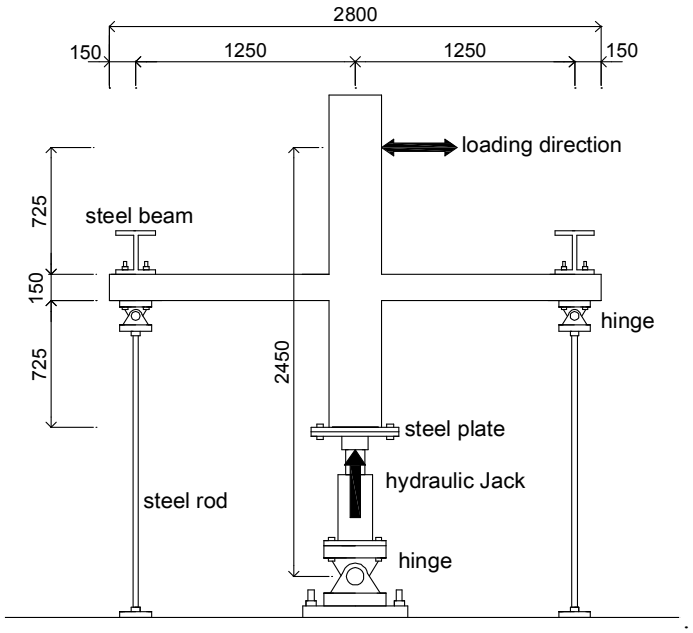

(a) Elevation plan

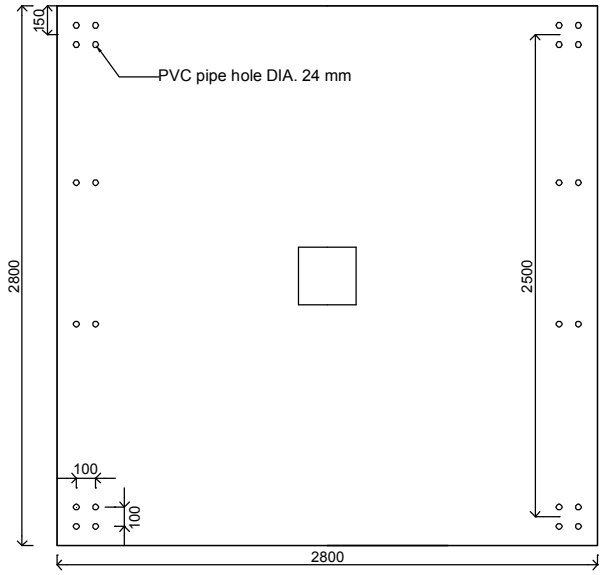

(b) Floor plan

Figure 4-15 Elevation and floor plan of unbalanced moment test (Unit: mm)

4.3.2 Punching shear

In the study by Pilakoutas and Li (2003), specimens were supported through tie rods on their several corners, and 8 hydraulic jacks of 100 kN capacity were used to apply the load symmetrically on the eight points of contraflexure on a circle of 1.7 m diameter (as previously shown in **Chapter 2**, **Figure 2-2**).

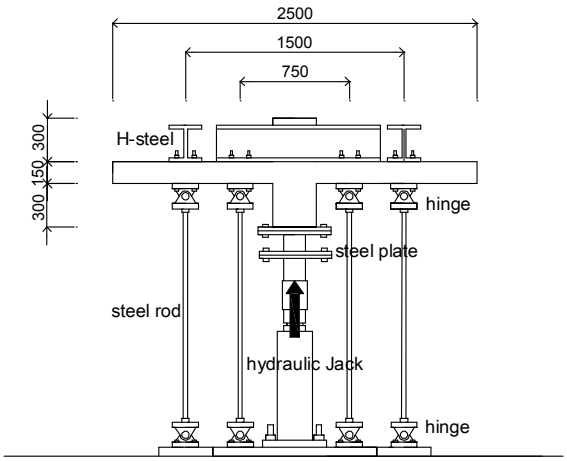

(a) Elevation plan

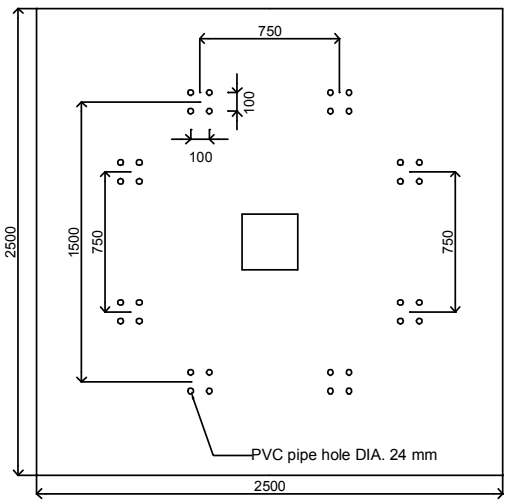

(b) Floor plan

Figure 4-16 Elevation and floor plan of punching shear test (Unit: mm)

Unlike Pilakoutas and Li's (2003) research, the punching shear test method with a concentrated load applied to the column was used in the current study. A gradually increasing gravity force was applied at the base of the column using a hydraulic jack for the duration of testing. The gravity force was controlled by displacement and transferred to a specimen after passing through a 25 mm steel plate. A total of 8 shores were set up for safety. Gravity load was applied until the specimen reached its peak load and showed a capacity deterioration of 80% of its maximum resistance. **Figure 4-16** shows the specimen setting for the punching shear experiment.

4.4 Gauge Plan

A number of steel gauges were attached in various locations in specimens to observe the shear reinforcement effect and to determine how external loads were transferred to the specimen (**Table 4-4**). The locations for gauges attached to the specimens for two experiments are drawn and the specific distance and locations are given in the following subsections.

Table 4-4 Gauge plan

ID	Slab				Column	Shear reinforcement	
	Top		Bottom				
	X-axis	Y-axis	X-axis	Y-axis		X-axis	Y-axis
UN	13 EA	10 EA	13 EA	4 EA	4 EA	NA	NA
US	13 EA	10 EA	13 EA	4 EA	4 EA	12 EA	12 EA
UB	13 EA	10 EA	13 EA	4 EA	4 EA	12 EA	12 EA
PN	13 EA	10 EA	13 EA	4 EA	4 EA	NA	NA
PS	13 EA	10 EA	13 EA	4 EA	4 EA	12 EA	12 EA
PB	13 EA	10 EA	13 EA	4 EA	4 EA	12 EA	12 EA

4.4.1 Unbalanced moment

A total of 10 steel bar strain gauges were arranged at transverse intervals of 160 mm and 240 mm within the column strip and middle strip, respectively, in the longitudinal direction, and a total of 13 steel gauges were attached to a transverse reinforcing bar at intervals of 120 mm or 240 mm for top slab flexural reinforcement.

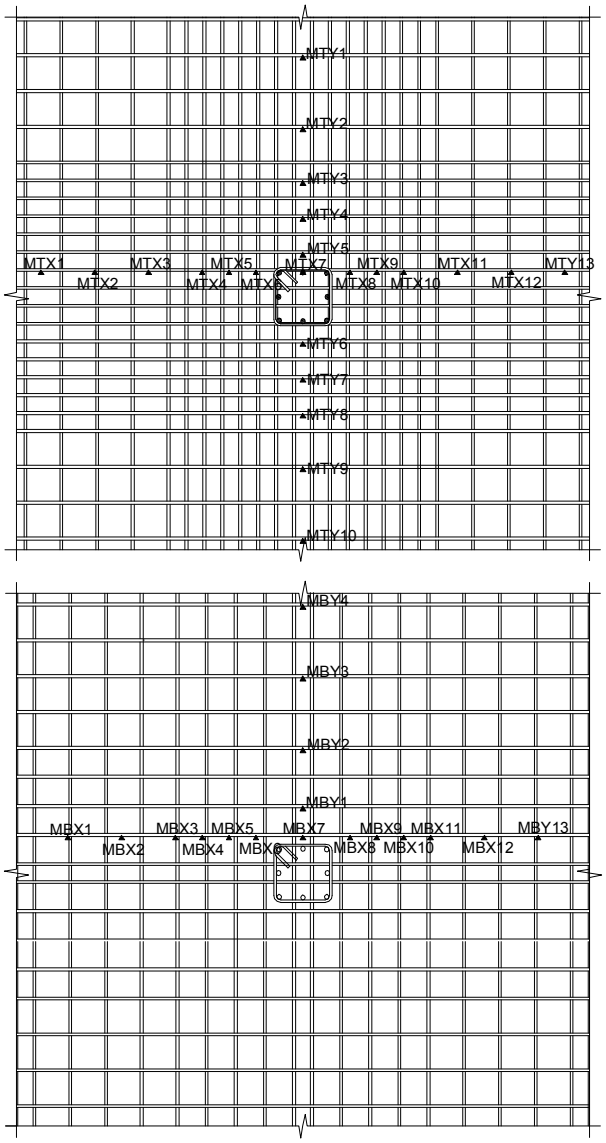

Figure 4-17 Gauge location in top and bottom slab reinforcement (Unbalanced moment test)

For bottom flexural reinforcement, 13 steel strain gauges were used in a transverse rebar at 120 mm to 240 mm spacing, and 10 steel strain gauges were attached in longitudinal rebars at points of -1080 mm, -760 mm, -520 mm, -360 mm, -200 mm, 200 mm, 360 mm, 520 mm, 760 mm and 1080 mm from the center of the column (**Figure 4-17**). As shown in **Figure 4-18**, 6 steel gauges in the longitudinal direction and 12 steel gauges in the transverse direction were set up at intervals of 60 mm in shear reinforcement. The gauge plans for the two different types of shear reinforcement were designed to be the same in order to readily compare their strains.

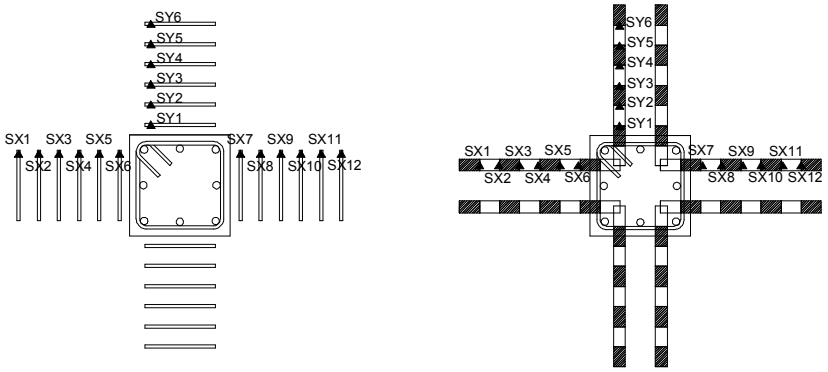

Figure 4-18 Gauge location of stirrup and shearbands

4.4.2 Punching shear

Ten steel strain gauges were installed at intervals of approximately 170 mm in the longitudinal direction and 13 steel gauges were attached to the transverse bar at intervals of 120 mm for the top slab reinforcement. For the bottom slab bar, 13 gauges were placed on the transverse bar with 120 mm or 240 mm spacing, and 4 gauges were installed at points adjacent to the north side interface between the slab and the column with 213 mm spacing (**Figure 4-19**). Strain gauge locations of both shear reinforcements (stirrup and shearbands) in punching shear experiment are the same as the one in unbalanced moment experiment as shown in **Figure 4-18**.

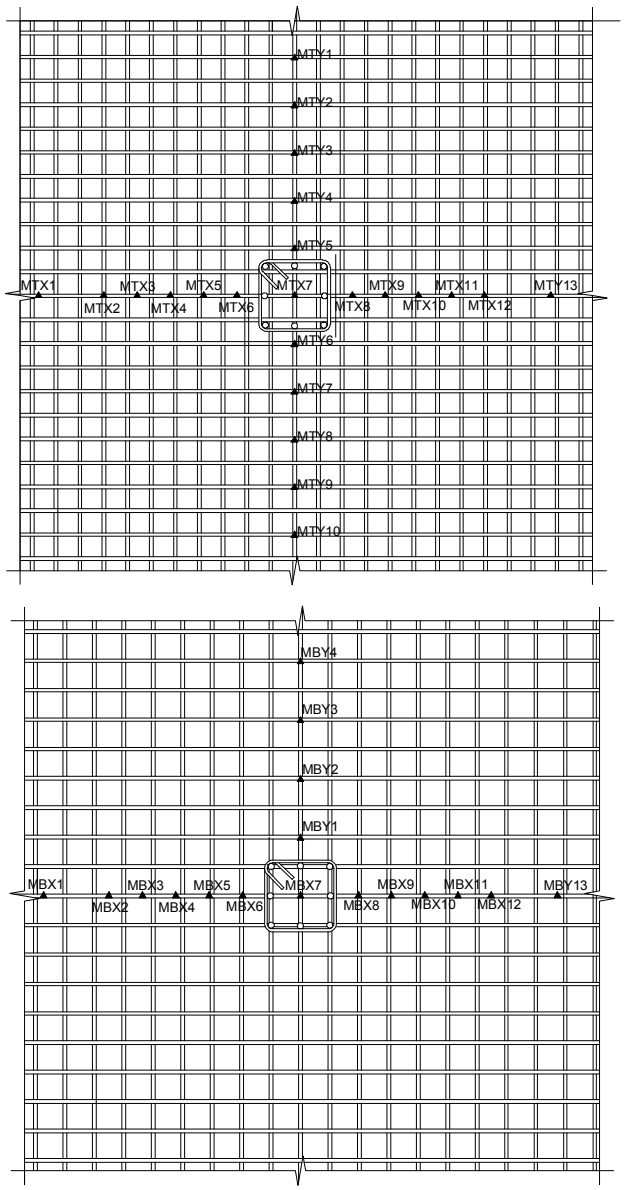

Figure 4-19 Gauge location in top and bottom slab reinforcement (Punching test)

4.5 Linear Variable Differential Transformer (LVDT) Plan

4.5.1 Unbalanced moment

A total of five linear variables differential transformers (LVDTs) were installed in order to measure the lateral deformations of specific parts of each member. LVDT1 measures the lateral displacement of the top part of a column connected to an actuator, and the displacement of the column near the slab-column connection was gauged by LVDT3 and LVDT4. LVDT2 measures the lateral drift of slab, and is shown in **Figure 4-20**.

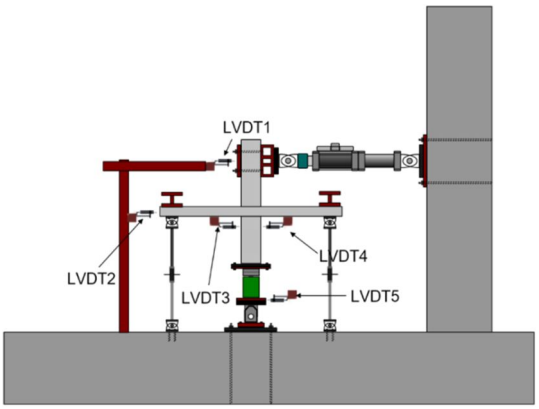

Figure 4-20 Detailed installation position of LVDTs (Unbalanced moment test)

4.5.2 Punching shear

A total of 7 LVDTs were installed to estimate the horizontal displacement in the punching shear experiment. LVDT 1 was set up over the center of the column, and LVDTs 2 and 5 were installed at location 30 mm from the column sides. Also, as shown in **Figure 4-21**, LVDTs 3, 4, 6 and 7 were installed at 120 mm intervals, which is a planned effective depth. Detail of installation position is figured in **Figure 4-21**.

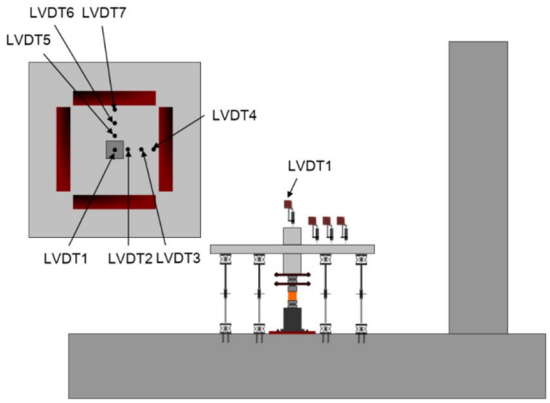

Figure 4-21 Detailed installation position of LVDTs (Punching test)

4.6 Materials

4.6.1 Concrete

In this experiment, the designed compressive concrete strength was 24 MPa. Two placements were made to construct specimens for the unbalanced moment test and specimens for the punching shear test. Since compressive concrete strength was needed in order to analyze structural performance, cylinder type concrete samples of 100 mm × 200 mm size were fabricated in accordance with KS F 2403, and cured in the same condition as that for the experimental specimens.

A compressive strength test was conducted as recommended in KS F 2405 on the same day as the experiment date. The measured mean compressive strengths of the concrete used in the unbalanced moment specimens and punching shear specimens were 24.1 MPa and 23.8 MPa, respectively, based on the concrete sample test in accordance with KS F 2405 as shown in **Figure 4-22**.

Punching shear experiment		Unbalanced moment experiment	
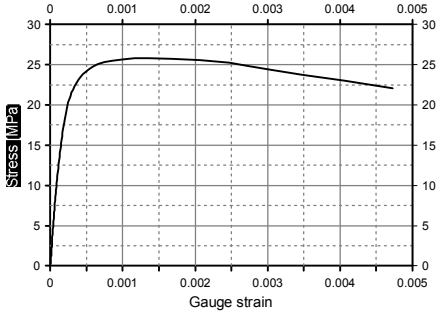		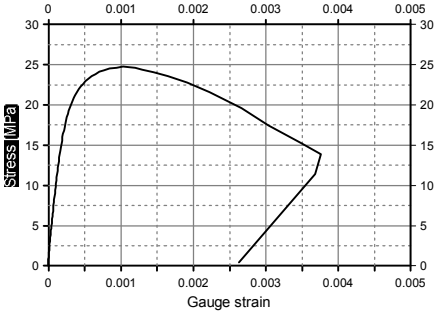	
Test Number	f'_c [MPa]	Test Number	f'_c [MPa]
1	25.8	1	21.7
2	22.5	2	25.2
3	23.0	3	24.7
Average	23.8	Average	23.9

Figure 4-22 Compressive concrete strength used in tests

4.6.2 Reinforcement

In this experiment, a total of 3 types of steel bars and one additional metallic material were used. D10 rebars and D13 rebars were used for stirrup and slab flexural bars, respectively, while D22 was used for the column main reinforcement. To analyze the property of the steel, a tensile test was conducted in accordance with KS B 0801. A band type shear reinforcement band was developed using a steel plate of 3 mm thickness to replace the stirrup shear reinforcement in this study as shown in **Figure 4-23**. A material test of the shearbands was conducted in accordance with KS B 0802.

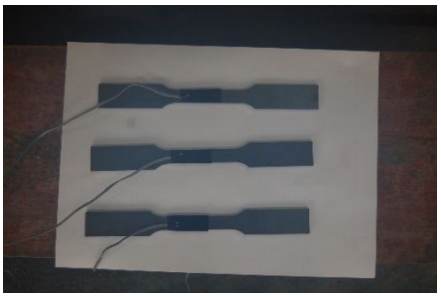

Figure 4-23 Specimen of band reinforcement for tensile test

For each type of steel reinforcement, three test specimens were made and tested. The averages of three test values were considered for yield strength and tensile strength. The tensile test results of the reinforcement used in this study are shown in **Figures 4-24**, **Figure 4-25**, **Figure 4-26**, and **4-27**.

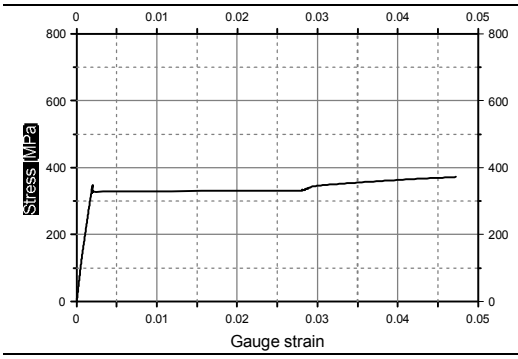

Test number	Yield strength [MPa]	Tensile strength [MPa]
1	328	416
2	329	414
3	334	422
Average	330	417

Figure 4-24 Yield and tensile strength of shearbands

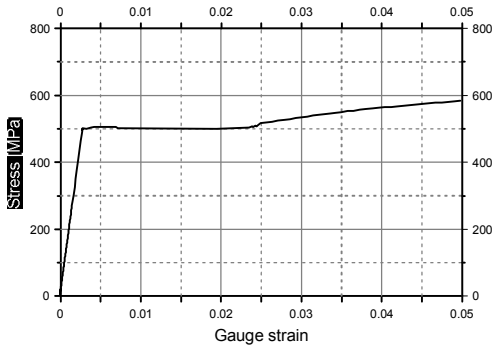

Test number	Yield strength [MPa]	Tensile strength [MPa]
1	499	630
2	490	618
3	510	643
Average	500	630

Figure 4-25 Yield and tensile strength of D10 rebar

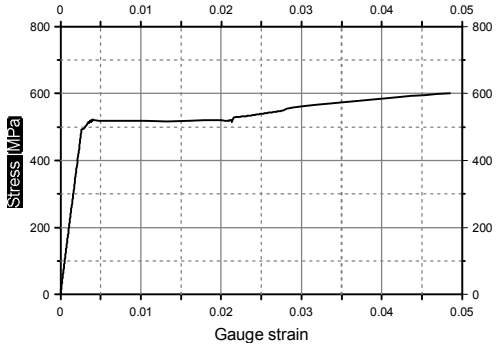

Test number	Yield strength [MPa]	Tensile strength [MPa]
1	526	596
2	518	640
3	533	654
Average	526	630

Figure 4-26 Yield and tensile strength of D13 rebar

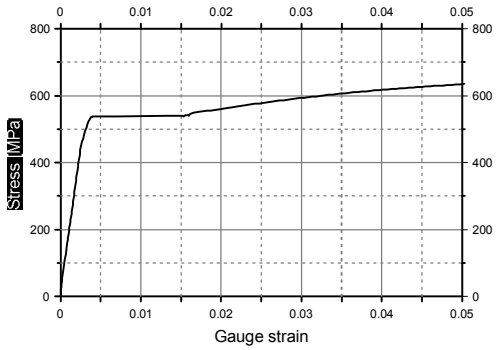

Test number	Yield strength [MPa]	Tensile strength [MPa]
1	538	636
2	546	631
3	541	638
Average	542	635

Figure 4-27 Yield and tensile strength of D22 rebar

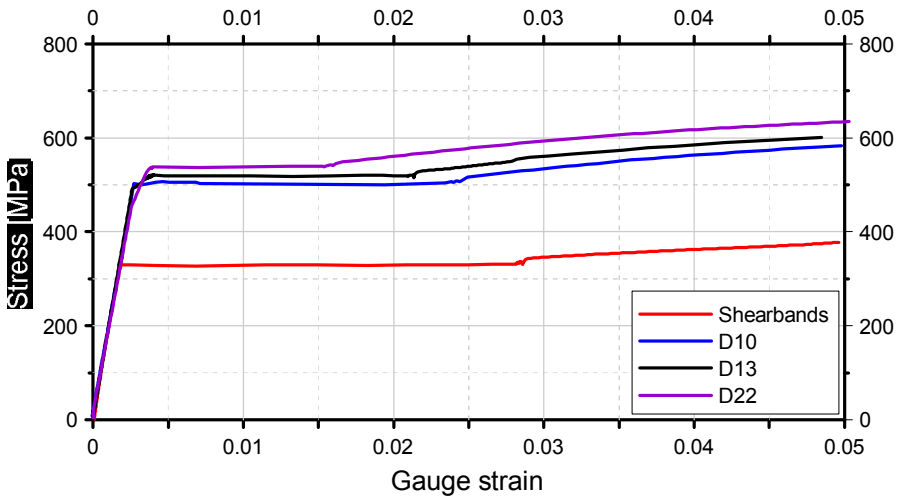

Figure 4-28 Comparison of four reinforcements

Chapter 5. Experiments and Experimental Data

The behavior of specimens was observed and cracks were marked while conducting the experiment. Experimental data was collected using the installed strain gauges and the LVDTs from the unbalanced moment test and punching shear test. Evaluations of experimental data obtained from both tests are presented in the following subsections.

Overall, the specimens showed the expected performance, and the shearbands reinforcement reached a performance almost corresponding to that of the stirrup shear reinforcement, although the stirrup shear reinforcement showed a slightly better performance overall.

5.1 Unbalanced moment experiment

5.1.1 Gravity and lateral load plan

Pan and Moehle (1989) insisted that a gravity shear ratio (V_g/V_c) should be limited less than 0.4 so as to ensure story drift capacity more than 1.5% based on their observation that for "values of V_g/V_c exceeding approximately 0.4, there is virtually no lateral displacement ductility", and ACI-ASCE Committee 352 accepted it. Therefore, the gravity load corresponding to 40% concrete shear strength was planned to be applied constantly during the test.

Three of the unbalanced moment specimens (UN, US and UB) were subjected to both gravity load and lateral load. Gravity load, which was applied constantly to the bottom of the specimens during experiment, was approximately 40% of V_c, which is the smallest value among **Eqs. (3-1)**, **(3-2)** and **(3-3)**. The measured values (V_g) when a specimen reached its maximum

strength were 140.29 kN, 143.95 kN, and 140.36 kN for the UN, US, and UB specimen, respectively. Besides gravity load, the reversed cyclic lateral loads were designed to be applied twice for each increasing 0.5% or 1.0% drift ratio from 0% to 5%; the relationship of time history vs. drift ratio is plotted in **Figure 5-1**.

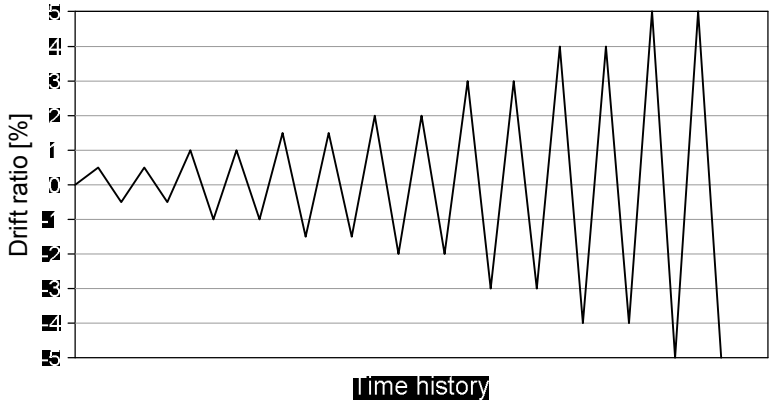

Figure 5-1 Cyclic lateral loading plan

For safety reasons, the experiment was planned to be performed when the moment capacity of a specimen decreases to below 80% of its peak moment in the first cycle of any drift, but the test was allowed to continue by engineering judgment.

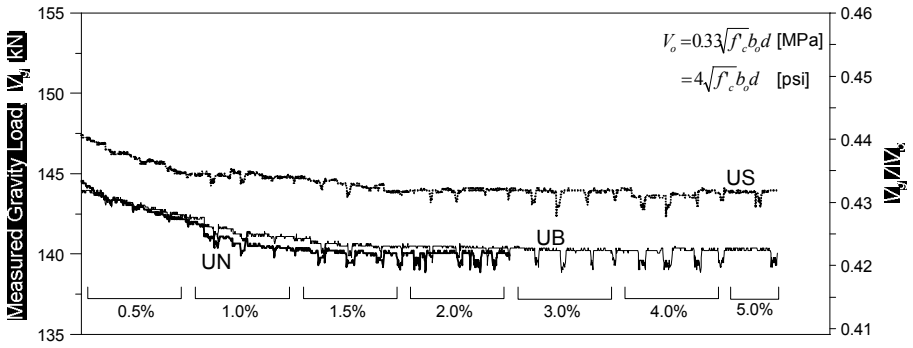

Figure 5-2 Measured gravity load during the test

According to the obtained gravity load history in **Figure 5-2**, gravity loads from 138.9 kN to 144.6 kN, 142.3 kN to 147.4 kN and 138.9 kN to 143.9 kN were consistently applied for Specimens UN, US and UB, respectively, during the test. Although applied gravity load was not constant and changed continuously depending on the drift level, differences between the largest and the smallest during each test were approximately 4.0%, 3.5% and 3.6 %, respectively, and these differences are considered to be negligible.

5.1.2 Moment vs. drift ratio

Moment-drift relations and the backbone curve obtained from three of the specimens for the unbalanced moment experiment are plotted in **Figure 5-3**. Also, to aid understanding, each drift ratio is marked with different colors (black line: 0.5%, blue line: 1.0%, red line: 1.5%, green line: 2.0%, pink line: 3.0%, orange line: 4.0%., gray line: 5.0% as indicated in the figure legends). While US reached its peak moment in the positive direction, the UN and UB specimens reached peak moment in the negative direction. The largest moment value in both directions was considered as a peak moment, and was marked in all load-story drift relation curves. The drift ratio, which was 80% of the peak moment, was interpolated in a backbone curve, and considered as a drift inducing punching failure (Kang and Wallace, 2008)

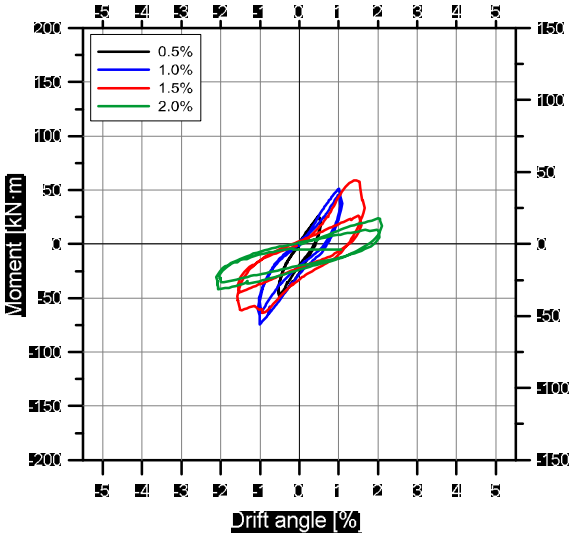

(a) Moment-story drift curve of UN specimen

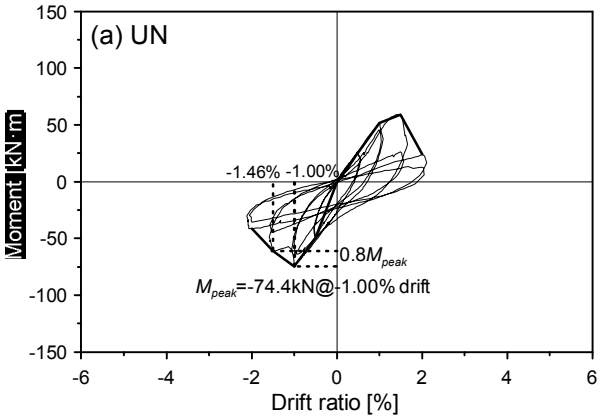

(b) Backbone curve of UN specimen

Figure 5-3 Moment - drift and backbone curves of UN specimen

As shown in **Figure 5-3(b)**, the moment strength of the UN specimen increased until it reached a peak value (maximum moment: -74.4 kN·m, maximum shear: 30.4 kN and maximum displacement: 8.01 mm) at the first cycle of 1.0% drift ratio (blue line in **Figure 5-3(a))** in the negative direction. The moment strength was maintained stably after accomplishing the maximum strength; however, it dramatically declined after the first cycle at 1.5% drift (see red line) to 35% and 60% of the peak moment for the positive

and negative directions, respectively. The experiment was continued, and brittle failure occurred while turning back from the 2nd cycle of the 2% drift (green line in **Figure 5-3(a)**) due to the concrete delamination near the column sides. The maximum shear force and moment in the positive direction were 24.1 kN and 59.1 kN·m, respectively, and those in negative direction were -30.4 kN and -74.4 kN·m. The crack conditions from the beginning to the end of the experiment at each drift ratio are shown in **Figures 5-4** and **5-5**.

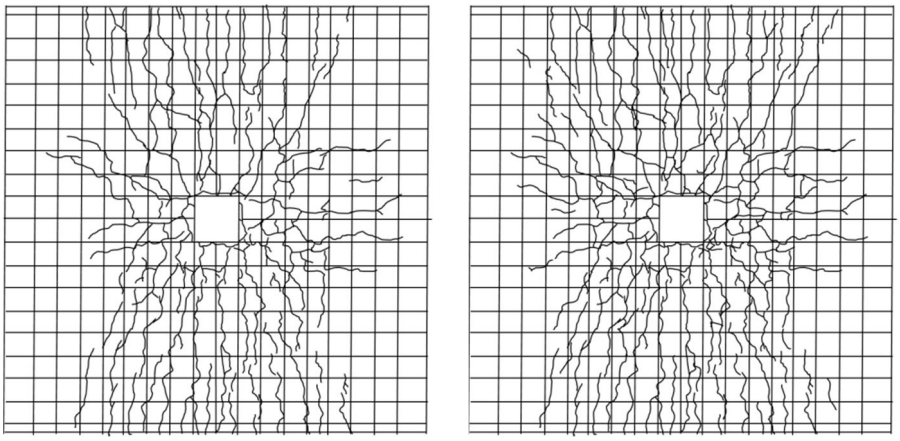

(a) Only gravity load applied (b) At 1.0% drift ratio

Figure 5-4 Crack condition of UN specimen at early phase

As shown in **Figure 5-4(a)**, a tension crack occurred in the Y-direction when only a gravity load was applied to the specimen and cracks then appeared at 1.0% drift ratio (**Figure 5-4(b)**). The crack width increased as the cracks started connecting to each other.

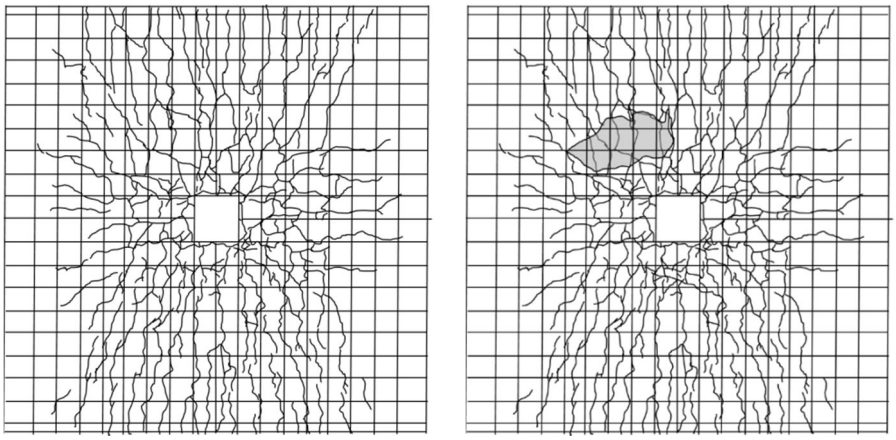

(c) At 1.5% drift ratio (d) Final condition

Figure 5-5 Crack condition of UN specimen at final phase

When the drift ratio reached 1.5%, cracks due to punching shear were found in the slab near the column. The top part of the slab was abruptly detached and drastic strength reduction appeared while loading to a negative 1.5% drift ratio. A cover spalling was widespread and the spalled concrete size was about 750 mm × 450 mm as shown in **Figure 5-5(d)**.

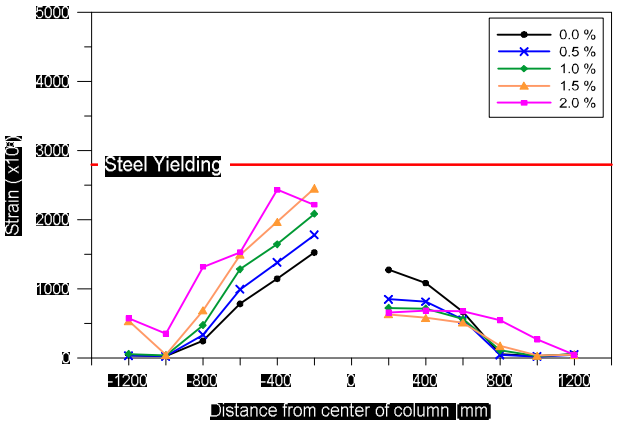

(a) Top reinforcement

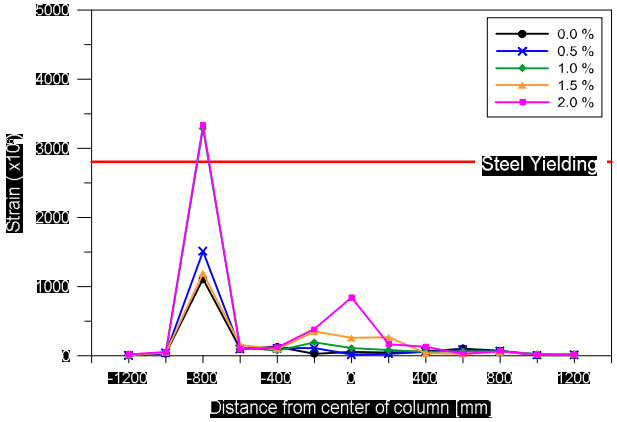

(b) Bottom reinforcement

Figure 5-6 Strain gauges attached to slab bars penetrating center of column (UN)

Figures 5-6(a) and **Figure 5-6(b)** show the strain changes of the top and bottom reinforcements penetrating the center of the column in the transverse direction according to the increasing load. As shown in **Figure 5-6(a)**, the top reinforcement already showed considerable strain before lateral load was applied (0.0% in the legend), and this indicates that tension cracks at 1.0% of drift ratio in the longitudinal direction occurred along the tension reinforcement. As the lateral load increased, the tension reinforcement stretched further but did not reach yield strain. Overall, the bottom reinforcement did not show remarkable changes, except at the -800 mm section (**Figure 5-6(b)**), which was considered to be caused by the concentrated load near the support.

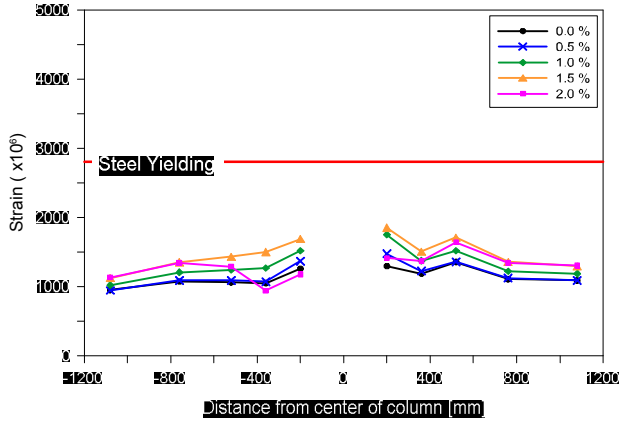

(a) Top reinforcement

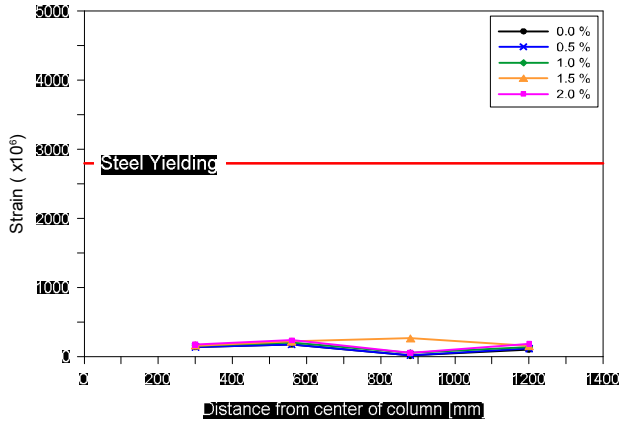

(b) Bottom reinforcement

Figure 5-7 Strains at flexural critical section of UN attached to main reinforcements away from center of column in transverse direction

Figure 5-7 shows that the top slab bars in all sections were already strained due to gravity load and then kept being stretched until 1.5% drift ratio. At 2.0% drift ratio, the strains in the top bars were reduced because the external load had been concentrated on the cracked concrete, which was a relatively weak part. The bottom slab bars showed only small changes as seen in **Figure 5-7(b)**. These figures show that the top and bottom slab bars in the UN specimen did not reach yield strength, regardless of the location of rebar. Therefore, punching failure occurred before reaching flexural failure as

expected.

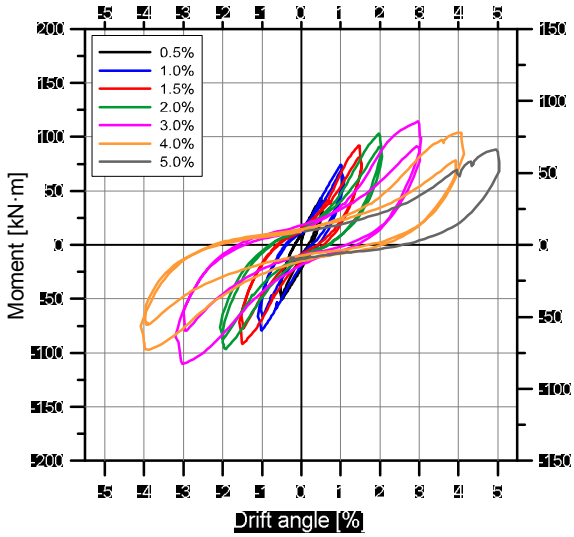

(a) Moment-story drift curve of US specimen

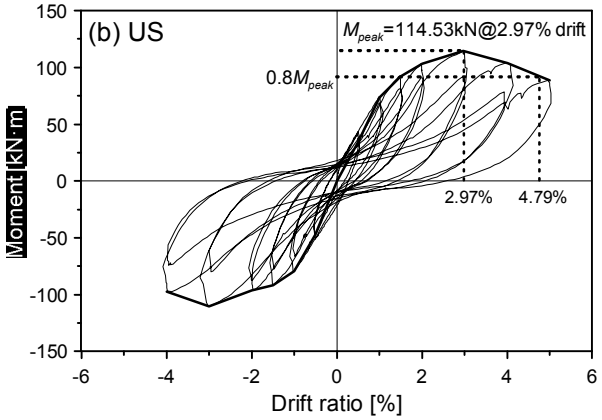

(b) Backbone curve of US specimen

Figure 5-8 Moment - drift and backbone curves of US specimen

The US specimen, strengthened with stirrup shear reinforcement, showed considerably stable behavior and substantial moment strength compared to the UN specimen. The moment strength of the specimen increased steadily until the specimen accomplished its maximum value (applied load: 46.7 kN, moment: 114.5 kN·m and displacement: 23.8 mm) at the 1st cycle of 3% drift

ratio. After that, the strength deteriorated gradually while passing through the 2nd cycle of the 3% drift ratio and two cycles of 4% drift ratio. Eighty percent of the peak moment, which was defined as a moment causing punching failure was interpolated between drift ratios of 4% and 5% in the backbone curve (**Figure 5-8**). The experiment was performed after the first cycle of 5% drift ratio in the positive direction, since the moment capacity was 77% of peak moment (under 80%).

The crack pattern of the US specimen at the initial stages (only an axial load of about 140 kN was applied) was similar to that of the UN specimen (**Figure 5-9(a)**). Tensile cracks occurred along the top slab reinforcements, but the number and size of cracks were slightly less than those of the UN specimen due to shear reinforcement effect. While increasing lateral load, the size of the existing cracks increased, and the shear cracks then started appearing at 1.0% drift ratio.

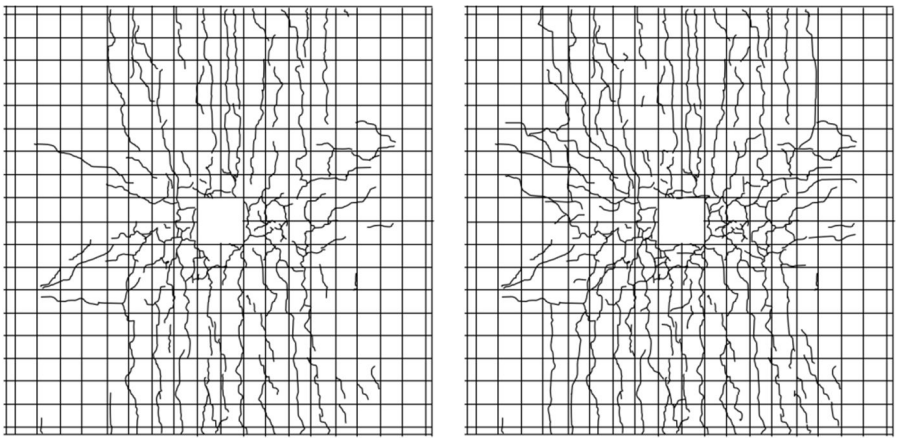

(a) Only gravity load applied (b) At 1.0% drift ratio

Figure 5-9 Crack condition of US specimen at early phase

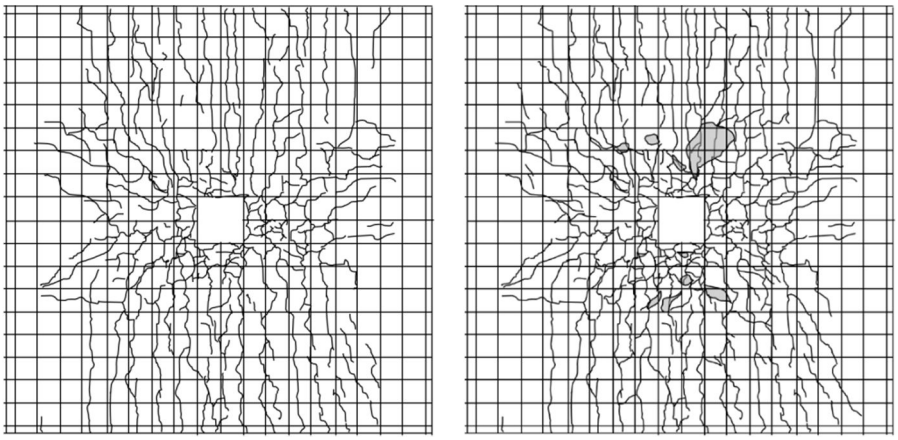

(c) At 3.0% drift ratio (d) Final crack condition

Figure 5-10 Crack condition of US specimen at final phase

As soon as the maximum strength of US specimen was reached at 3.0% drift ratio, the top part of the concrete slab started flaking near the critical section. Shear cracks became intensified and the specimen's strength was reduced by 85% of its maximum strength while reaching towards 4.0% drift ratio. At the end of the test, it was found that concrete damage was widely distributed and the maximum size of spalled concrete piece (approximately 450 mm × 300 mm) was smaller than that of the PN specimen, as shown in **Figure 5-10(d)**. From this observation, it is known that the stirrup shear reinforcement enhanced the specimen's overall performance by reducing and distributing critical cracks.

The strain changes of the US specimen according to the increasing load are shown in **Figures 5-11** and **5-12**. Unlike the strain gauges in the UN specimen, those in the US specimen showed a significant increase near the column sides, and some slab bars near the column reached to their yield strain.

To be specific, the top transverse main reinforcement yielded at a point 210 mm from the center of the column after 1.5% drift ratio as shown in **Figure 5-11(a)**, and the bottom slab bar showed expansion only near the column, as

seen in **Figure 5-11(b)**.

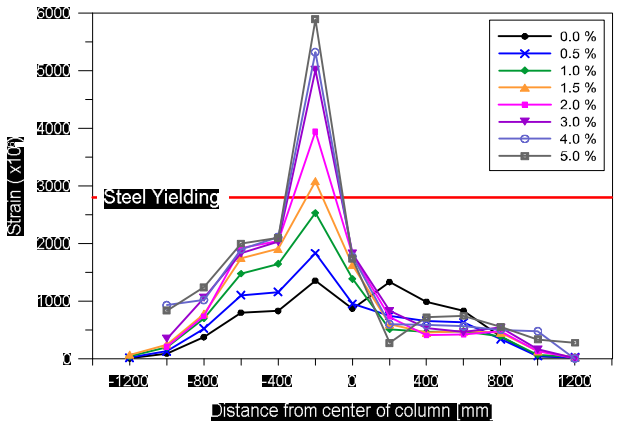

(a) Top reinforcement

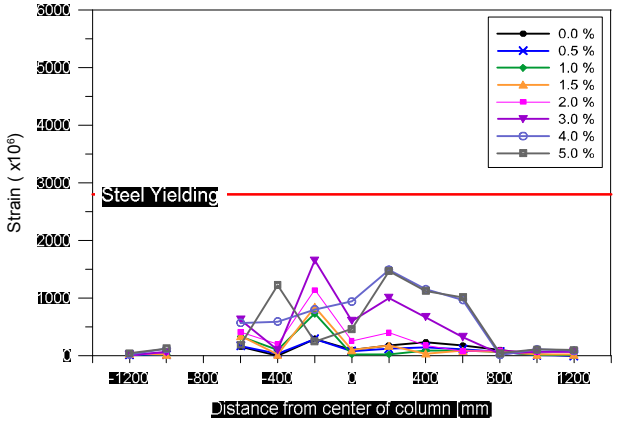

(b) Bottom reinforcement

Figure 5-11 Strain gauges attached to slab bars penetrating center of column (US)

The top transverse main reinforcement, installed 360mm from the center of the column, yielded after reaching gravity load, and continued to stretch as seen in **Figure 5-12(a)**. A drastic change was not observed in the bottom reinforcement, except in the 1200 mm section shown in **Figure 5-12(b)**. The negative moment that occurred at the section is thought to be the reason for this change.

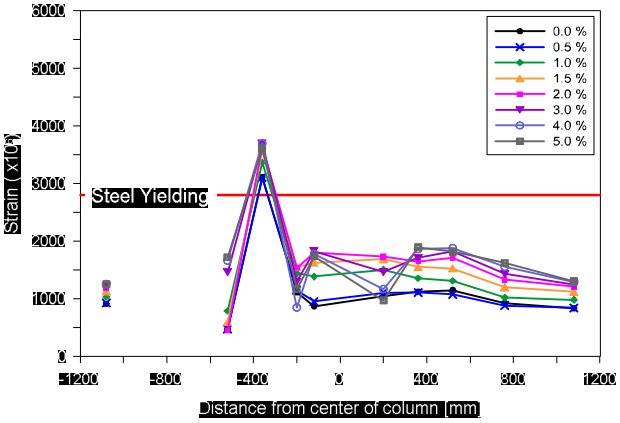

(a) Top reinforcement

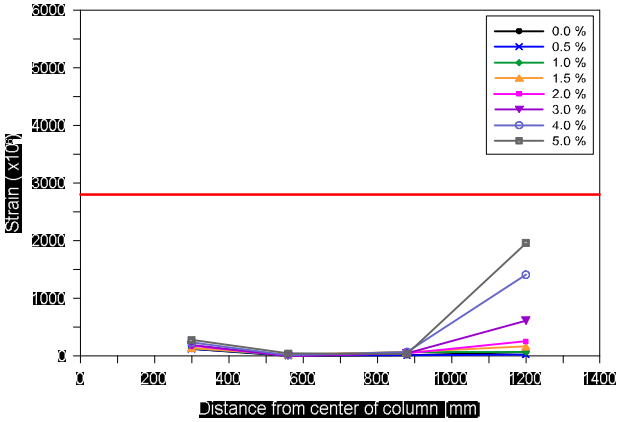

(b) Bottom reinforcement

Figure 5-12 Strains at flexural critical section of US attached to main reinforcements away from center of column in transverse direction

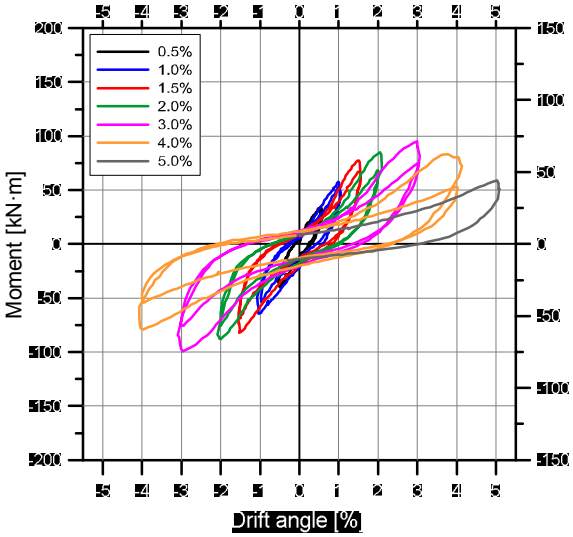

(a) Moment-story drift curve of UB specimen

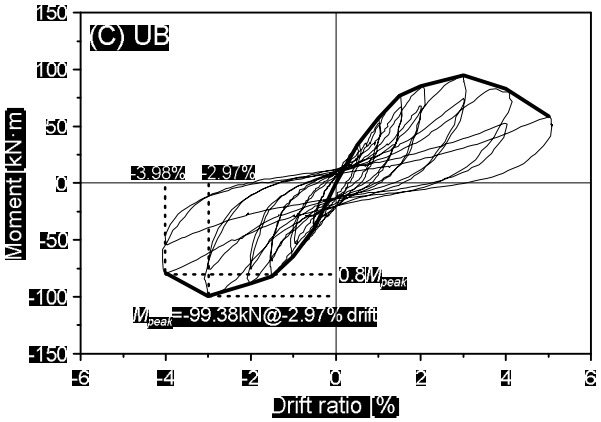

(b) Backbone curve of UB specimen

Figure 5-13 Moment - drift and backbone curves of UB specimen

The UB specimen, reinforced by the shearbands, showed similar behavior to that of the US specimen, but the maximum strength was slightly less than that of the US specimen (**Figure 5-13**). The maximum value (applied load: -40.56 kN, moment: -99.38 kN·m and displacement: -23.72 mm) was reached at the 1st cycle of 3% drift ratio in the negative direction, and the strength gradually reduced. The moment capacity decreased to 80% of the peak moment at 3.98% drift ratio, and this was considered as a drift inducing punching failure. The

experiment was stopped when the moment capacity in the first cycle of 5% was under 80% of the UB specimen's peak moment.

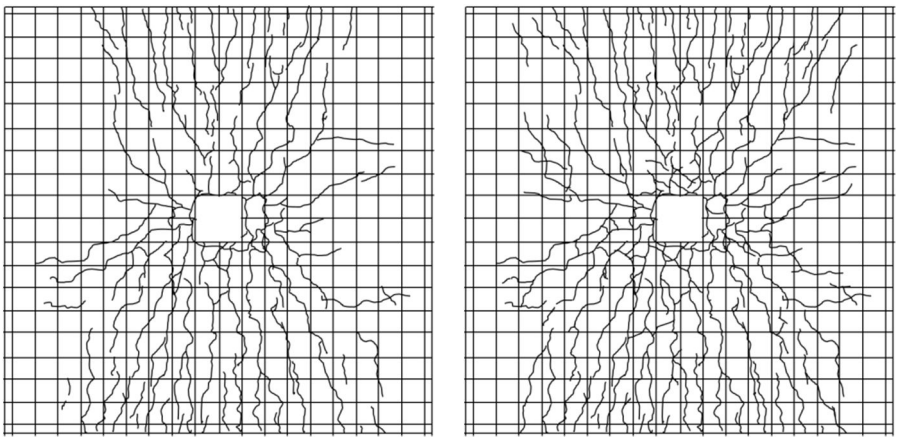

(a) Only gravity load applied (b) At 1.0% drift ratio

Figure 5-14 Crack condition of UB specimen at early phase

When only the gravity load (140.3 kN) was applied to the UB specimen, a similar crack pattern to that of the UN and US specimens was made (**Figure 5-14**). Many tension cracks appeared along with the top longitudinal main reinforcement, and a number of cracks were larger than that of the US specimen. It is presumed that this was due to concrete cover depth that was greater than that of the planned cover depth. While fabricating specimen UB, the specimen was stepped by workers, and the arranged rebars were inadvertently pressured depressed. This increased concrete cover depth (or decreased effective depth) can then generate more cracks on the concrete surface. After the lateral load was applied, the size of the cracks became increased and shear cracks were generated especially near the column-slab connection (**Figure 5-14(b)**).

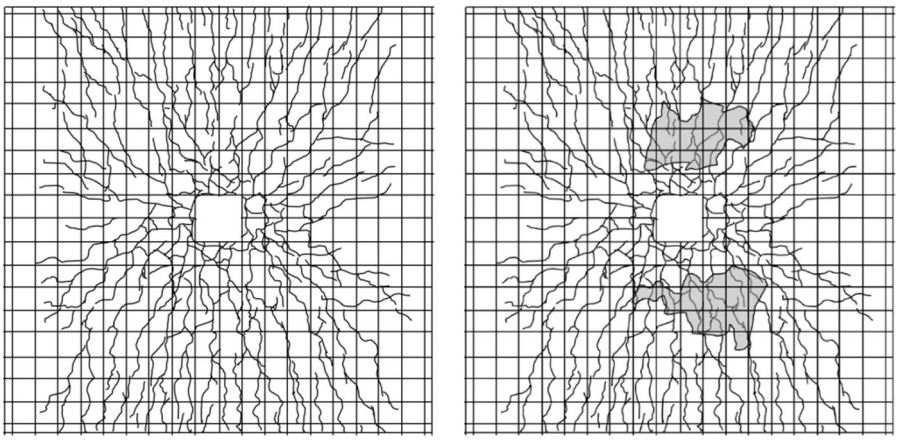

(c) At 3.0% drift ratio (d) Final crack condition

Figure 5-15 Crack condition of UB specimen at final phase

At 3.0% drift ratio, the UB specimen reached at the maximum strength, and an expansion of the shear cracks and flakes on the concrete surface was found as the drift ratio further increased (**Figure 5-15**). The moment strength was degraded to 85% of its maximum strength at 4.0% drift ratio due to aggravation of concrete disintegration. The maximum spalled concrete size was 900 mm × 600 mm and the damage range was wider than that of the US specimen. From this observation, the shearbands is presumed to have distributed the external load more effectively than the stirrup shear reinforcement.

Figure 5-16(a) and **Figure 5-17**(a) show that while the stresses were concentrated on the reinforcement adjacent to the column in the US specimen, in the UB specimen, the stresses were less concentrated on a critical section but were distributed in a wider section. It is presumed that the bottom slab reinforcement in the UB specimen contributed more effectively to resist lateral load since the bottom slab bars in the UB specimen showed considerable strain changes unlike those in the US specimen (**Figure 5-11**(b)).

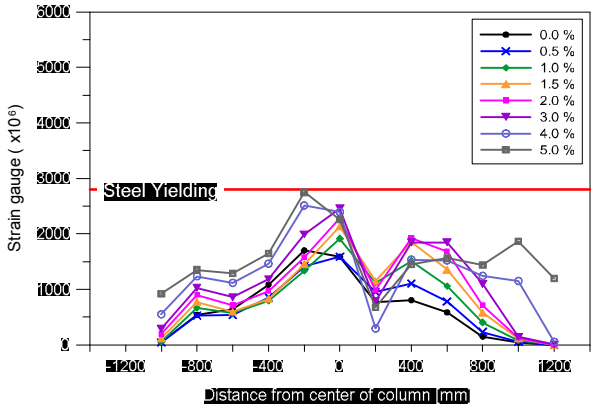

(a) Top reinforcement

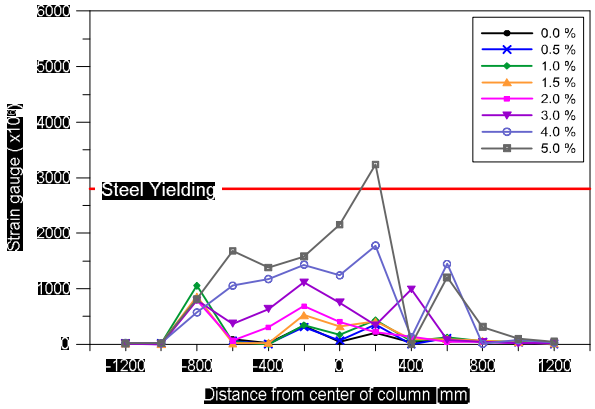

(b) Bottom reinforcement

Figure 5-16 Strain gauges attached to slab bars penetrating center of column (UB)

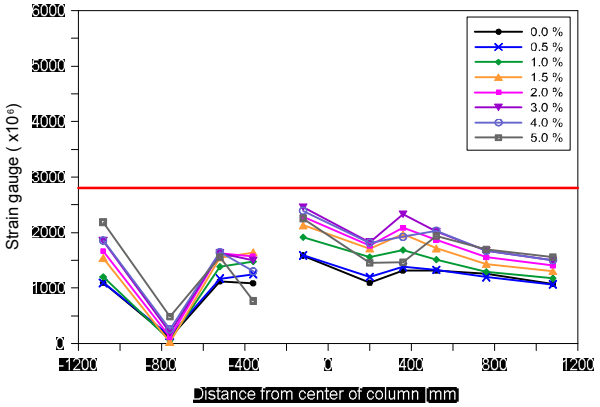

(a) Top reinforcement

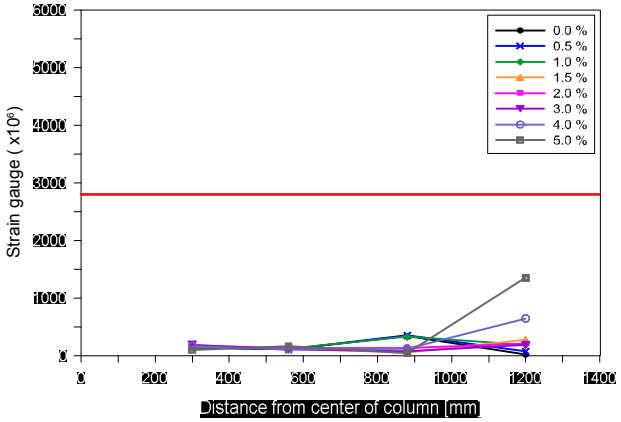

(b) Bottom reinforcement

Figure 5-17 Strains at flexural critical section of UB attached to main reinforcements away from center of column in transverse direction

5.1.3 Comparison of lateral displacement capacity

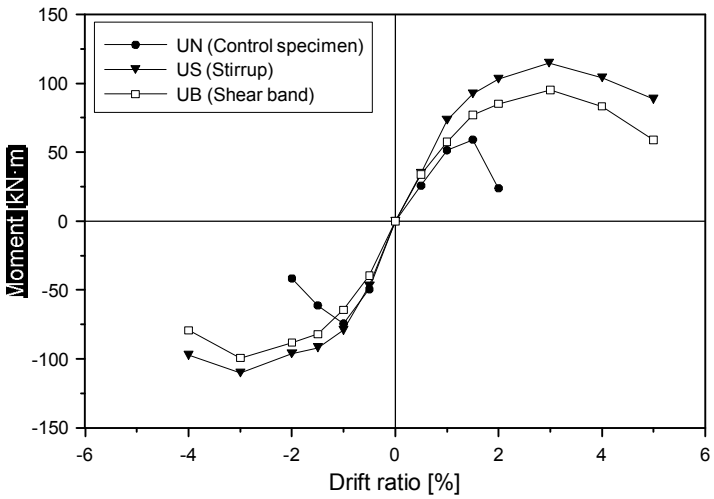

Figure 5-18 Backbone curves of three specimens

As shown in **Figure 5-18**, shear-reinforced specimens (US and UB) showed substantial improvement regarding load-carrying capacity and deformation capacity as well. For more specific comparison, the experimental results such as maximum load and deformation in each specimen are tabulated in **Table**

5-1.

Table 5-1 Maximum values on negative direction

ID	Values at maximum load							
	Drift ratio (%)		Load (kN)		Moment (kN·m)		Displacement (mm)	
	(+)	(−)	(+)	(−)	(+)	(−)	(+)	(−)
UN	1.5	1.0	24.1	30.4	59.1	74.4	11.6	8.0
US	3.0	3.0	46.7	45.0	114.5	110.2	23.8	24.2
UB	3.0	3.0	38.8	40.6	95.1	99.4	24.0	23.7

The test results and comparisons of the control specimen (UN) and shear-reinforced specimens (US and UB) are summarized in **Table 5-2**. The table also includes the previous seismic test result of slab-column connections strengthened with the shearband by Kang and Wallace (2008) and Park et al. (2012).

Table 5-2 Test result and comparison

ID	V_u/V_c	Test result		Comparison of results	
		M_{peak} [1] [kN-m]	δ_{exp} [2] [%]	M_{exp}/M_{exp}(control) [3] (3)=(1)/ (5) or (1)/ (7) or (1)/ (8) or (1)/ (9)	$\delta_{exp}/\delta_{exp}$(control) [4] (4)=(2)/(10) or (2)/(11) or (2)/(12) or (2)/(13)
Current test					
UN	0.40	74.4[5]	1.46[10]	1.00	1.00
US	0.41	114.5	4.79	1.54	3.28
UB	0.40	99.4	3.98	1.34	2.73
Kang and Wallace (2008)					
C0	0.33	83.2[7]	1.85[11]	1.00	1.00
PS2.5	0.33	107.7	4.85	1.29	2.62
PS3.5	0.33	104.6	3.45	1.26	1.86
Park and el. (2012)					
RC-A	0.40	64.5[8]	1.5[12]	1.00	1.00
SB-A	0.40	96.7	5.1	1.49	3.10
RC-B	0.40	70.5[9]	1.6[13]	1.00	1.00
SB-B	0.40	86.8	6.5	1.23	4.06

Note: [1] Maximum value of the unbalanced moment; [2] Maximum drift ratio at $0.8M_{peak}$; [3]

Ratio of strength of shear-reinforced specimen to that of control specimen; (4) Ratio of maximum drift ratio of shear-reinforced specimen to that of control specimen

In this study, the specimen with stirrup shear reinforcement showed approximately 1.54 and 3.28 times better performance in the moment and deformation capacity, respectively, and the specimen with the shearband indicates 1.54 times greater moment strength and 2.73 times better deformation capacity, respectively, than the specimen without shear reinforcement. The improvement of moment strength in this study (34%) corresponds to that from previous studies which showed 49%, 23%, 29% and 26%; however, the improvement of deformability varied from 40% to 306% depending on test conditions.

5.1.4 Effective flexural transfer width

While ACI 318-11 defines the section of c_2+3h as a transfer width, a certain flexural transfer width is difficult because the effective transfer width can change according to many variables such as the existence of shear reinforcement and crack condition, etc. By comparing data from strain gauges attached to the top and bottom slab bars and shear reinforcement, the effect of shear reinforcement on effective flexural transfer width is evaluated in this subsection.

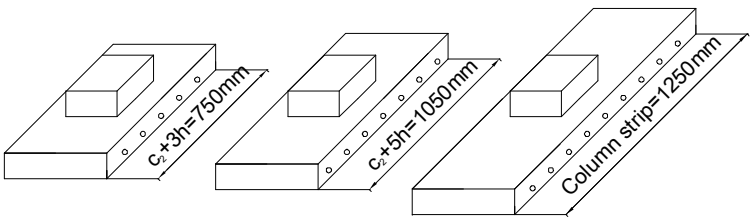

Figure 5-19 Effective transfer width

Rebar strains of each specimen for the top main reinforcement are plotted in **Figure 5-20**, and only five stages of drift ratios (0.0%, 0.5%, 1.0%, 1.5% and

2.0%) are given for better comparison.

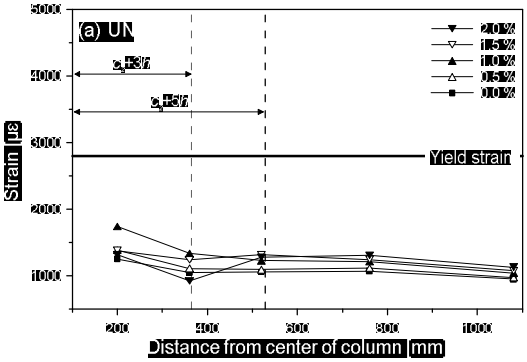

(a) Specimen without shear reinforcement (UN)

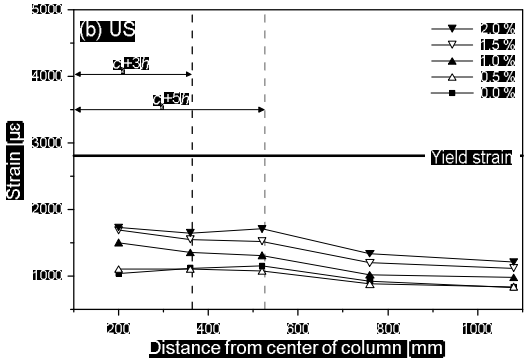

(b) Specimen with stirrup shear reinforcement (US)

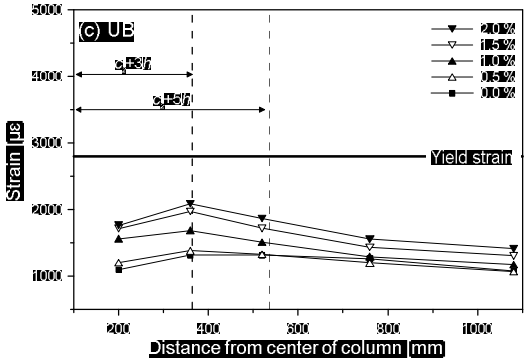

(c) Specimen with band shear reinforcement (UB)

Figure 5-20 Distribution in steel strain of top bar

At 0.0% drift ratio (only gravity load was applied), the measured strains of all specimens (which were evenly distributed along the entire span regardless of

the presence or absence of shear reinforcement) indicate that not only the top bars within c_2+3h but also all the arranged top reinforcement resisted the applied gravity load. As the drift ratio continued to increase, the rebar strains became concentrated near the column in specimen UN (without shear reinforcement), while the rebar strains in specimens US and UB (with shear reinforcement) were widely distributed over the c_2+3h length. The UN specimen's rebar strains near the column started decreasing after 1.0% drift ratio due to the concrete failure around the connection, but the rebar strains arranged beyond the c_2+3h length continued to increase instead.

In specimens US and UB, although the bars within c_2+5h showed especially large strains, the rebar strains were also observed to continuously increase across the entire length. From this observation, it was concluded that a range of effective transfer widths which transfer unbalanced moment from slabs to column can be expanded in the case where shear reinforcement is correctly added, and this makes the flexural transferred moment efficiently distribute to a wider range.

5.1.5 Energy dissipation capacity

This subsection deals with the energy dissipation capacity of the interior slab-column connections in the flat plate structures having unbalanced moment. Energy dissipation capacity is one of the most important aspects in structures since it determines a structure's integrity and ductility. The energy dissipation capacity of each specimen was calculated using the enclosed area of the load-deformation curve seen in **Figures 5-21**, **5-22** and **5-23**. The column's lateral displacement (LVDT1 data) minus the slab's lateral displacement (LVDT2 data) was taken as a deformation, and the sum of the enclosed areas of the 1st and 2nd cycle at each drift ratio was calculated.

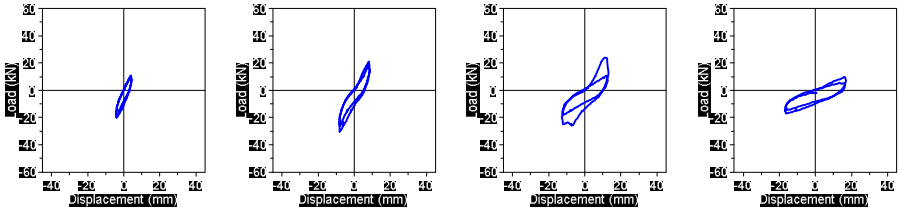

(a) 0.5% (b) 1.0% (c) 1.5% (d) 2.0%

Figure 5-21 Load-displacement curve at each drift (UN)

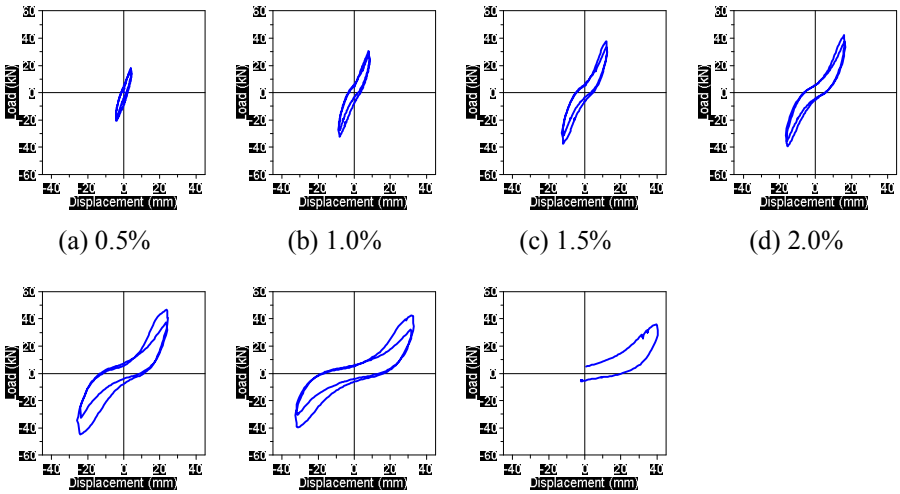

(a) 0.5% (b) 1.0% (c) 1.5% (d) 2.0%

(e) 3.0% (f) 4.0% (g) 5.0%

Figure 5-22 Load-displacement curve at each drift (US)

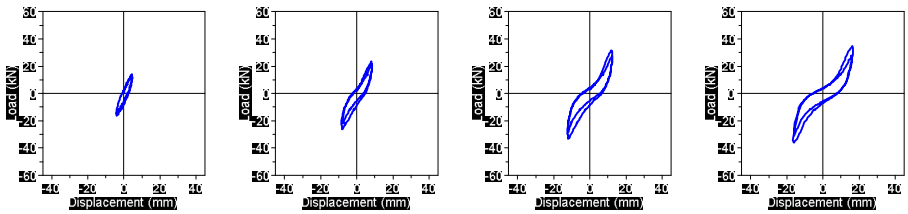

(a) 0.5% (b) 1.0% (c) 1.5% (d) 2.0%

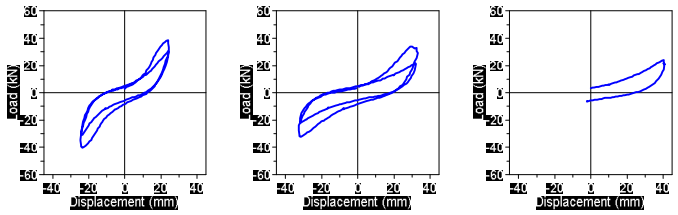

(e) 3.0% (f) 4.0% (g) 5.0%

Figure 5-23 Load-displacement curve at each drift (UB)

The calculated energy at each drift ratio and the accumulated energy are specified in **Figure 5-24**. The UN specimen showed maximum plastic deformation capacity at a drift ratio of 1.5% and the total dissipation energy was 1,738 kN·mm as presented in **Figure 5-24**(a).

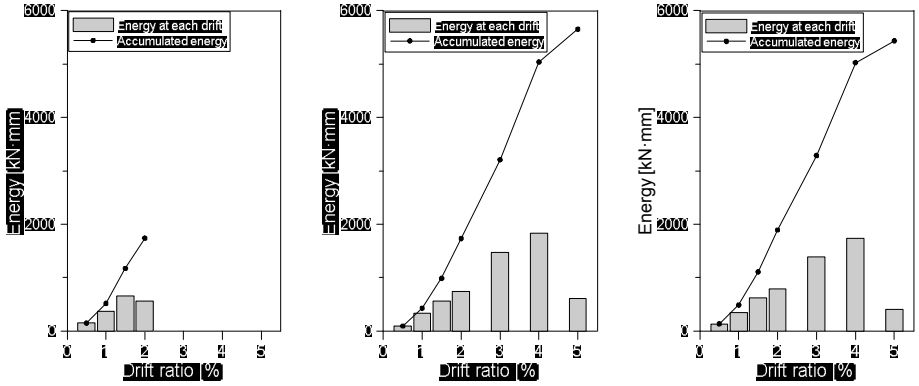

(a) UN specimen (b) US specimen (c) UB specimen

Figure 5-24 Energy at each drift and accumulated energy

The dissipation energy capacity of the US and UB specimens increased gradually, and both specimens achieved the highest energy absorbing capacity at a drift ratio of 4% (**Figures 5-24**(b) and **5-24**(c)). The total amounts of dissipation energy of the US and UB specimens were 5,649 kN·mm and 5,433 kN·mm, respectively, and these show an improved capacity of approximately 225% and 212%, compared to that of UN specimen.

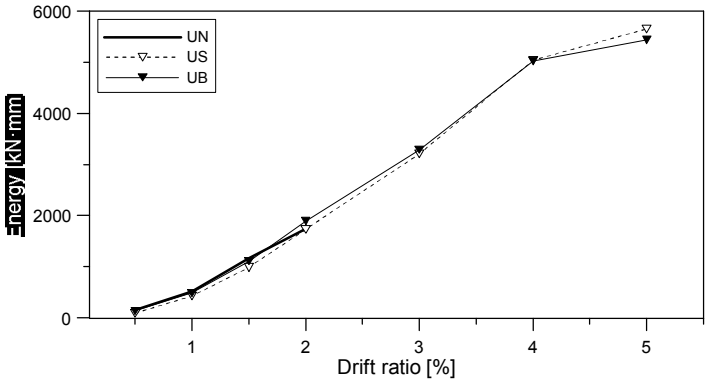

Figure 5-25 Comparison of accumulated dissipation energies

The accumulated dissipation energy for each case is compared in **Figure 5-25**. At the early stages (0.5% and 1.0%), the absorbing energy capacity showed no significant difference among specimens, regardless of the presence or absence of shear reinforcement. The absorbing energy gap between specimens with or without shear reinforcement started to be seen from the drift ratio of 1.5%, and it became increasingly greater as the drift ratio increased. The UN specimen (without shear reinforcement) stopped absorbing energy after its failure at a 2% drift ratio, but specimens US and UB (with shear reinforcement) continued to absorb energy up to a 5% drift ratio. Based on this observation, it is concluded that the correctly arranged shear reinforcement significantly improves energy dissipation capacity.

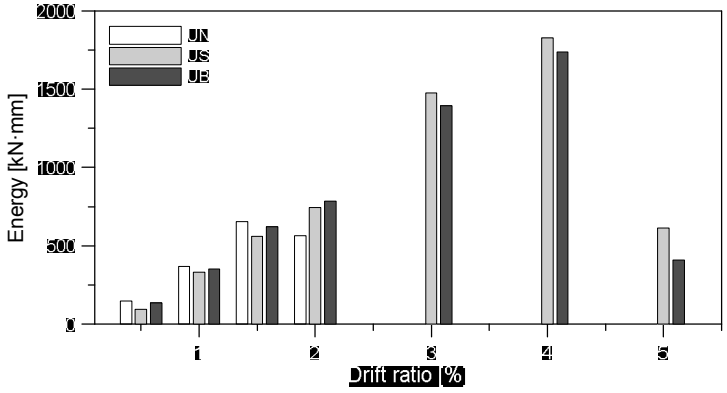

Figure 5-26 Dissipation energy comparison of all specimens

As presented in **Figure 5-26**, the specimen with stirrup shear reinforcement shows better energy dissipation capacity than the specimen with shear band reinforcement for almost all stages, and this may be due to the previously mentioned construction error that occurred when securing an effective depth in the UB specimen.

5.1.6 Strains in top bar

The strain gauge measurements on the top slab bars and shear reinforcement are shown in **Figures 5-27** and **5-28**, respectively, and these figures also validate the effectiveness of shear reinforcement for specimens US and UB. As shown in **Figure 5-27**, the strains on the top reinforcing bars continued to increase and decrease in accordance with the applied load, and the strains of several rebars dwindled after punching shear failure (for example: top bar within c_2+3h for Specimens UN and UB; top bar within c_2 for Specimen US). As intended, none of the top reinforcement within the flexural transfer width yielded, implying that punching shear failure occurred before the yielding of the top reinforcement (this is close to a stress-induced punching failure).

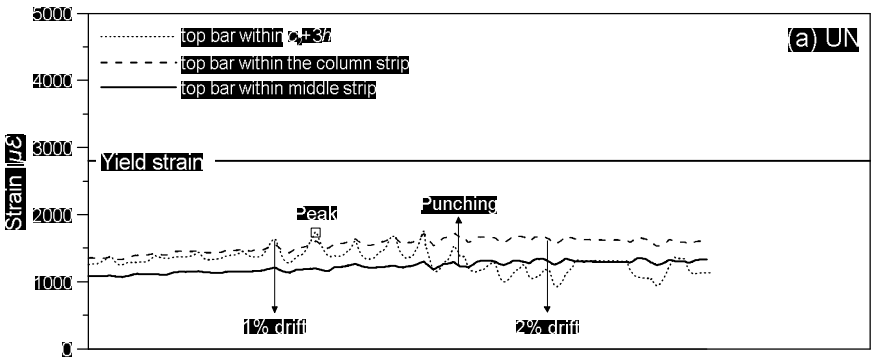

(a) UN specimen

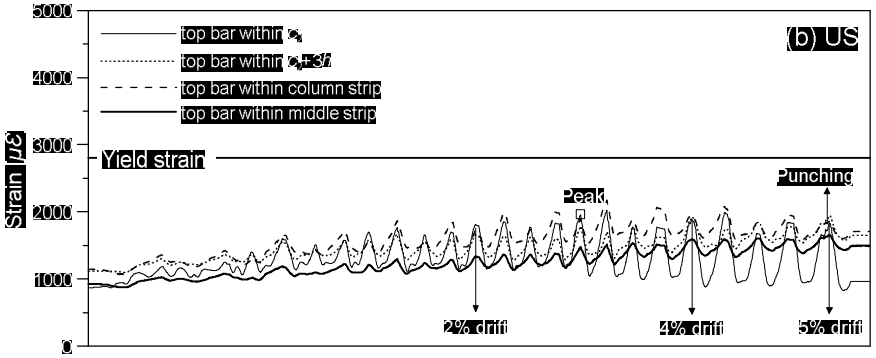

(b) US specimen

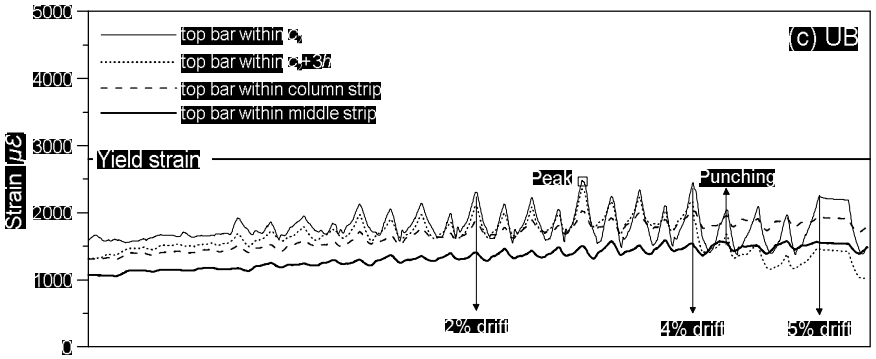

(c) UB specimen

Figure 5-27 Strains in top slab bars

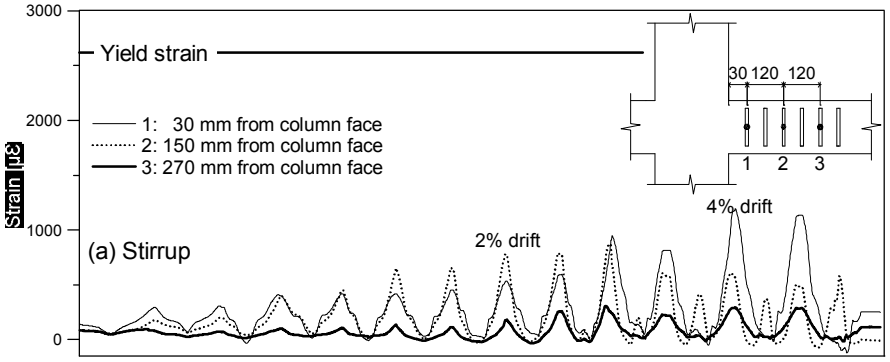

(a) Stirrup shear reinforcement

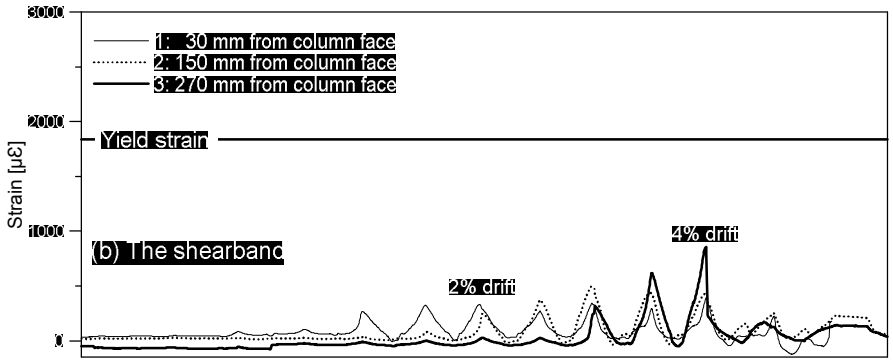

(b) Shearbands shear reinforcement

Figure 5-28 Strains in shear reinforcement on the east side of the connection

Strains in shear reinforcement reached a maximum of 1196.2 με and 856.9 με for specimens US and UB, respectively, indicating that shear reinforcement controlled cracks effectively, but did not reach the yield strains of 2620 με and 1840 με for stirrup and the shearband respectively (**Figure 5-28**).

5.2 Punching shear experiment

5.2.1 Load plan

An actuator (1,000 kN capacity) was used to provide gravity load, which was controlled by the increased displacement by 0.5 kN. As mentioned earlier in **Chapter 4.3.2**, the traditional punching shear test method was used in this study, in which a concentrated gravity load is applied to the column under the column base. Gravity load was applied until the specimen reached its peak load and showed capacity deterioration of 80% of its maximum resistance.

5.2.2 Load vs. displacement curve

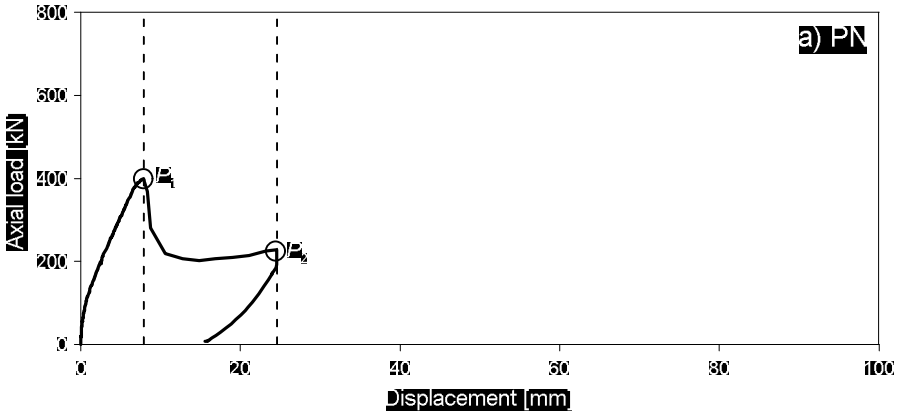

Figure 5-29 Load vs. displacement (PN specimen)

For the PN specimen (without shear reinforcement) stiffness deterioration was observed at around 90 kN due to the initial flexural crack, and an almost proportional relation between displacement and axial load was then maintained before it reached its peak load (399.0 kN). After reaching its peak load, the concrete cover was pulled out by punching shear, causing subsequent substantial strength deterioration. The PN specimen did not fail immediately after achieving peak strength and the axial load started increasing slightly again near the point of 200 kN and 10 mm. This corresponded to the research performed by Park et al. (2007) in which the load-carrying capacity of the specimen without shear reinforcement suddenly decreased at the first peak strength (marked as P_1 in **Figure 5-29**). However, the load-carrying capacity of the non-shear-reinforced specimen gradually increased again up to the second peak strength (marked as P_2). This is because the continuous slab bars placed within the slab-column connection maintained the integrity of the connection by developing cable action; however, the PN specimen finally failed to recover further strength and the experiment was stopped at around 24 mm displacement.

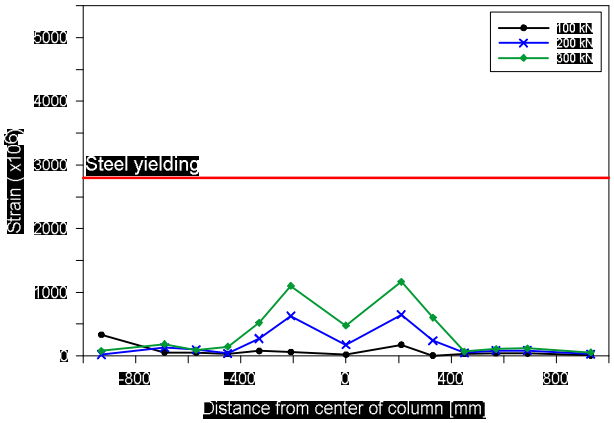

(a) Top reinforcement

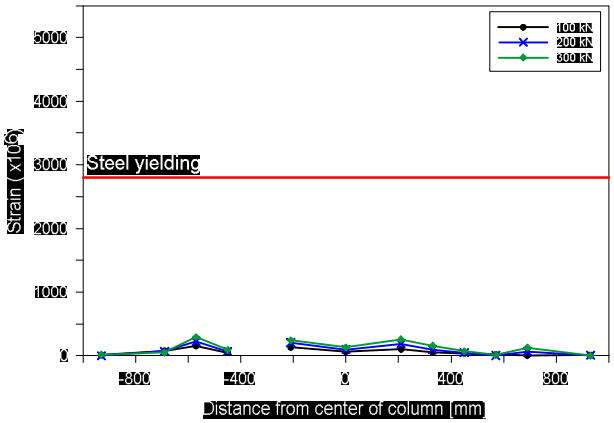

(b) Bottom reinforcement

Figure 5-30 Strains attached to one top bar and one bottom bar penetrating column center (PN)

Figures 5-30 and 5-31 show how the strain gauge values changed depending on the distance from the center of the column as loading increased. The obtained strain gauge data show that none of the main reinforcement reached yield strain, providing evidence that the drastic strength degradation occurred due to concrete fracture as conjectured from the load-displacement relation.

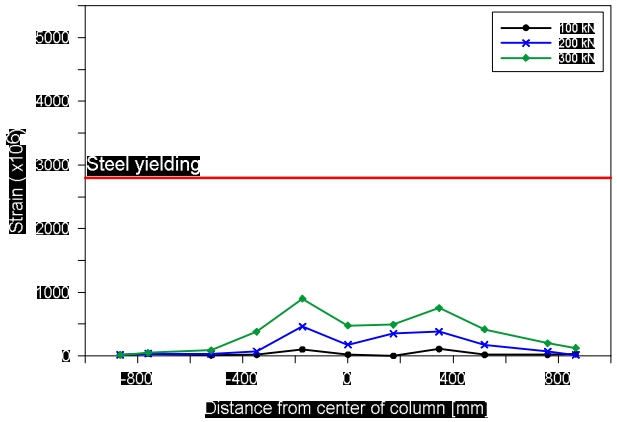

(a) Top reinforcement

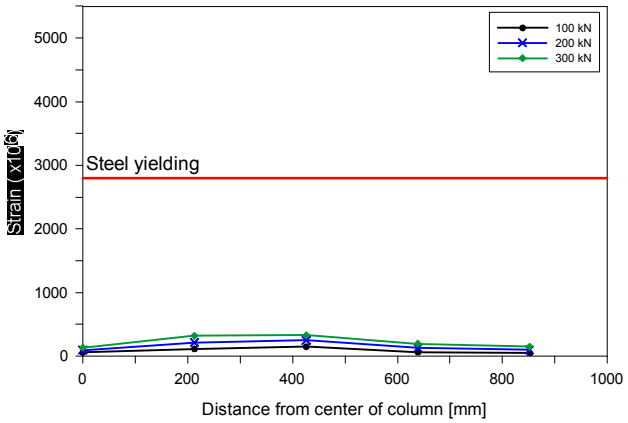

(b) Bottom reinforcement

Figure 5-31 Strains of multiple top & bottom bars along center line (PN)

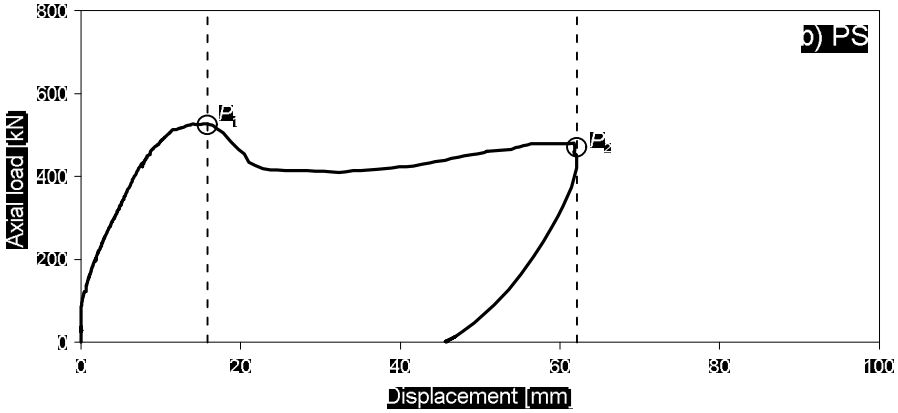

Figure 5-32 Load vs. displacement (PS specimen)

The PS specimen also showed an almost linear relation between axial load and displacement from 110 kN, in which a stiffness deduction occurred due to an initial flexural crack to the peak load point as shown in **Figure 5-32**. At the point of 16.06 mm displacement, the PS specimen reached its maximum axial load P_1 (526.5 kN) (which is significantly greater than that of the PN specimen), and started to deteriorate. The curve descended but the PS specimen was not as brittle as the PN specimen. This is because the width of the concrete area resisting external force increased and the main reinforcement effectively withstood the external load due to the confinement effect by shear reinforcement. Load carrying capacity increased again and finally reached P_2.

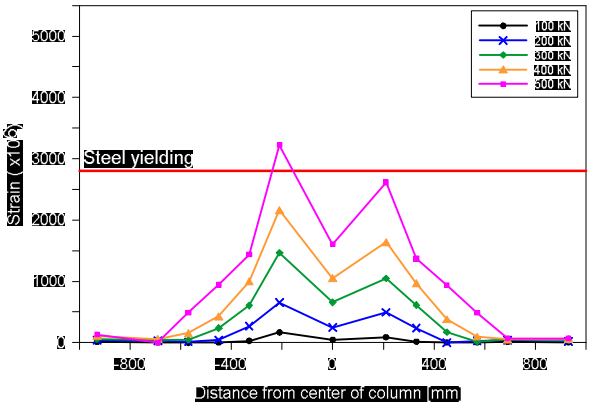

(a) Top reinforcement

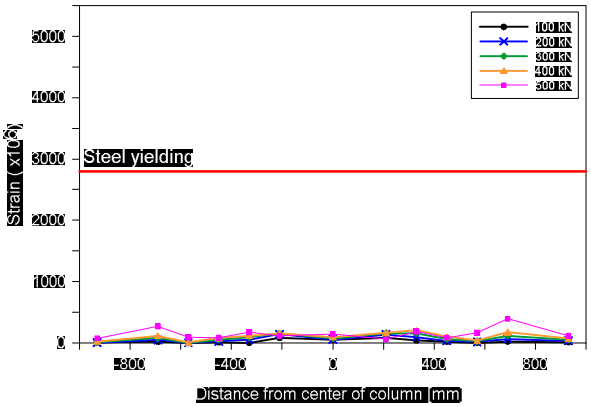

(b) Bottom reinforcement

Figure 5-33 Strains attached to one top bar and one bottom bar penetrating column center (PS)

Figure 5-33 shows the strain changes of one slab bar penetrating the column. Even though external force was concentrated on the center of the column, deformations occurred near the sides of the column rather than at the central part of the main bar. This is because the central part was completely confined to the column so that the force was concentrated on the vulnerable part which is a connection (column sides). The bottom bar did not stretch significantly compared to the top rebar, implying that the compression bar absorbed comparatively smaller charges when only gravity load was applied.

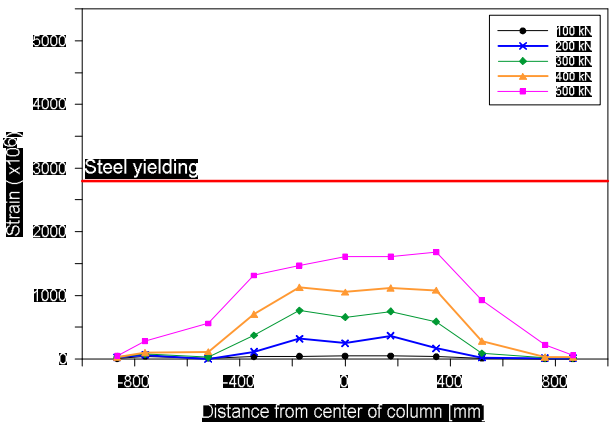

(a) Top reinforcement

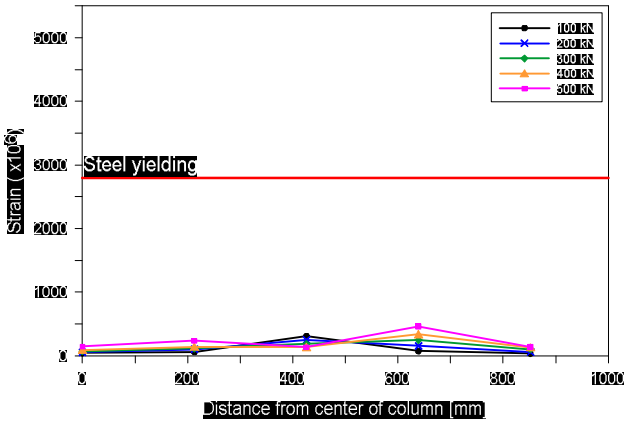

(b) Bottom reinforcement

Figure 5-34 Strains of multiple top & bottom bars along center line (PS)

Figure 5-34 shows the changes of strain gauges attached to the transverse slab bars along with the distance from the center of the column. The strain change pattern of PS was similar to that of PN, in which the strain gauges within approximately 200 mm of the column sides showed intensively increasing strain of 300 kN, although this range increased to about 370 mm as loading increased. This is because the main reinforcement in the wider range resisted the external load due to shear reinforcement installed in the PS specimen. Similar to the PN experiment, strains occurred more near the slab-column connection than at the center of the column due to constraint effect, and compressive reinforcement showed slight deformation until the end of the experiment.

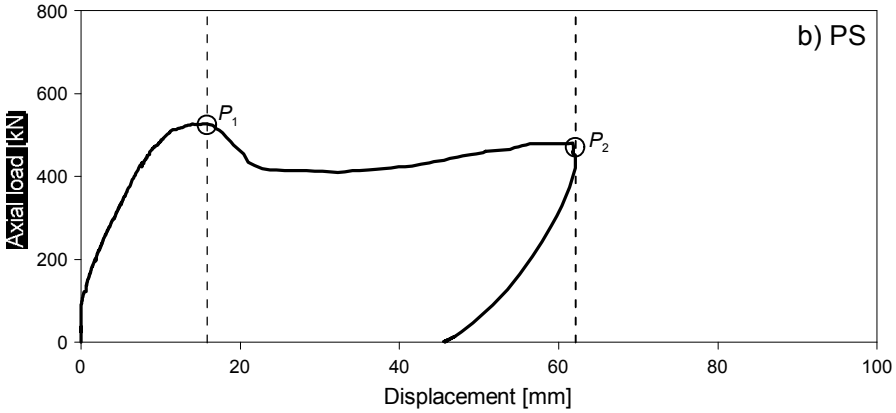

Figure 5-35 Load vs. displacement (PB specimen)

Similar to the previous two specimens, after the first decrease of stiffness at 80 kN in the PB specimen, the axial load increased as the displacement increased until it reached the peak load (**Figure 5-35**). The maximum load (503 kN) was accomplished when displacement was 18.06 mm, and strength degradation occurred. The axial load continued to reduce until 350 kN and increased at the 25 mm point. The axial load increased slowly as displacement increased, and an almost linear relation appeared again at this section. The deformation and axial load continued to increase until they reached the second peak point (P_2), and the experiment was then stopped because the concrete surface was pulled out.

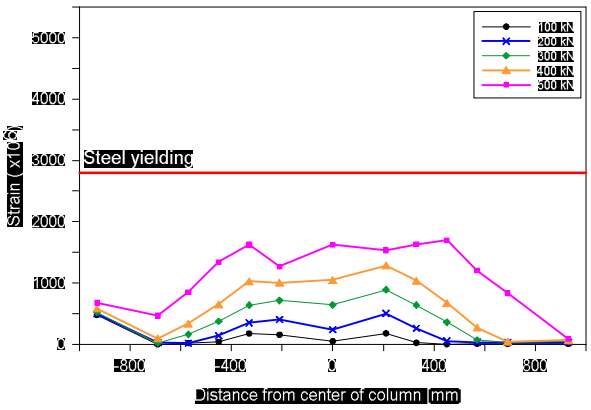

(a) Top reinforcement

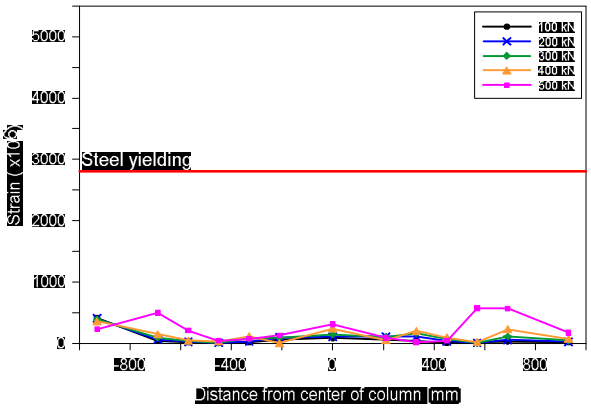

(b) Bottom reinforcement

Figure 5-36 Strains attached to one top bar and one bottom bar penetrating column center (PB)

While the PS specimen showed intensive strain deformations near the column, the strain gauges on the PB specimen were evenly stretched through almost the entire span (**Figure 5-36**). It is therefore inferred that the external load on the PB specimen was widely and evenly spread out.

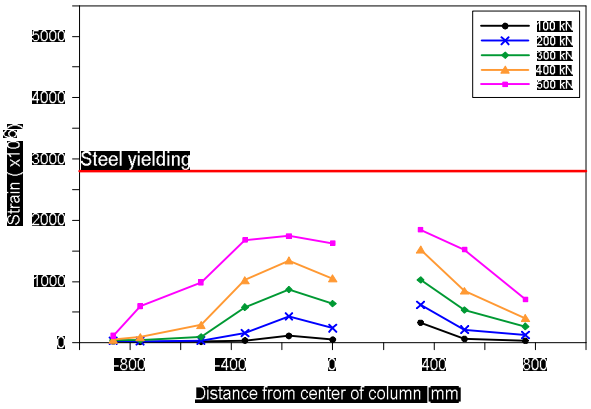

(a) Top reinforcement

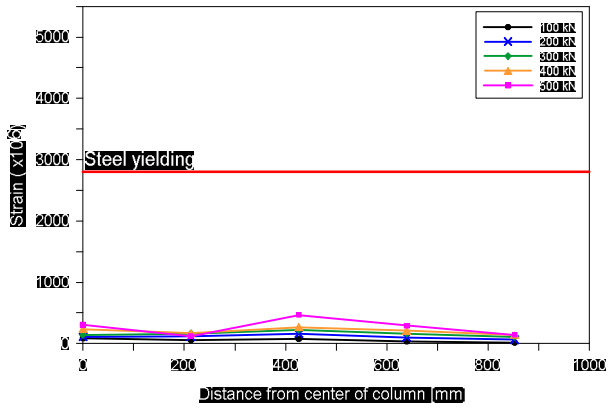

(b) Bottom reinforcement

Figure 5-37 Strains of multiple top & bottom bars along center line (PB)

Although a strain gauge installed at 170 mm from the center was damaged, the strain gauge is assumed to be greater than strain at the point of 0 mm (**Figure 5-37**). None of the main reinforcement attained yield strain, but the main reinforcement sustained considerable external load. The distribution range was wider and strains were spread out more evenly than in the previous two specimens. This implied that the area resisting against external load was widened more with the shearbands reinforcement than with the stirrup shear reinforcement. Compression reinforcement in the PB specimen did not show remarkable changes in most of the parts, but at the point of 930 mm strain, it gradually kept increasing, unlike for the PN and PS specimens. This might be due to the unexpected transfer of loading near supports (tie rod).

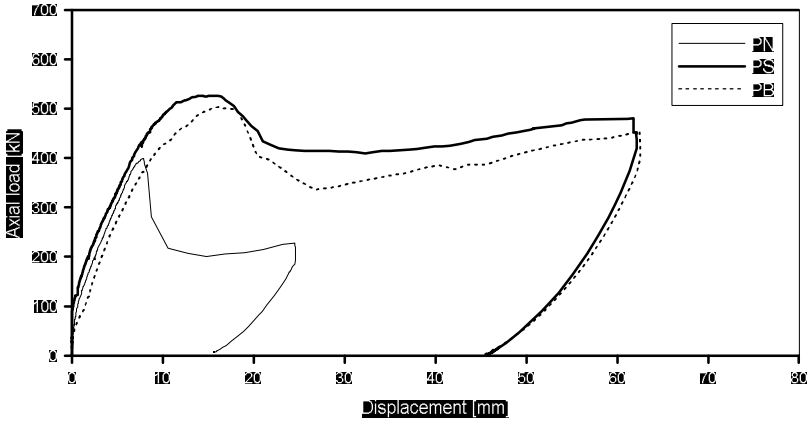

Figure 5-38 Comparison of three specimens

Displacement–axial load relations of the three specimens (non-shear-reinforced, reinforced with stirrup, and reinforced with the shearband) are shown together in **Figure 5-38** to assist understanding, and the test results and comparison are summarized in **Table 5-3**. In concurrence with the previous study by Park et al. (2007), the deformation at the first peak strength P_1 was considered as the deformation capacity of the slab without shear reinforcement for the following reasons: 1) typically non-shear-reinforced slab-column connections are severely damaged after the first peak strength; 2) the second peak strength P_2 is significantly smaller than that of P_1 (about 55%); and 3) the load-carrying capacity was not maintained after the first peak strength P_1. These reasons are clearly observed in the load-displacement relation of the PN specimen. While in shear reinforced specimens, because the load-carrying capacities maintained stable for large displacements after the first peak strength and the second peak strengths of PS and PB were 85.6% and 80% of their first peak strengths, respectively, the deformation at the second peak strength P_2 was taken as the deformation capacity of the slab with shear reinforcement. The strength ratio was obtained by dividing the maximum strengths of PS and PB by that of PN, respectively, and the deformation capacity ratio was defined as the ratio of the maximum deformation of PS and PB at the second peak strength P_2 to the maximum

deformation of PN at the first peak strength P_1.

Table 5-3 Test results and comparison (punching test)

Specimens	Test results		Comparison of results	
	Strength [kN]	Deformation [mm]	Strength ratio*	Deformation capacity ratio*
PN	399.0	7.86†	–	–
PS	526.5	62.12‡	1.32	7.90
PB	503.0	62.54‡	1.26	7.96

Note: *Test results of shear-reinforced specimens divided by those of non-shear-reinforced specimens. Deformation at P_1 of non-shear-reinforced specimens; †Deformation at P_1 of non-shear-reinforced specimens; ‡Deformation at P_2 of shear reinforced specimens

The larger punching shear strengths were observed for both shear reinforced specimens than the specimen without shear reinforcement. To be specific, specimen PS with stirrup shear reinforcement showed 1.32 times larger strength, and specimen PB with the shearband showed 1.26 times larger strength.

Remarkable improvement of deformation capacity was also achieved for both shear reinforced specimens. The deformation capacity of specimen PS with stirrup shear reinforcement improved to 7.9 times the deformation capacity without shear reinforcement (PN), and that of specimen PB improved to 7.96 times.

The obtained results demonstrate that properly installed shear reinforcement substantially improved the punching shear strength as well as the deformation capacity. Especially, the suggested shearband shear reinforcement improved the punching shear strength as much as did the stirrup shear reinforcement, and it was even more effective in improving the deformation capacity.

5.2.3 Strains in top bars

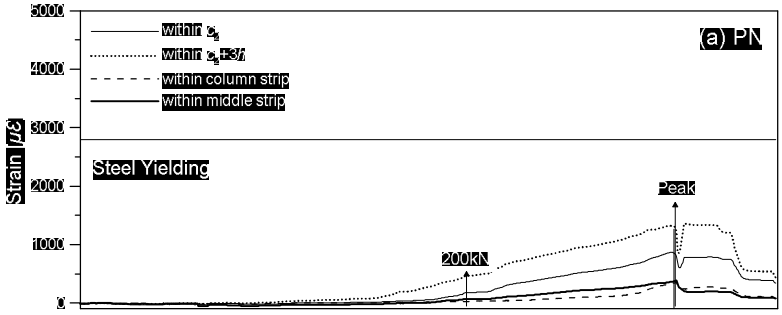

(a) PN specimen

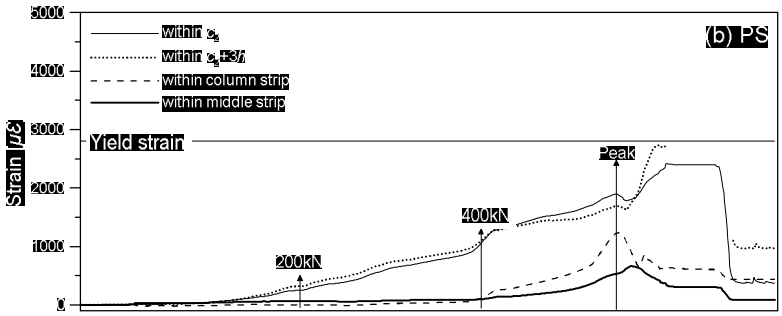

(b) PS specimen

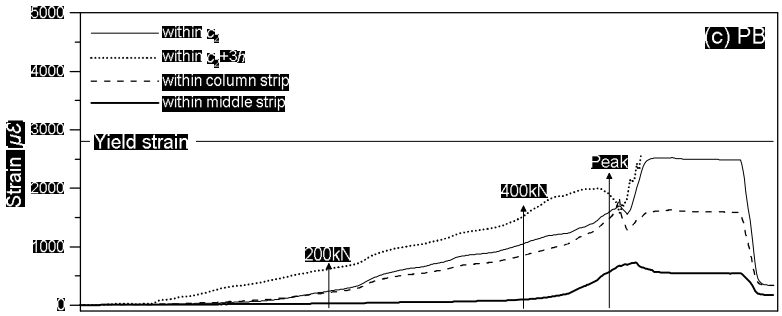

(c) PB specimen

Figure 5-39 Strains in top bars between slab and column

Figure 5-39 shows how the strain gauge values varied depending on their location. All top reinforcing bars were subject to compression at the very beginning of the test due to the self-weight of concrete, but as soon as the hydraulic jack started to push the base of the column bottom, the reinforcing

top bars began to be subject to tension. The strains of the top reinforcing bar within c_2+3h tended to show the greatest value for all specimens, which was followed by the strains of the reinforcing bar within c_2, the column strip, and the middle strip, indicating that the reinforcing bars near the column resist gravity load more effectively. Although the top reinforcing bars of specimens PS and PB within c_2+3h were close to the yield strain in tension at the peak strength (considering that strains measured by strain gauges generally underestimated actual strains due to the bond effect between the reinforcement and concrete (Park et al. (2007), those reinforcing bars might have yielded), most reinforcing bars did not yield. This indicates that although a few reinforcing bars within c_2+3h yielded, the degradation of concrete shear strength induced the punching shear failure before all reinforcing bars yielded. This corresponds to the load-displacement relationship curves of the PS and PB specimens in which the specimen's strength maintained ductile behavior after the first peak strength because the flexural reinforcing bars were within c_2+3h, but sharply deteriorated after concrete fracture at P_2.

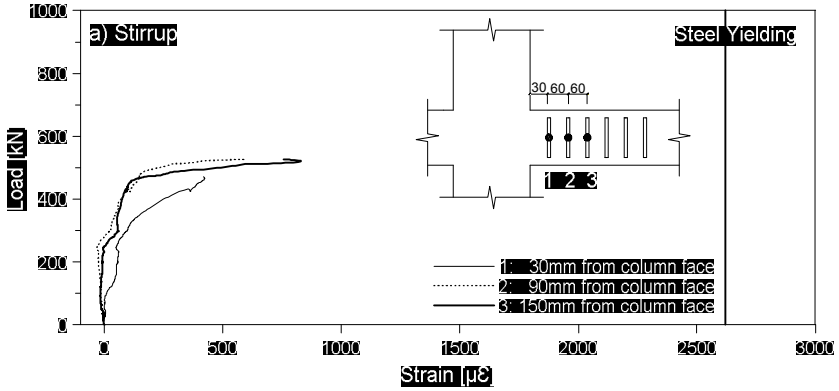

(a) Stirrup shear reinforcement

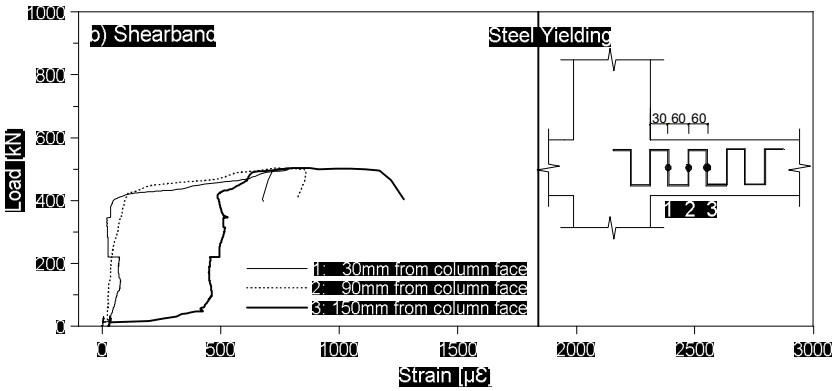

(b) shearbands reinforcement

Figure 5-40 Strains in shear reinforcement on east side of connection

Figure 5-40 indicates the strains in shear reinforcement at three points, 30 mm, 90 mm, and 150 mm from the column side, respectively. The measured strain values indicated similar behaviors for the PS and PB specimens, and neither specimen yielded. Strains on the shearband showed less stable behavior possibly due to the less bonding condition between the shearband and concrete due to the flat and slippery surface of the shearband.

Chapter 6. Experimental Result and Analysis

6.1 Design code comparison

This chapter compares the experimental result and design strengths in accordance with the three design codes for unbalanced moment and punching shear experiments. All reduction factors for each design code are neglected to observe the actual strength. The measured material properties suggested in **Chapter 4.6** are used for the calculation.

6.1.1 Punching shear experiment

The critical perimeters of each design code are suggested in **Table 6-1**. According to the table, the critical perimeter of Eurocode 2 ("Design", 2004) is larger than that of ACI 318-11 ("Building", 2011) and KCI 2012 ("Korean", 2012).

Table 6-1 Analysis for code provisions using punching shear

Code	ACI 318-11	KCI 2012	Eurocode 2
Shear perimeter	Square + $d/2$	Square + $d/2$	Square + $2d$
	1620.0 mm	1620.0 mm	2519.5 mm
	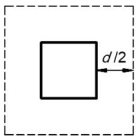	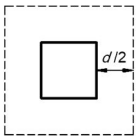	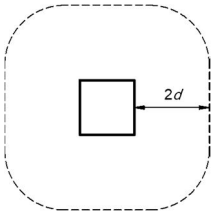

Punching shear strengths at the considered critical perimeter are calculated in accordance with ACI 318-11, KCI 2012 and Eurocode 2, respectively, and suggested in **Table 6-2**. In the table, shear strengths provided by concrete and shear reinforcement are classified and their ratios are given.

Table 6-2 Analysis for code provisions for punching shear

Code		ACI 318-11		KCI 2012		Eurocode 2	
Shear strength		kN	(%)	kN	(%)	kN	(%)
PN	V_c	275.6	100	308.2	100	300.2	100
	V_s	–	–	–	–	–	–
	V_n	**275.6**	100	**320.5**	100	**322.3**	100
PS	V_c	142.0	34	320.5	62	322.3	49
	V_s	275.5	66	199.7	38	333.2	51
	V_n	**417.5**	100	**520.2**	100	**655.5**	100
PB	V_c	142.0	34	320.5	57	322.3	38
	V_s	275.5	66	242.6	43	528..6	62
	V_n	**417.5**	100	**563.1**	100	**850.9**	100

For better understanding, bar charts showing each shear strength provided by concrete and shear reinforcement, and their ratios are drawn in **Figure 6-1**. As shown in the figure, the overall design punching shear strengths of ACI 318-11 are smaller for both control and shear-reinforced specimens, followed by KCI 2012 and Eurocode 2. This suggests nominal strength at the considered critical section might be the most conservative with ACI 318-11 among the three design codes.

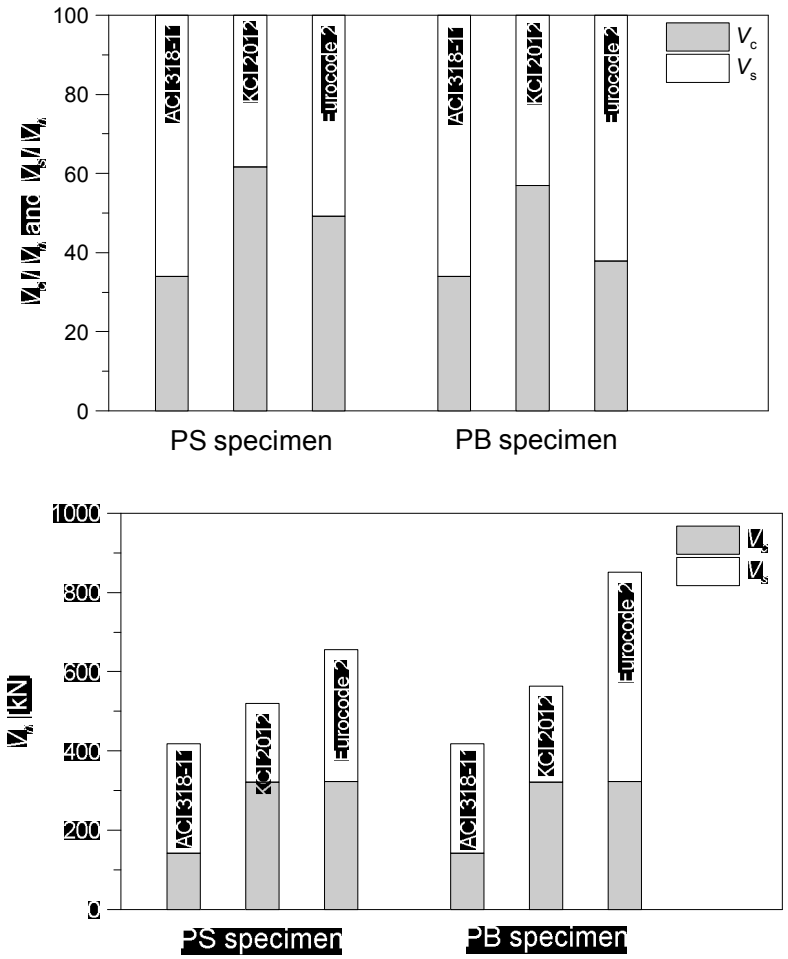

Figure 6-1 Design shear strength ($V_n = V_c + V_s$) and (V_c / V_n) and (V_c / V_n) ratios for each design code

The percentage shares of concrete and shear reinforcement in nominal shear strengths at each considered critical sections are drawn in **Figure 6-1**. According to **Figure 6-1**, when shear reinforcement is used, the nominal shear strengths calculated by ACI 318-11 and Eurocode 2 are more dependent on shear reinforcement (approximately 66% and 51% for Specimen PS, and 66% and 62% for Specimen PB, respectively), while nominal shear strength in accordance with KCI 2012 is more dependent on concrete (62% and 57% for PS and PB, respectively). To avoid overestimating nominal shear strength

when shear reinforcement is arranged, ACI 318-11 presumes concrete shear strength (V_c) is reduced by half, and this makes nominal shear strength (V_n) dependent on shear strength provided by shear reinforcement (V_s) more.

From this observation, it is found that ACI 318-11 is more conservative for shear strength of concrete (V_c) but less conservative for shear reinforcement (V_s). Essentially, KCI 2012 and ACI 318-11 have a similar philosophy and design procedure whereby design strength is the sum of V_c and V_s [**Eq. (3-15)**]; however, differences occur when calculating the shear strength of concrete and shear reinforcement. KCI 2012 uses a specific equation [**Eq. (3-16)**] to calculate concrete shear strength when structures behave as two-way, regardless of the existence of shear reinforcement, while ACI 318-11 uses the smallest of **Eqs. (3-1)** ~ **(3-3)** or **Eq. (3-5)** depending on the existence of shear reinforcement. In addition, while KCI 2012 reduces V_s by half [**Eq. (3-24)**], ACI 318-11 does not reduce. This difference results in about a 20% gap between the two design values.

The design shear strength of each specimen according to ACI 318-11 was calculated, the expected governing section (a further critical section between the two sections) was determined. These design shear strengths are shown in **Table 6-3**.

Table 6-3 Design shear strength according to ACI 318-11

ID	Critical section	b_0, [mm]	V_n at Column [kN]	V_n at Outer [kN]	Governing section
PN	Column*	1659.2	**275.6**	–	Column*
PS	Column*	1659.2	**417.5**	474.3	Column*
	Outer**	3443.5			
PB	Column*	1659.2	**417.5**	482.9	Column*
	Outer**	3543.2			

Note: *Column critical section (at $d/2$ from the column face); **Outer critical section (at $d/2$ from the outmost vertical elements of shear reinforcement)

According to the table, shear strength at the column critical section is smaller than that of the outer critical section, and this indicates that punching shear is expected to occur at the column critical section.

Table 6-4 summarizes the calculated design values at the column and outer critical sections for each specimen in accordance with KCI 2012. As shown in the table, punching shear is expected to occur at the column critical section for PN specimen, but at the outer critical section for shear-reinforced specimens (PS and PB), and this differs from the prediction by ACI 318-11.

Table 6-4 Design strength calculated according to the KCI code

ID	Critical section	b_0, mm	V_n at Column [kN]	V_n at Outer [kN]	Governing section
PN	Column*	1659.2	**320.5**	–	Column*
PS	Column*	1659.2	520.2	**467.2**	Outer**
	Outer**	3443.5			
PN	Column*	1659.2	563.0	**473.9**	Outer **
	Outer**	3543.2			

Note: *Column critical section (at $d/2$ from the column face); **Outer critical section (at $d/2$ from the outmost vertical elements of shear reinforcement)

In Eurocode 2, the punching shear strengths at the three control perimeters are determined and compared to determine the governing perimeter having the least punching shear strength. **Table 6-5** indicates the design punching shear resistance obtained using Eurocode 2. As a result of the analysis, it is anticipated that punching shear occurs at the outermost perimeter of shear reinforcement, and this is in contrast to ACI 318-11.

Table 6-5 Design strength of unbalanced moment specimens by Eurocode 2

ID	Control perimeter	u_i, [mm]	$V_{Rd,c}$ at column* [kN]	$V_{Rd,cs}$ at perimeter† [kN]	$V_{Rd,c}$ at outer‡ [kN]	Governing section
PN	Column*	1200	699.7	**322.3**	–	Perimeter†
	Perimeter†	2519				
PS	Column*	1200	699.7	655.6	**435.1**	Outer‡
	Perimeter†	2519				
	Outer‡	3401				
PB	Column*	1200	699.7	850.9	**403.9**	Outer‡
	Perimeter†	2519				
	Outer‡	3157				

Note: *at the adjacent to the column; †at control perimeters within 2*d* from the periphery of the column; ‡at the outermost perimeter of shear reinforcement

Test results and design strengths in accordance to ACI 318-11, Eurocode 2 and KCI 2012 of specimens in punching shear experiment are presented in following figures.

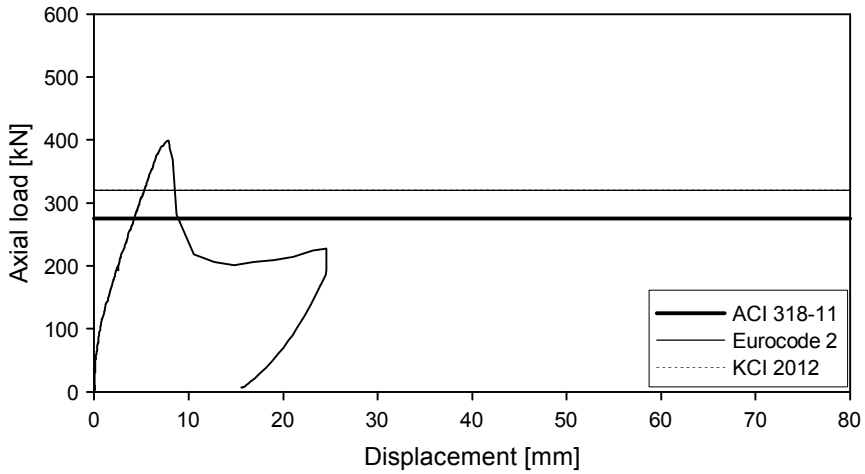

Figure 6-2 Test result vs. design strengths (PN specimen)

The peak load of the UN specimen during the test is beyond the design strengths of the three codes (**Figure 6-2**). The closest to the experiment data is Eurocode 2, and then KCI 2012 and ACI 318-11. Calculated design values by three design codes are similar. Especially the difference between Eurocode 2 and KCI 2012 is only about 0.6% and clear distinction of two graphs is difficult in the figure, although both code use completely different equations to obtain a punching shear strength. All design values are quite conservative compared to the test result in PN specimen.

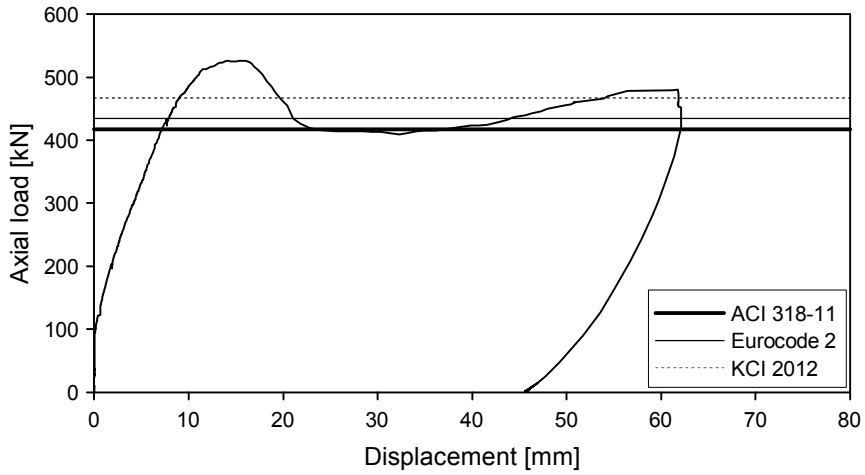

Figure 6-3 Test result vs. design strengths (PS specimen)

Similarly, in US specimen, the peak axial load is greater than three design strengths as shown in **Figure 6-3**. The design strength of the US specimen calculated from KCI 2012 is the nearest to the test result, followed by those from Eurocode 2 and ACI 318-11. Similar to non-shear-reinforced specimen (PN), design values of three design codes show small difference, and all show a reasonably conservative aspect compared to the peak axial load obtained from the test.

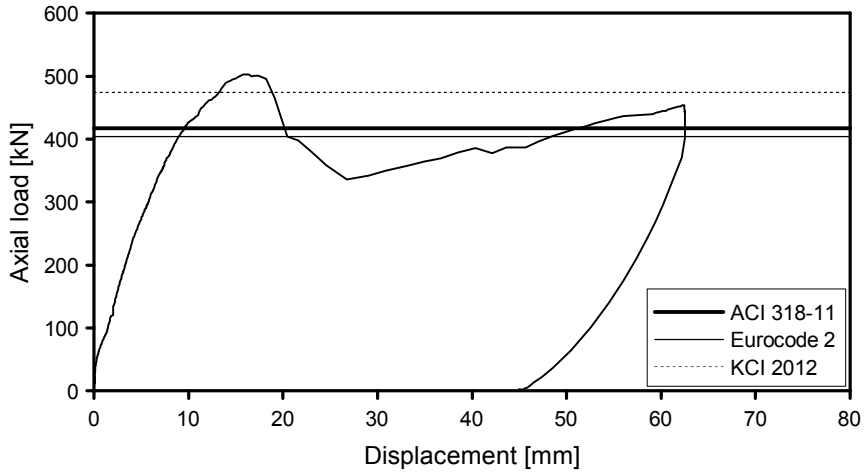

Figure 6-4 Test result vs. design strengths (PB specimen)

The test result and the design strengths of the specimen reinforced with the shearbands is shown in **Figure 6-4**. The peak strength of PB specimen is greater than the design strengths of three codes. KCI 2012 showed the greatest design strength, which is followed by ACI 318-11 and Eurocode 2 and the nearest to the test result is the same order. Design values of PB specimen in accordance with three design codes are also conservative as previous two tests of PN and PS specimens. This implies that although a detail design about shearbands such as requirement on installation or manufacturing features is not specified yet in three codes punching shear design of slabs specified in design codes used in this study (ACI 318-11, Eurocode 2 and KCI 2012) can be applicable to shearbands.

Comparison of the test result and design strengths of the non-shear-reinforced specimen and shear-reinforced specimens in punching shear test reveals that three design codes are quite conservative considering the fact that reduction factors are not considered in this analysis. This seems reasonable in punching shear design because punching shear strength is difficult to estimate due to too many variables. Thus, the observation implies that punching shear design of flat plate with / without shear reinforcement using ACI 318-11, Eurocode 2

and KCI 2012 may be safe even in the case where unusual reinforcing ratio is used and reduction factors are not considered.

Three design codes show similar design values for both non-shear or shear reinforced connections although each code has its own equation which is completely different to others based on different background. Several observations are made by comparing design values and equations.

According to **Eqs. (3-4)**, **(3-15)** and **(3-42)**, nominal shear strengths of ACI 318-11, Eurocode 2 and KCI 2012 are proportionally increased as $A_v f_{yt}$ increases, and used value of $A_v f_{yt}$ of PB specimen is almost the same as the of PS specimen ($A_v f_{yt}$ of PB specimen is approximately 1% greater), where A_v is the cross-sectional area of shear reinforcement, f_{yt} is the yield strength of transverse reinforcement; however, while the design strength of PS specimen is the smaller than that of PB specimen in KCI 2012, the design strength of PS specimen equals to that of PB in ACI 318-11, the design strength of PS is greater than that of PB specimen in Eurocode 2. There are some reasons causing this happen.

When shear reinforcement is provided, nominal shear strength (V_n) is the sum of shear strength provided by concrete (V_c) and shear reinforcement (V_s) and shall not be greater than $0.5\sqrt{f'_c}b_o d$ in ACI 318-11. This limitation restricts excessive increase of nominal shear strength by shear reinforcement and causes two specimen (PS and PB) to have the same design strength.

On the other hands, KCI 2012 has a limitation for shear reinforcement whereby f_{yt} should not be greater than 400 MPa. The D10 rebar (71.33 mm^2) used for stirrups was proved to have 500 MPa yield strength from the property test, and its yield strength is underestimated due to the limitation. However, in the case of shearbands, the yield strength (f_{yt}) obtained was 330 MPa, and the total strength (330 MPa) is used without reduction. This limitation on shear stress of shear reinforcement causes design strength of PB specimen has

greater shear strength than that of PS specimen in KCI 2012.

For Eurocode 2, the effective design strength of shear reinforcement ($f_{ywd,ef}$) is calculated by $f_{ywd,ef} = 250+0.25d$. The equation does not concern the strength of the reinforcement, but only the effective depth. Moreover, outermost perimeter of shear reinforcement governs shear failure in Eurocode 2, and the way Eurocode 2 considers outermost perimeter differs from ACI 318-11 and KCI 2012 (**Figure 3-4** and **Figure 3-10**). Eurocode 2 takes curved portion in **Figure 6-6** as the critical perimeter at outer shear reinforcement (dotted line). The outer perimeter of PS is longer than that of PB in Eurocode 2 and this made PS has greater shear strength than PB. All codes are considered to lack enough specifications for different strengths of shear reinforcement.

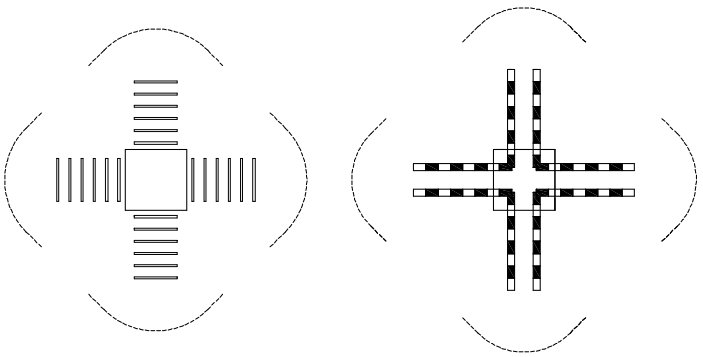

Figure 6-5 outer critical perimeter of PS and PB specimens defined by Eurocode 2

Figure 6-6 shows V_{exp} / V_n (test result / design value) according to the specimens and design codes, while specific data are summarized in **Table 6-6**. As seen in **Figure 6-6**, ACI 318-11 is consistently conservative for all specimens, and the strength is especially underestimated for PN specimen (45%). The average punching shear of ACI 318-11 is the farthest from the test result among the three design codes. In Eurocode 2, the punching strength of specimens is consistently and moderately underestimated. Similar to ACI 318-11 and Eurocode 2, the design strengths of KCI 2012 for the three specimens show a conservative aspect, but is generally closer to the test result than ACI

318-11 and Eurocode 2 in that the error average for KCI 2012 of V_{exp}/V_n is 0.14 while those for ACI 318-11 and Eurocode 2 are 0.30 and 0.23, respectively.

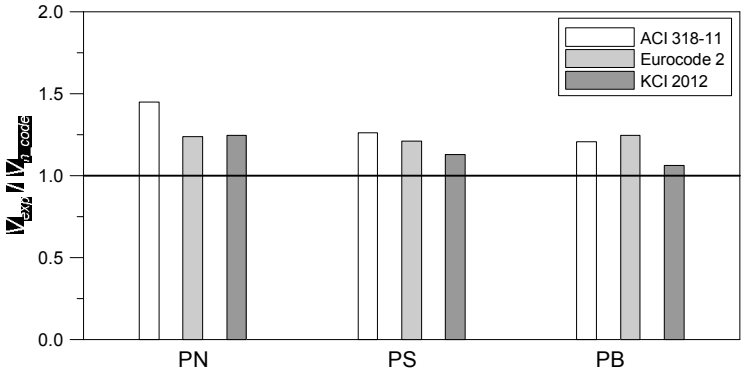

(a) V_{exp} / V_n ordered by specimens

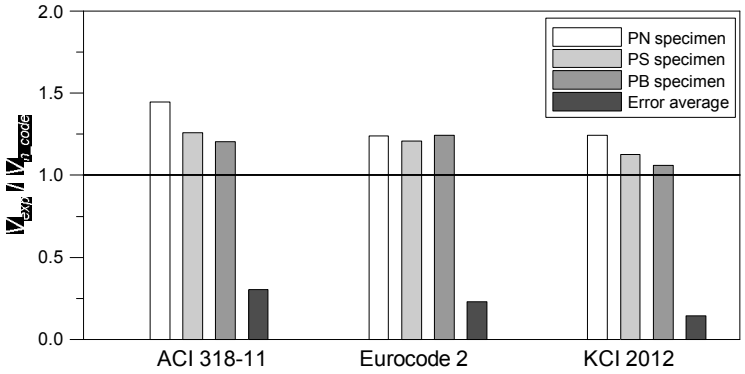

(b) V_{exp} / V_n ordered by design codes

Figure 6-6 V_{exp}/V_n (Test result / Design value)

Table 6-6 Summarized V_{exp}/V_n (test result / design value)

ID	Test result	ACI 318-11		Eurocode 2		KCI 2012	
	V_{exp} (1)	V_n (2)	V_{exp}/V_n =(1)/(2)	V_n (3)	V_{exp}/V_n =(1)/(3)	V_n (4)	V_{exp}/V_n =(1)/(4)
PN	399.0 kN	275.6	1.45	322.3 kN	1.24	320.5 kN	1.24
PS	526.5 kN	417.5	1.26	435.1 kN	1.21	467.2 kN	1.13
PB	503.0 kN	417.5	1.20	403.9 kN	1.25	473.9 kN	1.06

Error average	−	0.30	−	0.23	−	0.14

6.1.2 Unbalanced moment experiment

Design strength calculated by ACI 318-11 and flexural moment capacity within various effective widths are compared in **Table 6-7**. According to the calculation by ACI 318-11, punching shear failure is expected prior to reaching the yield capacity of the reinforcement provided within c_2+3h, c_2+5h and column strip for UN, US and UB specimens.

Table 6-7 Design strength of unbalanced moment specimens by ACI 318-11

ID	b_0, [mm]	Flexural failure			Shear failure	
		M_{Slab_c+3h} [kN·m]	M_{Slab_c+5h} [kN·m]	$M_{Slab\_c.s}$ [kN·m]	$M_{n\_unb,col}$ * [kN·m]	$M_{n\_unb,outer}$ ** [kN·m]
UN	1659.2	154.8	198.7	253.3	**46.5**	NA
US	1659.2	154.8	198.7	253.3	**93.9**	190.4
	3443.5					
UB	1659.2	154.8	198.7	253.3	**95.1**	206.7
	3543.2					

Note: * varies depending on what transfer is considered (c_2+3h, c_2+5h and column strip); *Column critical section (at d/2 from the column face); **Outer critical section (at d/2 from the outmost vertical elements of shear reinforcement); M_{Slab} is the flexural moment capacity within the considered section; M_{n_unb} is the unbalanced moment within considered section

The unbalanced moment strengths in accordance with KCI 2012 of the UN, US and UB specimens in the current study are calculated, and are suggested in **Table 6-8**. As discussed in **Chapter 3.2.2**, unbalanced moment resistance provided by the eccentric shear stress (M_S), the flexural strength (M_F) and the torsional moment (M_T) are considered, and the nominal unbalanced moment capacity is the sum of three values. Unlike ACI 318-11, when unbalanced moment exists, KCI 2012 only concerns the critical perimeter at d/2 from the column face without considering outer critical section at d/2 from the outmost vertical elements of shear reinforcement. Thus, calculated values are the

strengths at the critical perimeter, and failure is expected at this perimeter.

Table 6-8 Design strength calculated from KCI 2012

ID	M_F [kN-m]	M_S [kN-m]	M_T [kN-m]	M_n [kN-m]
UN	56.38	18.25	13.02	**87.65**
US	56.38	26.34	15.87	**98.58**
UB	56.38	28.06	15.87	**100.30**

Note: M_F is the sum of moment strengths of front and rear slab; M_S is the flexural strength by eccentric shear in front and rear slab; M_T is the torsion strength by eccentric shear in sides; M_n is the design unbalanced moment

The unbalanced moment carrying capacity in accordance with Eurocode 2 and needed specifications for the calculation are given in **Table 6-9**. Because Eurocode 2 recommends checking three critical perimeters; 1) column perimeter; 2) basic control perimeter; 3) outer perimeter; design strength at each critical section was calculated and compared to determine the governing perimeter.

Table 6-9 Design punching shear resistance by Eurocode 2

ID	Control perimeter	u_i [mm]		V_{Ed} [kN]	v_{Ed} [MPa]	M_{Ed} at u_i [kN-m]
UN	Column	u_0	1200	140.2	5.55	235.1
	Control	u_1	2519		1.22	**76.6**
US	Column	u_0	1200	143.9	5.55	233.6
	Control	u_1	2519		2.48	215.0
	Outer	u_{out}	3400		1.22	**122.4**
UB	Column	u_0	1200	140.4	5.55	235.1
	Control	u_1	2519		3.15	291.2
	Outer	u_{out}	3157		1.22	**110.7**

Note: u_i is the length of considered perimeter; u_0 is the column perimeter; u_1 is the basic control perimeter; u_{out} is the outer perimeter; V_{Ed} is the measured shear force at peak load in this study; V_{Ed} is the shear capacity of considered perimeter; M_{Ed} is the design value of the applied internal

bending moment

Data obtained from the unbalanced moment experiment and expected strengths calculated from ACI 318-11, Eurocode 2, and KCI 2012 are shown together in the following figures and compared. From the comparison, analysis is made to see whether each code is conservative or not, and equations suggested by codes are examined.

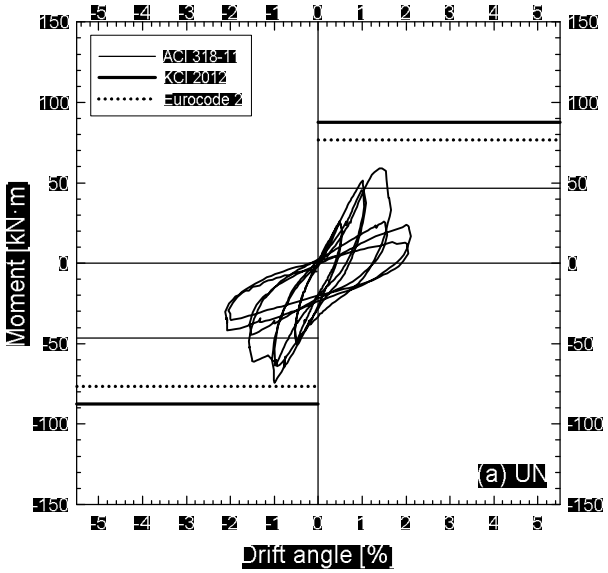

Figure 6-7 Experimental results and design strengths (UN)

In the UN specimen without shear reinforcement the design strength in accordance with ACI 318-11 shows the smallest value, which is followed by those of Eurocode 2 and KCI 2012 as shown in **Figure 6-7**. According to the figure, the design strength from ACI 318-11 is smaller than the maximum strength obtained from the experiment. This indicates that ACI 318-11 is conservative in terms of concrete shear strength, while KCI 2012 overestimates concrete shear strength quite substantially. Although this error will be reduced by considering reduction factors, it shows an excessively large gap with the experimental data (15% error). This appeared to occur due to the

relatively over-reinforced flexural reinforcement causing punching failure without yielding of slab reinforcing bars since an unbalanced moment strength of a slab increases as reinforcing bar increases.

This result implies that Eurocode 2 and KCI 2012 may be somewhat unreliable when designing a flat plate with too much flexural reinforcement but without shear reinforcement. On the other hand, ACI 318-11 conservatively predicts the punching shear strength of the concrete connection without shear reinforcement.

Additionally, the two previously tested specimens with large tension reinforcing ratios but without shear reinforcement are assessed. The specimens of RC-A and RC-B were tested by Park et al. (2012). The tension reinforcing ratio within c_2+3h of two specimens was 0.0095 and both specimens were subjected to constant gravity loads (V_g / V_o = 0.45 and 0.41, respectively) and cyclic lateral loads. The calculated strengths of Specimens RC-A and RC-B using each code show similar patterns with Specimen UN of the current study. ACI 318-11 shows conservative aspects, while Eurocode 2 and KCI 2012 give unconservative estimations. Test results of Specimen RC-A and RC-B are shown in **Figure 6-8**, along with the calculated strengths values by three design codes.

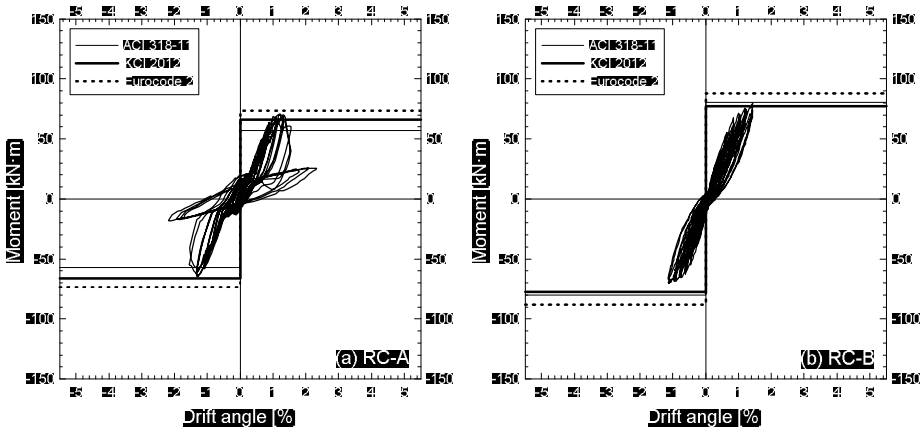

Figure 6-8 Experimental results and design strengths (Park et al., 2012)

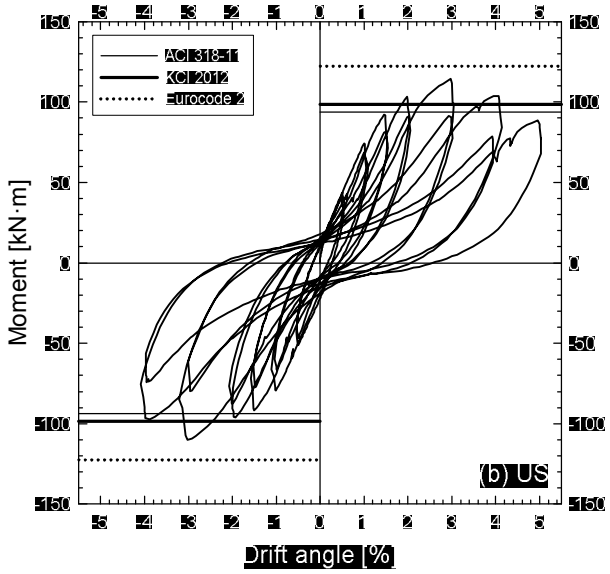

Figure 6-9 Experimental results and design strengths (US)

The design values of ACI 318-11 and KCI 2012 for the US specimen are smaller than the maximum test value, but that of Eurocode 2 is greater than the maximum test value (**Figure 6-9**). Unlike the concrete connection without shear reinforcement (UN specimen) that , the design value of the concrete connection with stirrup shear reinforcement (US specimen) from Eurocode 2 is nearest to the test result, followed by KCI 2012 and ACI 318-11; However, while ACI 318-11 and KCI 2012 show a conservative aspect, Eurocode 2 is not conservative.

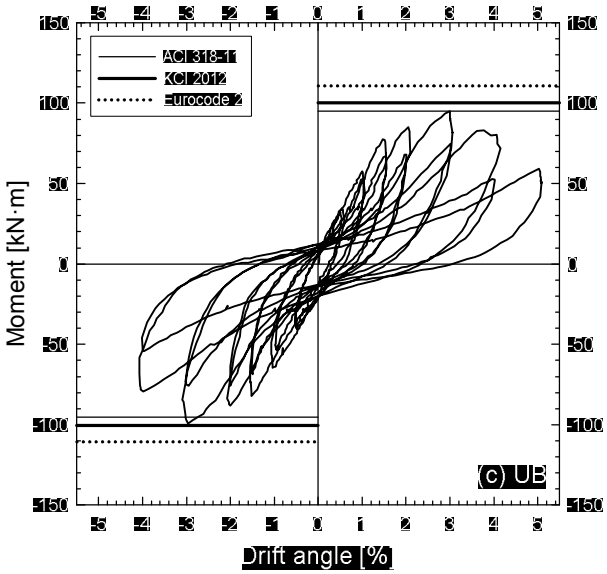

Figure 6-10 Experimental results and design strengths (UB)

The comparison of the test result and the design strengths of UB specimen is given in **Figure 6-10**. According to the figure, Eurocode 2 shows the largest design strength, which is followed by KCI 2012 and ACI 318-11, and this order is the same as US specimen. KCI 2012 (99%) is the closest to the test result with 99% and followed by ACI 318-11 (104%) and Eurocode 2 (90%). ACI 318-11 is reasonably conservative, and Eurocode 2 and KCI 2012 are unconservative in UB specimen.

Figure 6-11 shows the ratio of experimental results to design strengths, and the error averages for the three design codes. In the UN specimen, the test result / design value differs compared to the design codes. (While the design strength using Eurocode 2 is reasonable, that using ACI 318-11 and KCI 2012 is underestimated or overestimated). For the US and UB specimens, ACI 318-11 and KCI 2012 show somewhat conservative results but for Eurocode 2 design strengths of the US and UB specimens are unconservative. The M_{exp} / M_{n_code} values are closer to 1 for the UB specimen than for the US specimen in ACI 318-11 and KCI 2012. The design values of the UN specimen using

Eurocode 2 and KCI 2012 are smaller than 1, which might not be safe for heavily reinforced slabs.

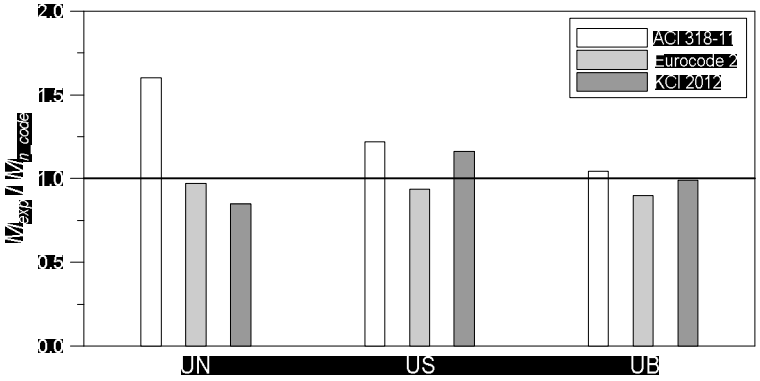

(a) M_{exp} / M_n ordered by specimens

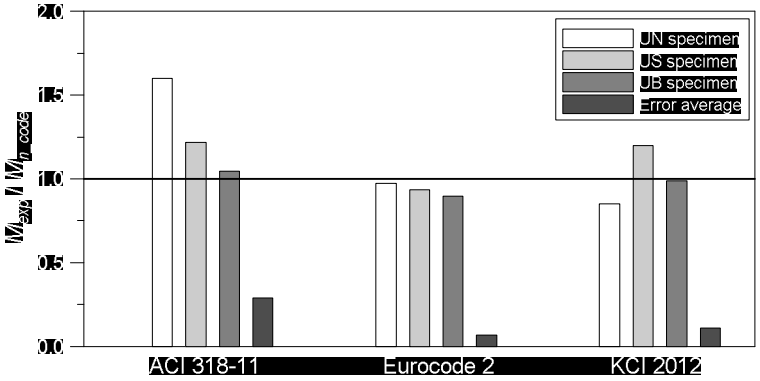

(b) M_{exp} / M_n ordered by design codes

Figure 6-11 M_{exp} / M_n (Test result / Design value)

From the observation on **Figure 6-11** and **Table 6-10**, ACI 318-11 shows the greatest error average (29%) followed by KCI 2012 (11%) and Eurocode 2 (7%). The design strength using ACI 318-11 is conservative regardless of the presence of shear reinforcement. The overall design strengths in accordance with Eurocode 2 are relatively close to the test results, but unconservative and it is not ideal in shear design. KCI 2012 accurately estimates the strength of the connections with shear reinforcement, but overestimates the strength of connection without shear reinforcement.

Table 6-10 Summarized M_{exp} / M_n (test result / design value)

ID	Test result	ACI 318-11		Eurocode 2		KCI 2012	
	M_{exp} [kN·m] (1)	M_n [kN·m] (2)	M_{exp} / M_n =(1)/(2)	M_n [kN·m] (3)	M_{exp} / M_n =(1)/(3)	M_n [kN·m] (4)	M_{exp} / M_n =(1)/(4)
UN	74.4	46.5	1.60	76.6	0.97	87.7	0.85
US	114.5	93.9	1.22	122.4	0.94	95.6	1.16
UB	99.3	95.1	1.04	110.7	0.90	100.3	0.99
Difference		−	0.29	−	0.07	−	0.11

6.2 Consideration

6.2.1 Transfer width

Figure 6-11 presents the test result and design strengths of the US and UB specimens that were strengthened with stirrups or shearbands. In these figures, there are no significant differences between the expected strengths of codes. However, this does not imply that all design codes would have similar design strengths for any case. Unlike KCI 2012 and Eurocode 2 that focus on concrete failure rather than flexural failure of reinforcement, in ACI 318-11, flexural transfer strength is taken at the transfer width of c_2+3h and then compared with the shear failure value to determine design strength (Kang, 2004). As previously discussed in **Chapter 5.1.4**, not only flexural reinforcement within c_2+3h but also beyond c_2+3h considerably resisted lateral force and this corresponds to previous studies (Choi et al., 2008; Song et al., 2012). Therefore, a significant difference would occur if flexural reinforcement was arranged more intensively within c_2+3h and less intensively within c_2+5h as typically constructed, or a different transfer width was used such as c_2+5h or column strip instead of c_2+3h. This subchapter demonstrates how design strength in accordance with ACI 318-11 could be varied depending on different transfer widths.

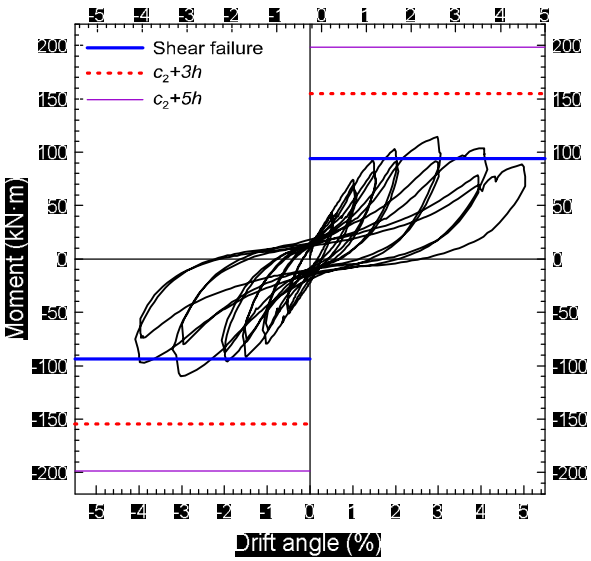

(a) US specimen

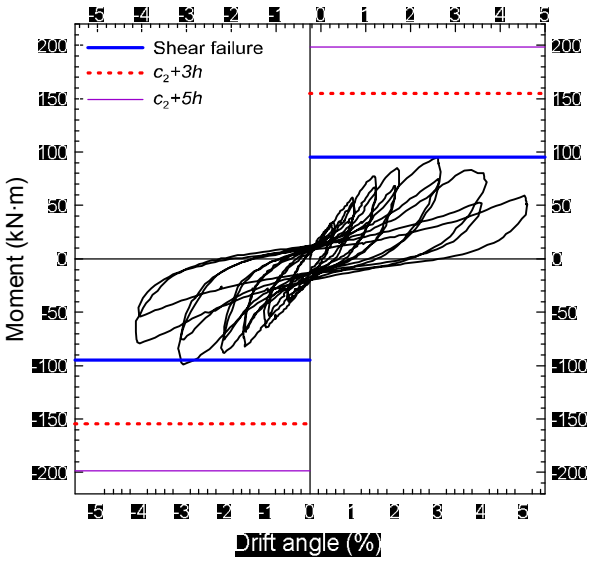

(b) UB specimen

Figure 6-12 Experimental results and design strengths as per ACI 318-11

As shown in **Figure 6-12**, for the US and UB specimens, the design strength inducing shear failure is significantly smaller than the flexural transfer strengths of both c_2+3h and c_2+5h. This is because the reinforcing ratio was designed to be fairly high in order to induce stress-induced punching failure as

mentioned in **Chapter 4.2.2**. Therefore, if c_2+5h were taken as a transfer width instead of c_2+3h, the result would not change since strength associated with punching shear is significantly smaller than the flexural transfer strengths of both c_2+3h and c_2+5h, and in this case, the design strength is somewhat close to the test result. However, usually reinforcement is not as intensively arranged as it was in this study, and it is also not recommended due to the brittle failure of concrete (instead of ductile failure by yielding of reinforcement). Therefore, a parametric study using various reinforcing ratios is conducted to discuss the effect of different transfer widths. The reinforcing ratios of bottom bars obtained from previously published papers are used, and M_{n_c+3h} and M_{n_c+5h} are obtained by varying the reinforcing ratio of the top bars. The information of the used reinforcing ratio is summarized in **Table 6-11**

Table 6-11 Flexural reinforcing ratio for each experimet

Kang and Wallace (2008)					
ρ^-_{c+3h}	ρ^+_{c+3h}	$\rho^-_{c.s}$	$\rho^+_{c.s}$	$\rho^-_{f.s}$	$\rho^+_{f.s}$
0.0052	0.0022	0.0052	0.0021	0.0038	0.0021
Park et al. (2012)					
ρ^-_{c+3h}	ρ^+_{c+3h}	$\rho^-_{c.s}$	$\rho^+_{c.s}$	$\rho^-_{f.s}$	$\rho^+_{f.s}$
0.0095	0.0054	0.0096	0.0064	0.0070	0.0051
Current study					
ρ^-_{c+3h}	ρ^+_{c+3h}	$\rho^-_{c.s}$	$\rho^+_{c.s}$	$\rho^-_{f.s}$	$\rho^+_{f.s}$
0.0147	0.0088	0.0141	0.0088	0.0103	0.0086

Note: ρ is the ratio of A_s to bd (=A_s/bd); A_s is the cross-sectional area of slab reinforcement within b; b is the considered width; d is the effective depth (top layer); ρ_{c+3h} is the reinforcing ratio for the width of c_2+3h; c_2 is the column width; h is the slab thickness; $\rho_{c.s}$ is the reinforcing ratio for the column strip; $\rho_{f.s}$ is the reinforcing ratio for the full span width; – means top bars for negative bending; + means bottom bars for positive bending

As shown in the above table, no significant difference is observed between the reinforcing ratios c_2+3h and the column strip, and the flexural reinforcement placement shown in the figures of the papers indicate that same spacing was used in c_2+3h and the column strip. Therefore, a reinforcing ratio at c_2+3h is used to calculate the amount of reinforcement in c_2+3h and c_2+5h for each

individual study, and M_{slab_c+3h} and M_{slab_c+5h} are found by considering the amount of arranged reinforcement in c_2+3h and c_2+5h, respectively (Note that M_{Slab} is $\sum M_n$ / γ_f as shown in **Eq. (3.13)**, where $\sum M_n$ is the sum of positive and negative nominal moment strength of the slab; γ_f is the representative factor to determine the unbalanced moment transferred by flexure at slab-column connections and 0.6 is used in this study). The obtained reinforcing ratio vs. the unbalanced moment relationships are shown in **Figure 6-13**.

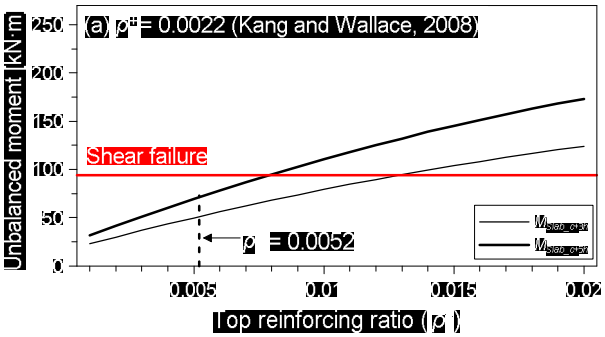

(a) Kang and Wallce (2008) (ρ^+ = 0.0022)

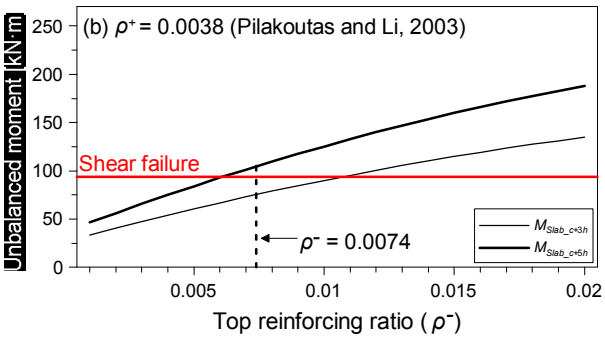

(b) Pilakoutas and Li (2003) (ρ^+ = 0.0038)

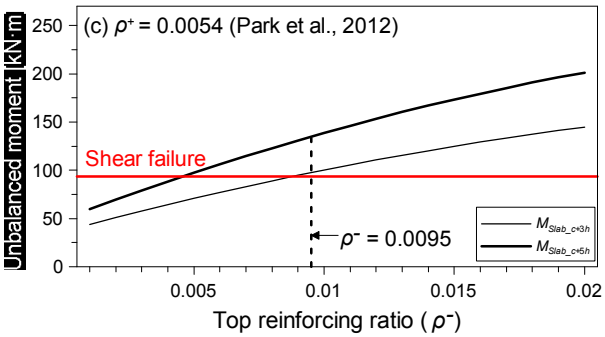

(c) Park et al. (2012) (ρ^+ = 0.0054)

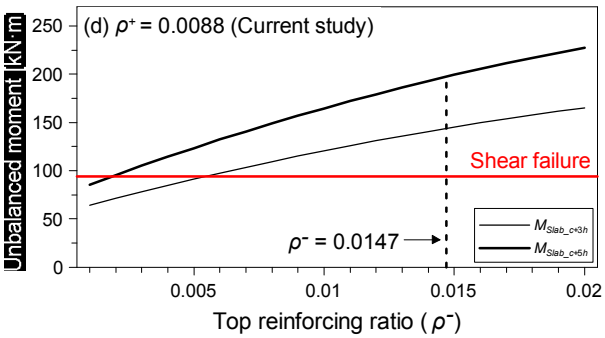

(d) Current study (ρ^+ = 0.0088)

Figure 6-13 Reinforcing ratio vs. unbalanced moment relationship (ordered by bottom reinforcing ratio)

While unbalanced moment values associated with M_{n_c+3h} and M_{n_c+5h} shown in **Figures 6-13(a)**, **6-13(b)** and **6-13(c)** are close to the unbalanced moment inducing punching failure, those of this research as shown in **Figure 6-13(d)** show a clear boundary between the M_{slab_c+3h} and M_{slab_c+5h} values and the moment inducing punching failure. The graph obviously indicates that stress-induced punching failure would occur regardless of the transfer width used, and this was demonstrated by the experiment. However, if the reinforcing ratio were lower, determining a transfer width could be an important matter. For example, in the study performed by Kang and Wallace (2008), an unbalanced moment inducing stress-induced punching failure is located over M_{slab_c+3h} and M_{slab_c+5h} in the graph, and the design strength could be varied depending on the transfer width in this case. **Figure 6-13(b)**, in which ρ^+=0.0038 and ρ^+=0.0074 were used, also shows that a design value could be changeable up to the transfer width. This occurs when the flexural reinforcement is moderately arranged.

A further parameter study is conducted to observe the effects of other variables such as concrete strength and shear reinforcement on the design strength of structures subjected to a combined constant gravity and reversed

cyclic lateral loading. **Figure 6-14** shows changes of the specimen's shear failure limitation according to concrete strength from 20 MPa to 80 MPa when the areas of shear reinforcement (A_v) are 500 mm, 1000 mm, and 1500 mm. As shown in the figure, a moment causing shear failure is under the c_2+3h line when the compressive strength of concrete is within 20 MPa to 50 MPa. Within this range, shear failure is expected to occur first so that the outcome is not importantly changed, and it does not matter whether c_2+3h or c_2+5h is taken as a transfer width. However, a significant design error may occur when the concrete strength is greater than 50 MPa and more than two shearbands are installed in one direction. As shown in **Figure 6-14**, it is difficult to predict failure mode and design strength since they vary depending on the transfer width.

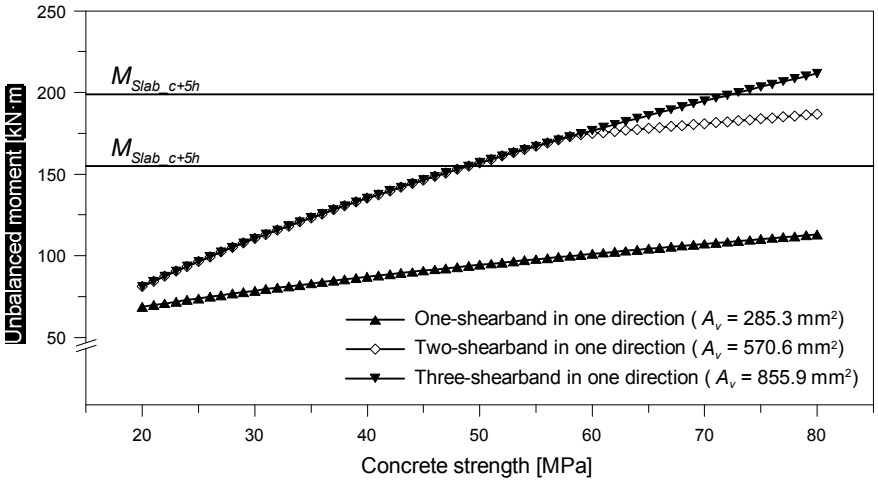

Figure 6-14 Design strength when changing concrete strength

The result of another parametric study in which the area of shear reinforcement varies is presented in **Figure 6-15**. The area of shear reinforcement is varied from 100 mm^2 to 1000 mm^2 and 20, 24, 40, 60, and 80 MPa concrete is considered. As drawn in the figure, moment curves linearly

increase when the shear reinforcement increases and maintains a constant strength at a certain point. This is because shear strength has a limitation [**Eq. (3-4)**], and after that point, additional shear reinforcement is no longer counted. The 570.6 mm^2 of the area of shear reinforcement and 24.1 MPa concrete were used in the experiment.

The curves of 20, 24 and 40 MPa concrete are located below than the M_{Slab_c+3h} line up to 570.64 mm^2 point in all cases, but curves of 60 and 80 MPa concrete are not within this range. According to **Figure 6-15**, it could be unreliable if 80 MPa concrete and more than about 450 mm^2 shear reinforcement were used since the difference between M_{Slab_c+3h} (154.77 kN·m) and M_{Slab_c+5h} (198.67 kN·m) is approximately 28.3%, and this is a significant gap.

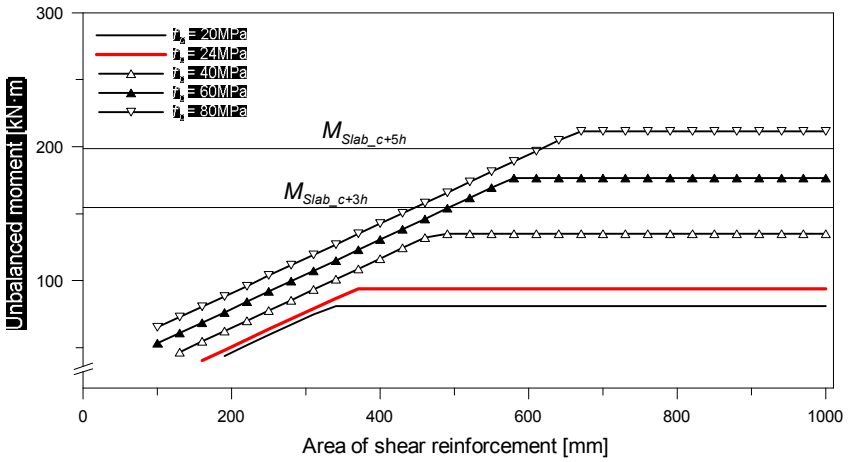

Figure 6-15 Design strength when changing area of shear reinforcement

Various parametric studies reveal that a great difference might occur between the test results and design strength according to ACI 318-11, if variables are changed such as the amount of flexural or shear reinforcement and the strength of concrete. The flat plate design in accordance with ACI 318-11 may not be efficient and reliable in some cases. It is recommended that in ACI318-11, the effect of interactions among shear reinforcement, flexural

reinforcement and concrete needs to be considered, as it is in KCI 2012 and Eurocode 2.

6.2.2 Effective depth

As mentioned earlier, the effective depth of the UB specimen was not secure. After unbalanced moment experiments, the concrete cover depths for the US and UB specimens were measured in order to inspect the amount of construction error that occurred compared with the original plan.

(a) Measured concrete cover depth of US specimen

(b) Measured concrete cover depth of UB specimen

Figure 6-16 Measured concrete cover depth after experiments

Based on the measured lengths shown in **Figure 6-16**, the concrete cover depths of the US and UB specimens were about 35 mm and 46 mm, respectively. Because concrete deformation can occur during experiments, it is not possible to speculate the intact concrete cover depths before tests with data measured after experiments. However, the figure clearly indicates that effective depth was better secured in the US specimen than in the UB specimen. To observe the influence of effective depth to moment capacity, a parametric study is performed by varying the effective depth from 90 mm to 110 mm.

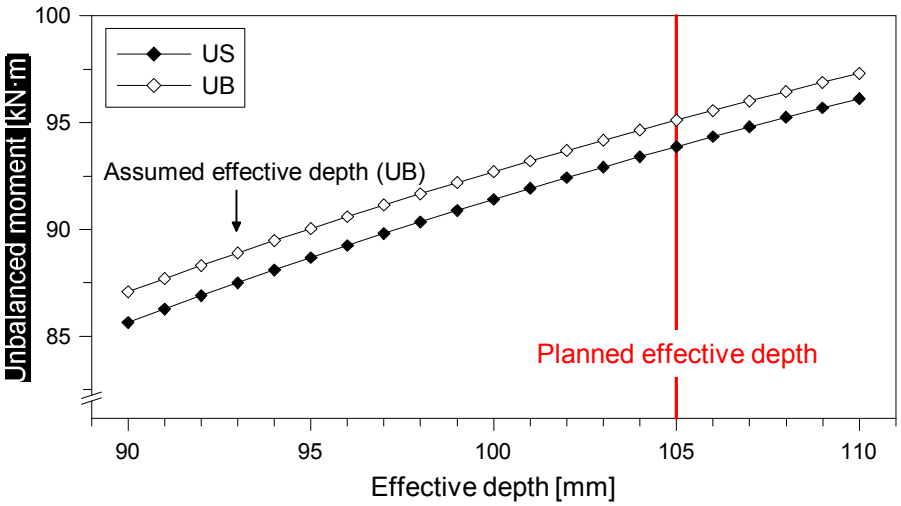

Figure 6-17 Parametric study by varying effective depth (US and UB)

As shown in **Figure 6-17**, the moment capacity of the UB specimen was intended to be greater than that of the US specimen when they were placed at the same effective depth. At the same time, the figure also indicates that about a 10 mm difference (obtained from the measured value in **Figure 6-16**) could play an important role in changing the moment carrying capacity.

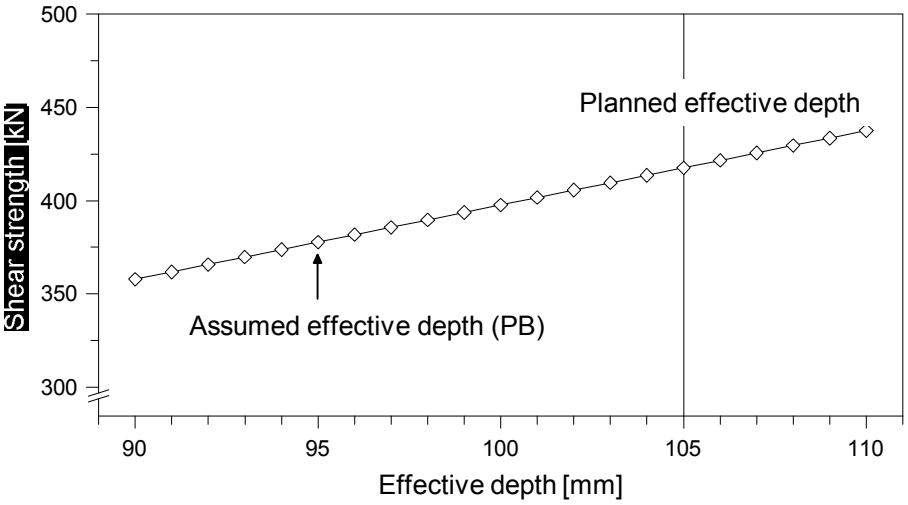

Figure 6-18 Parametric study by varying effective depth (PB)

The same phenomenon might influence the punching shear experiment as shown in **Figure 6-18**. Therefore, the unsecured effective depth is thought to be one of reasons why the UB and PB specimens had less load carrying capacity than the US and PS specimens.

Chapter 7. Conclusion

In this research, the band type shear reinforcement for the flat plate system is suggested and its performance is demonstrated by experimental analysis. A total of six specimens, having different types of shear reinforcement, were fabricated to investigate and compare structural performance. Two specimens were without shear reinforcement and two other specimens were strengthened by stirrup shear reinforcement, while the remaining two specimens were strengthened using the band type shear reinforcement. The specimens were tested under two different conditions of only gravity load and gravity load with lateral load. Based on the studies, several important observations and conclusions are drawn as follows:

1) On analysis of the result of the experiment, it was found that all specimens reached the design strength calculated in accordance with ACI 318-11 using the measured properties. Specimens with stirrups or shearbands showed superior performance in terms of load carrying capacity, ductility, and energy dissipation in both the unbalanced moment and punching shear experiments compared to specimens without shear reinforcement.

2) In the unbalanced moment experiment, the moment carrying capacity and deformation capacity of the specimen with stirrup shear reinforcement (specimen US) were increased by 54% and 228% (vs. UN), respectively, and those of the specimen with shearbands (specimen UB) were increased by 34% and 173%. The dissipation energy capacities of the US and UB specimens were 3.25 and 3.12 times that of UN, respectively.

3) In the punching shear experiment, specimens PS and PB with stirrups and shearbands, respectively, showed 1.32 times and 1.26 times improved load carrying capacities, and achieved 7.9 times and 7.96 times enhanced deformation capacities, compared to the specimen without shear reinforcement (PN). Therefore, given the advantageous constructability of the shearbands, the shearbands can be effectively used in actual construction sites.

4) The flat plate designs in accordance with ACI 318-11, KCI 2012 and Eurocode 2 are compared. Since all specimens showed somewhat brittle shear failure rather than flexural failure without yielding of slab flexural reinforcement, comparing design strength with test values may be thought to be fair in terms of nominal punching shear strength. Design strength by ACI 318-11 tends to be constantly conservative in both punching shear test (difference average = 0.30) and unbalanced moment test (difference average = 0.29) regardless of the presence of shear reinforcement. Calculation by Eurocode 2 gives difference average of test result to design strength of 0.23 and 0.07 for punching shear strength and unbalanced moment strength, respectively, which are closer to the test result, but unconservative for all specimens in the unbalanced moment test. Design strength by KCI 2012 is almost same as test results in punching shear (difference average = 0.14) but shows unsafe aspect in estimating unbalanced moment capacity (difference average = 0.11), especially for specimen UN which had no shear reinforcement.

References

1. ACI-ASCE Committee 352 (1988). "*Recommendations for Design of Slab-Column Connections in Monolithic Reinforced Concrete Structures* (ACI 352.1R-89)," ACI Structural Journal, 85(6), 675-696.

2. Ann, K.-S. (2004). "*Shear Reinforcement for Flat Plate-Column Connections using Lattice Bars*," MS Thesis, Department of Architecture & Architectural Engineering, Seoul National University, Seoul, Korea. (in Korean)

3. Ann, K.-S., and Park, H.-G. (2005). "Shear Reinforcement for Flat Plate-Column Connections Using Lattice Bars," *Journal of the Korea Concrete Institute*, 17(2), 191-200. (in Korean)

4. Broms, C. E. (1990). "Shear Reinforcement for Deflection Ductility of Flat Plates," *ACI Structural Journal*, 87(6), 696-705.

5. "*Building Code Requirement for Structural Concrete* (ACI 318-08)," American Concrete Institute, Farmington Hills, MI, 2008.

6. "*Building Code Requirement for Structural Concrete* (ACI 318-11)," American Concrete Institute, Farmington Hills, MI, 2011.

7. Choi, C.-S., Bae, B.-I., Choi, Y.-C., and Choi, H.-K. (2012). "The Effect of Anchorage with Shear Reinforcement in Flat Plate System," *Journal of the Korea Concrete Institute*, 24(6), 667-675. (in Korean)

8. Choi, J.-W., and Song, J.-K. (2007). "The Punching Shear Strength of Lightly Reinforced Thick Flat Plates without Shear Reinforcement," *Journal of Architectural Institute of Korea,* 23(8), 67-74. (in Korean)

9. Choi, J.-W., Song, J.-K., Park, H.-G., and Kim, K.-H. (2007). "Lateral Capacity of Flat Plate-Column Connection with Shear Reinforcements," *Journal of Architectural Institute of Korea,* 23(9), 47-54. (in Korean)

10. Choi, J.-W., Song, J.-K., and Song, H.-B. (2008). "The Failure Model of RC Flat Plates Considering Interrelation between Punching Shear and Unbalanced Moment," *Journal of the Korea Concrete Institute*, 20(4), 523-530. (in Korean)

11. Choi, K.-K. Shin, D.-W., and Park, H.-G. (2014), "Shear-Strength Model for Slab-Column Connections Subjected to Unbalanced Moment," *ACI Structural Journal*, 111(3), 491-502.

12. "*Eurocode 2, Design of Concrete Structures - Part1-1: General Rules and Rules for Buildings*," EN 1992-1-1, Brussels, Belgium, 2004.

13. Ferreira, M. P., Melo, G. S., Regan, P. E., and Vollum, R. L. (2014). "Punching of Reinforced Concrete Flat Slabs with Doulble-Headed Shear Reinforcement" *ACI Structural Journal*, 111(2), 363-374

14. Gardner, N., J. (2011). "Verification of Punching Shear Provisions for Reinforced Concrete Flat Slabs," *ACI Structural Journal*, 108(5), 572-580.

15. Hawkins, N. M., Bao, A., and J. Yamazaki (1989). "Moment Transfer from Concrete Slabs to Columns," *ACI Structural Journal*, 86(6), 705-716.

16. Hwang, S. J. (1989). "*An Experimental Study of Flat-Plate Structures under Vertical and Lateral Loads*," PhD Thesis, Department of Civil Engineering, University of California at Berkeley, CA.

17. Kang, T. H.-K. (2004). "*Shake Table Tests and Analytical Studies of Reinforced and Post-tensioned Concrete Flat Plate Frames*," PhD Thesis, Department of Civil and Environmental Engineering, University of California at Los Angeles, CA.

18. Kang, T. H.-K., and Wallace, J.W. (2008). "Seismic Performance of Reinforced Concrete Slab-Column Connections with Thin Plate Stirrups," *ACI Structural Journal*, 105(5), 617-625.

19. Kang, T. H.-K., and Park, H.-G. (2012). "Performance of Shearbands in Concrete Slab-Column Connections," *SP-287-4 ACI Special Publication*, Recent Development in Reinforced Concrete Slab Analysis, Design and Serviceability, 16.

20. "*Korean Structural Design Code* (KCI 2012)," Korean Concrete Institute, Seoul, Korea, 2012. (in Korean)

21. "*Method of Tensile for Metallic Materials* (KS F 0802: 2003)," Korean Standard Association, 2003. (in Korean)

22. Mirzaei, Y. (2011). "*Post-Punching Behavior of Reinforced Concrete Slabs*," Phd Thesis, Earthquake Engineering and Structural Dynamics Laboratory, Ecole Polythchnique Federale de Lausanne, Switzerland.

23. Pan, A., and Moehle, J. P. (1989). "Lateral Displacement Ductility of Reinforced Concrete Flat Plates," *ACI Structural Journal*, 86(3), 696-705.

24. Park, H.-G., Ann, K.-S., Choi, K.-K., and Chung, L. (2007). "Lattice Shear Reinforcement for Slab-Column Connections," *ACI Structural Journal*, 104(3), 294-303.

25. Park, H.-G., Kim, Y.-N., Song, J.-G., and Kang, S.-M. (2012). "Lattice Shear Reinforcement for Enhancement of Slab-Column Connections," *ASCE Journal of Structural Engineering*, 138(3), 425-437.

26. Pilakoutas, K., and Li, X. (1995). "*Alternative shear reinforcement in flat slabs*," Rep. No. CCC/94/0030A, Center for Cememt and Concrete, Dept. of Civil and Structural Engineering, Univ. of Sheffield, U.K.

27. Pilakoutas, K., and Li, X. (2003). "Alternative Shear Reinforcement for Reinforced Concrete Flat Slabs," *ASCE*

Journal of Structural Engineering, 129(9), 1164-1172.

28. "*Prestandard and Commentary for the Seismic Rehabilitation of Buildings*," Report No. 356, Fedral Emergency Management Agency, 2000.

29. Song, J.-K., Kim, J., Song, H.-B., and Song, J.-W. (2012). "Effective Punching Shear and Moment Capacity of Flat Plate-Column Connection with Shear Reinforcements for Lateral Loading," *International Journal of Concrete Structures and Materials*, 6(1), 19-29.

30. "*Standard Test for Making and Curing Concrete Specimens* (KS F 2403: 2010)," Korean Standard Association, 2010. (in Korean)

31. "*Standard Test for Method for Compressive Strength of Concrete* (KS F 2405: 2010)," Korean Standard Association, 2010. (in Korean)

32. "*Test Pieces for Tensile Teset for Metallic Materials* (KS F 0801: 2007)," Korean Standard Association, 2007. (in Korean)

국 문 초 록

전단밴드로 보강된 철근콘크리트 플랫 플레이트 내부 접합부의 실험적 연구

무량판 구조는 보 없이 기둥만으로 바닥판을 지지하는 구조 시스템으로 층고 감소로 인한 경제적 설계를 가능하게하며, 비교적 단순한 거푸집 작업으로 시공성을 확보할 수 있는 유용한 시스템이다. 뿐만 아니라 유연한 공간 구성이 가능하므로 평면을 계획할 때나 추후 리모델링이 필요할 때 유리한 가변성을 활용할 수 있는 장점이 있다. 하지만 삼풍백화점에서 경험하였듯 무량판 구조는 설계 및 시공에서의 오류가 발생할 때 기둥과 슬래브 접합부에서 과다한 중력 하중 하에 취성적인 전단파괴가 발생하거나 제한된 횡변위각 성능으로 지진 발생 시 전단파괴가 발생할 수 있다. 최근 고층 건물의 활성화와 가변형 건축평면 요구의 증가로 인해 무량판 구조에 대한 수요는 꾸준히 증가하고 있는 추세이다. 따라서 보다 간편하고 효과적으로 슬래브-기둥 접합부를 보강할 수 있는 방법에 대한 연구가 필요한 실정이다.

이 연구에서는 쉽게 조립이 가능하며 우수한 전단 보강 효과를 기대할 수 있는 전단밴드가 제시되었고 그 성능을 증명하기 위하여

실험적 연구가 수행되었다. 성능 비교를 위하여 전단 보강되지 않은 접합부, 스터럽 / 전단밴드로 전단 보강된 접합부가 각각 2 개씩 총 6 개 제작되었다. 그 중 3 개의 실험체는 중력하중 하에서 실험이 진행되었고, 나머지 3 개의 실험체는 40%의 콘크리트 전단강도에 상응하는 중력 하중과 반복 횡 하중을 동시에 받는 하중 조건에서 실험이 진행되었다. 실험결과 제작된 실험체 모두 ACI 318-11 에 의해 계산된 설계 강도를 상회하였고, 실험에 사용된 두 전단보강제 모두 접합부의 펀칭전단강도, 연성능력, 소산에너지 성능을 크게 향상시키며 전단 보강제로서의 역할을 충분히 발휘하였다. 전단 보강되지 않은 접합부와 비교하였을 때 전단밴드는 중력 하중 실험에서 접합부의 전단성능을 1.26 배, 연성능력을 7.96 배 향상시켰으며, 지진하중 실험에서는 횡저항 성능을 1.34 배, 횡변형능력을 2.73 배 향상시켰다. 실험결과에 근거하면 접합부의 강도와 연성 능력을 크게 향상시키는 전단밴드는 매우 효과적으로 접합부를 보강할 수 있는 전단보강제이며, 향상된 연성능력으로 미루어볼 때 이는 중력저항 시스템뿐만 아니라 횡저항 시스템에서도 효과적으로 사용될 수 있을 것으로 판단된다. 무엇보다 설치가 간편한 전단밴드는 시공 현장에서 향후 유용하게 쓰일 것으로 예상된다.

핵심용어: 무량판구조, 전단보강, 펀칭전단, 불균형모멘트, 전단밴드

학번: 2013-20569